Study of Liquid Jets at Transcritical to Supercritical Conditions in Single and Multicomponent Systems

A Thesis submitted

in partial fulfilment for the degree of

Doctor of Philosophy

by

Dhanesh Ayyappan

Department of Aerospace Engineering

INDIAN INSTITUTE OF SPACE SCIENCE AND TECHNOLOGY

THIRUVANANTHAPURAM - 695 547

May 2022

CERTIFICATE

This is to certify that the thesis titled ***Study of Liquid Jets at Transcritical to Supercritical Conditions in Single and Multicomponent Systems*** submitted by **Dhanesh Ayyappan**, to the Indian Institute of Space Science and Technology, Thiruvananthapuram, in partial fulfillment for the award of the degree of **Doctor of Philosophy**, is a bonafide record of the original work carried out by him under my supervision. The contents of this thesis, in full or in parts, have not been submitted to any other Institute or University for the award of any degree or diploma.

Dr. K Nandakumar
Co-Supervisor
Director Research
Hindustan Institute of Science and Technology

Dr. Aravind Vaidyanathan
Supervisor & Head of the department
Department of Aerospace Engineering
IIST

Place: IIST, Thiruvanathapuram
Date: 30 May 2022

Declaration

I declare that this thesis titled ***Study of Liquid Jets at Transcritical to Supercritical Conditions in Single and Multicomponent Systems*** submitted in partial fulfillment for the award of the degree of **Doctor of Philosophy** is a record of the original work carried out by me under the supervision of **Dr. Aravind Vaidyanatahan** and **Dr. Nandakumar K** and has not formed the basis for the award of any degree, diploma, associateship, fellowship, or other titles in this or any other Institution or University of higher learning. In keeping with the ethical practice in reporting scientific information, due acknowledgments have been made wherever the findings of others have been cited.

Place: IIST, Thiruvanathapuram
Date: 30 May 2022

Dhanesh Ayyappan
SC16D032

Acknowledgements

Firstly I would like to express my sincere gratitude towards my research advisor, Dr. Aravind Vaidyanathan, for giving me the opportunity to work under his guidance. I am very thankful to him for his continuous support, motivation, and guidance throughout my Ph.D. research in moulding me into a better researcher and also helping me to complete this project successfully.

I am very grateful to my co-guide Dr. K Nandakumar and all my doctoral committee members, Dr. Manoj. T Nair (DC Chairman, Associate Professor, Dept. of Aerospace Engineering, IIST), Dr. Pradeep Kumar (Associate Professor, Dept. of Aerospace Engineering) Dr. Deepak Mishra. (Associate Professor, Dept. of Avionics, IIST), and Dr. Sunil Kumar (Deputy Director, LPSC/ISRO), for their valuable suggestions, guidance, and constructive criticisms in each phase of my research work, which helped me a lot in improving the quality of the research outputs.

I also express my gratitude and thanks to the Director of IIST, the Dean Academics, and the Dean R&D for providing an excellent research ambience during my tenure in IIST.

I would like to thank Dr. Muthukumaran C K., Mr. Vinil Kumar R R., Mr. Sujinraj KS., Mr. Prakash R S., and Mr. Virosh for all their help in carrying out the research work smoothly.

I cannot express enough thanks to my friends, Mr. Shajahan, Dr. Aravind G P., Dr. Aryadutt Oamjee, Mr. Muhammed Shiyas K M., Dr. Prabith K., Mr. Sarath K P., Mr. Ajith Kumar., Mr.Mayukh C, Dr. Namitha Issac, Ms. Sreelekshmi Mohan, Mr. Renjith A R., Mr. Prajith Kumar, Mr. Gaurab Khanra, Ms. Risha Raju, Mr. Manu K Sukesan, Mr. Rithwik Sankar A.,Mr. Dayal, Mr. Pavanam Thomas, Mr. Abhijith Ajayakumar, Ms. Resmi V L., Ms. Anuja Vijayan S, Ms. Anju, Ms. Divya, Mr. Amal, Ms. Sunena, Mr. Raghul and Kurumpil family for all their support in many initiatives we have taken, both academic and non-academic, during these years, and also for all the wonderful memories.

I am extremely, grateful to my parents, my siblings and my wife for all their love and unconditional support throughout my years of study. Without them, this thesis would not have been possible.

Abstract

The physics of a liquid jet and its breakup has been of interest to researchers over the last many decades. It finds its applications in various areas like spray painting, liquid-fueled diesel engines, jet engines, rocket engines, etc. In applications like diesel engines and rocket engines, the chamber conditions are often supercritical with respect to the fuel under consideration. The behaviour of the fluid in these conditions is significantly influenced by the properties of the liquid-gas interfaces. The nature of instabilities at the near-critical and supercritical conditions and the mixing process of the jet are greatly influenced by the thermodynamic properties of the injectant. Experiments were carried out to study the effect of the thermodynamic properties of the injecting jet on the instability nature and mixing characteristics. The fluid and thermodynamic properties of the injectant jet are varied from room temperature to near-critical temperature by preheating the injectant jet and chamber pressure is varied from subcritical to supercritical conditions. Axis-symmetric linear instability analysis is performed to derive further insight from jet characteristics caused by the flow and fluid properties. Dynamic Mode Decomposition is employed to extract different instability modes of the flow. The generation of various modes depended on various factors like flow and fluid properties, disturbances in the flow like surface roughness in the injector, etc,. The linear stability analysis typically helps to bring out the dominant modes whereas DMD analysis on the high-speed shadowgraphy images brings out the range of instability modes that cause the jet to disintegrate. The DMD results were compared with the results obtained from linear instability analysis to find the dominant modes in the flow. DMD analysis was employed for the first time to bring out the instability characteristics of a liquid jet at near-critical and supercritical conditions.

The fundamental mechanisms which cause the behaviour of liquid jet to alter from classic spray atomization to diffusion-dominated mixing, especially in multicomponent systems at critical conditions are investigated. In the present experimental study, the behaviour of a subcritical laminar fluoroketone liquid jet injected into its own environment and in a mixture of N_2-fluoroketone environment at varying Reynolds number and chamber pressure (subcritical to supercritical) conditions are investigated. The present work utilizes high-speed imaging techniques to understand the jet behaviour and fractal analysis of the jet

boundary is employed to comprehend the mixing nature of the liquid jet. The results show that the composition of fluids in the chamber environment plays a critical role in altering the jet behaviour. The thermodynamic transition of the liquid jet depends upon the injecting Reynolds number and chamber pressure for a single component system whereas in a binary component system transition depends heavily on the partial pressure of the respective fluid in the chamber environment.

The study is also performed to analyse the behaviour of a co-flowing Nitrogen and Helium jet on the mixing behaviour of a sub-critical circular liquid jet at sub-critical to supercritical environments. The flow rate of both the incoming jets was varied to study the effect of velocities and velocity ratio on the mixing behaviour. DMD analysis was carried out to investigate the instabilities and the core length of the jet was determined. With the introduction of a sub-critical gaseous jet as a co-flow, at super-critical chamber conditions, the sudden thermodynamic transition of the fluoroketone jet was not observed and the co-flow jet insulated the fluoroketone jet from the surrounding environment. This shielding distance is directly dependent on the velocity of the co-flow jet.

Table of contents

Nomenclature

D	Diameter, m
D_f	Fractal dimension
Fk	Fluoroketone
Fr	Froude number
He	Helium
I	Modified Bessel function of first kind
K	Modified Bessel function of second kind
L_b	Normalized Undisturbed core length
N_2	Nitrogen
Oh	Ohnesorge Number
P	Pressure, bar
P_c	Critical Pressure,bar
P_{fk}	Reduced partial pressure of fluoroketone, $P_{fk} = P_{fluoroketone}/P_c$
$P_{fluoroketone}$	Pressure of fluoroketone,bar
P_i	Reduced injection pressure, $P_i = P_{injection}/P_c$
P_r	Reduced chamber pressure, $P_r = P_{chamber}/P_c$
Re	Reynolds Number
T	Temperature, $Kelvin$

T_i	Reduced injection temperature, $T_i = T_{injection}/T_c$
T_r	Reduced chamber temperature, $T_r = T_{chamber}/T_c$
We	Weber Number
k	Complex non-dimensional wave number
k_i	Non-dimensional spatial growth rate
k_r	Non-dimensional spatial oscillation
m	Mass flow rate, *g/s*
q	Ratio between ambient fluid density to injectant fluid density
t	time,*s*
v	velocity, *m/s*
v_g	velocity of gas, *m/s*
v_l	velocity of liquid jet, *m/s*
λ	Wavelength, *m*
λ_d	Normalized disturbance Wavelength
μ	Viscosity, Ns/m^2
ω	Complex non-dimensional temporal oscillation
ω_i	Non-dimensional temporal growth rate
ω_r	Non-dimensional temporal oscillation
ρ	Density, kg/m^3
ρ_g	Density of gas, kg/m^3
ρ_l	Density of liquid, kg/m^3
σ	Surface Tension, N/m
DMD	Dynamic Mode Decomposition
SVD	Singular Value Decomposition

List of figures

List of tables

Chapter 1

Introduction

In this chapter, a detailed introduction to literatures related to the study of regimes of liquid jet breakup, the corresponding mechanism of instability and mixing nature of the jet is presented. A detailed review of the studies on liquid jets at super-critical conditions is also carried out. The need for the experimental study of the liquid jet from trans-critical to super-critical conditions is discussed. Finally, the scope and objectives of the work are presented.

1.1 Background

The studies of fluid jet disintegration have been an interest to researchers for more than many decades. Understanding the dynamics of liquid jets is very important in various engineering applications. For example, in the case of spray painting, diesel engine, ink-jet printing process, rocket engines, the pressure and temperature plays a very important role in deciding the nature of the instability and thereby the behaviour of jet mixing or its disintegration. At higher subcritical temperatures, where the evaporation process is significant, the liquid and vapour phase properties are evaluated by considering the liquid-vapour equilibrium condition at the interface.

In certain applications like those in the liquid propelled rocket engine, the pressure and temperature are mostly above the supercritical state, i.e., above the critical point of the fuel under consideration. Beyond the supercritical point, the distinction between liquid and vapour ceases to exist. At the supercritical state, the value of surface tension becomes nearly zero. The various anomalies that exist in the vicinity of the critical point is not completely understood so far, and it needs to be addressed for efficiently designing the injectors employed at supercritical conditions.

The study of a fluid jet at supercritical conditions is more complex as compared to the study of static droplets at supercritical conditions. The pressure inside the rocket engine

or a diesel engine is always more than the critical pressure, so that the injected fuel always undergoes changes in transport properties which in turn affect the dynamic behaviour of the jet. A thorough understanding of the fluid dynamics, as well as the thermodynamic aspect of the jet behaviour, is mandatory for the efficient design of an injector and the combustion chamber of the rocket engines. Also, for enhancing the design database of the combustion chamber, the investigation of the liquid jet dynamics at supercritical conditions is necessary. It is to be noted that mimicking the actual injector conditions of a rocket engine may not be possible in a laboratory scale experimental setup. But the conditions explored in this study could serve the scientific community in understanding the physics and also help modelling community to validate their results and improvise the models at conditions associated with fundamental studies.

1.2 Regimes of liquid jet breakup

When a circular liquid jet emanates from an orifice into a quiescent environment, it preserves the cylindrical shape with a distinct interface. The interface separates the injectant liquid from the ambient medium which is characterized by the surface tension. The formation of instabilities and the breaking of the jet into fine droplets is a pure fluid dynamical process. There are various fluid dynamic forces that are responsible for the generation of instabilities and breakup of liquid jets. The flow parameters such as the velocity of the jet, the mass flow rate of the jet, and fluid properties such as density, surface tension, and viscosity of the fluid medium determine these fluid dynamic forces namely, inertial force ($\rho L^2 V^2$), surface tension force (σL), viscous force (μLV) and gravity force ($\rho L^3 g$). These fluid dynamic forces can be represented as independent non-dimensional groups: they are Reynolds number Re, Weber Number We, Froude number Fr and Ohnesorge number Oh which is the ratio of the square root of Weber number to the Reynolds number (Mehring and Sirignano (2000)).

The Weber number is the ratio between inertial force and the surface tension force and it is used when the effect of viscosity is not significant and the jet breakup mechanism is mainly dependent on the surface tension force and the inertial force. The We is defined in the eq.1.1

$$We = \frac{\rho V^2 D}{\sigma} \tag{1.1}$$

where ρ is the density of the fluid jet, V is the velocity of the jet, D is the diameter of the jet and σ is the surface tension of the fluid jet.

For a viscous jet, the viscosity has the effect of dampening the disturbances of the jet. In the case of viscous fluids, the Reynolds number is generally used and is defined as the ratio of the inertial force to the viscous force; it is expressed in eq.1.2

$$Re = \frac{\rho V D}{\mu} \tag{1.2}$$

where μ is the viscosity of the jet fluid.

To study the effect of gravity on the liquid jet the Froude number is used. The Froude number is obtained as shown in eq.1.3.

$$Fr = \frac{V}{\sqrt{gD}} \tag{1.3}$$

The Ohnesorge number (Oh) is used to understand the time scale of the breakup of the jet (McKinley and Renardy (2011)). The Oh is the ratio of viscous force to the product of inertial force and surface tension force. The Ohnesorge number is defined as in eq.1.4.

$$Oh = \frac{\mu}{\rho D \sigma} = \frac{\sqrt{We}}{Re} \tag{1.4}$$

For a given set of fluid properties like viscosity and surface tension, the behavior of the liquid jet is heavily dependent on the injection velocity. A review on jet breakup by Chigier and Reitz (1996) brought out the presence of various regimes of jet breakup and the underlying physical mechanism. The authors divided the liquid jet breakup into four regimes: Rayleigh regime, First wind-induced regime, second wind-induced regime, and Taylor regime.

1.2.1 Rayleigh Regime

At low Weber number or low injection velocities, the liquid jet is initially cylindrical and at a certain downstream distance, it is subjected to the growth of axisymmetric waves which are generally in the longitudinal direction. These unstable waves grow in the downstream direction and eventually leads to the formation of drops which are of the order of jet diameter. In the Rayleigh regime, the disturbances with larger wavelengths are more unstable which eventually causes a jet breakup. Within the Rayleigh regime, the breakup length of the jet is observed to increase with an increase in We. This is attributed to the increase in the inertia of the jet.

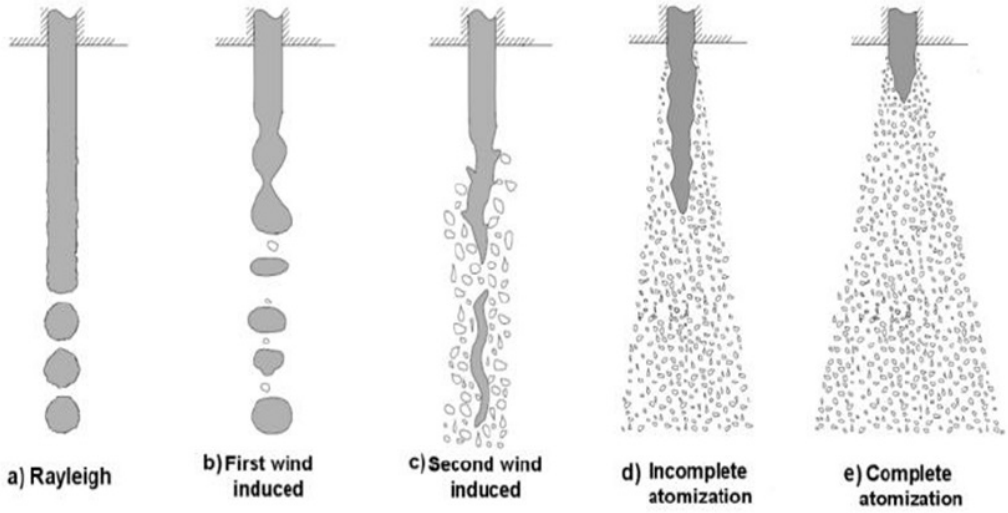

Figure 1.1: Regimes of atomization

1.2.2 First wind induced regime

In the first wind-induced regime, with a further increase in injection velocity, an asymmetric perturbation becomes possible due to the significant aerodynamic effect on the jet. The surrounding environment produces irregular weaving on the surface of the jet which results in a decrease in the breakup length of the jet. In the first wind-induced regime, the inertia of the surrounding gas is around one-tenth of the surface tension force. The size of the droplets produced is slightly smaller than those in the Rayleigh regime.

1.2.3 Second wind-induced regime

In the second wind-induced regime, with an increase in injection velocity, the inertia of the jet overcomes the aerodynamic shear which results in increased breakup length of the jet. But due to the increased flow turbulence and the due to aerodynamic effect, the disturbance wavelengths become shorter. The liquid jet shape is chaotic from the nozzle exit and the droplets are pinched from the surface of the jet. In the second wind-induced regime, the gas inertia force and the surface tension forces are of the same order of magnitude.

1.2.4 Taylor Regime or atomization

At high injection velocities, the jet breaks up into very fine droplets immediately as it emanates from the orifice. The drops formed in this regime are very fine due to strong wind effects. This regime is referred to as the Taylor mode of breakup and is typically associated

with atomization or spray formation. The Taylor regime is characterized by primary and secondary breakup processes. In the primary breakup, the liquid jet is distorted as it leaves the nozzle exit and the liquid fragments are pinched off from the jet surface. Due to the aerodynamic effect, these fragments further undergo distortion and break down into smaller fragments. This fragmentation continues until the surface tension force is strong enough to overcome the distortion due to the aerodynamic effect.

1.3 Instability analysis of circular liquid jets

The study of liquid jet instability dates back to Plateau when he performed the experiments in the static condition by placing the liquid between two disks. He observed that as the disks are moved apart, the length of the liquid cylinder formed between the two disks increases. He also explained that this phenomenon is similar to the liquid jet instability under gravity. Later Rayleigh through his extensive theoretical analysis described that the instability of the liquid jet and its breakup into droplets depends on the disturbances formed on the surface of the liquid jet. Based on the instability analysis by Rayleigh it was found that only the disturbance with a certain wavelength amplifies rapidly. The wavelength of disturbance with maximum growth rate corresponds to 1.437 times the circumference of the circular liquid jet. Rayleigh's analysis on the nature of instability included only the effect of surface tension, and the effect of viscosity and ambient medium were not considered.

The effect of viscosity and ambient medium on jet instability was first studied by Tomotika (1935). The author reported that an optimal ratio of viscosities of the jet and the ambient medium exists for which a disturbance of finite wavelength attains maximum growth rate. Mathematical analysis by Chandrasekhar (2013) showed that the viscosity tends to decrease the jet breakup length, and also increase the droplet size. The effect of density of the ambient gas on the liquid jet stability was studied by Weber (1931). Studies by Taylor (1940) revealed that the inertial force of the ambient gas significantly influenced the liquid-gas interface and the resulting droplet formation.

Leib and Goldstein (1986*a*), Lin et al. (1999) introduced the concept of convective and absolute instabilities which are often used to describe the nature of the instabilities in fluid flow. When the velocity distribution of the jet is non-uniform with a near-zero velocity at the interface, the instability wave propagates in both the upstream and downstream directions. This type of instabilities is termed absolute instability as reported by Lin and Jiang (2003). When the velocity profile is uniform, the instability waves propagate only in the downstream direction, and these types of instabilities are termed as convective instabilties (Leib and Goldstein (1986*a*,*b*)). The experimental evidence of the transition from convective

to absolute instability was reported by O'Donnell et al. (2001). The authors experimentally determined the critical Weber numbers above which a jet is convectively unstable and below which it is absolutely unstable for various Reynolds numbers. The influence of gravity on the convective and absolute instabilities of a viscoelastic jet was studied by Edwards et al. (2002) and Alhushaybari and Uddin (2019). Works by Ibrahim and Marshall (2000) showed that increasing injectant Weber number or gas to liquid density ratio enhances instability. An instability analysis by Hasan (2016*b*) also reported that the density ratio of the fluids plays a critical role in stabilizing or destabilizing the jets. The authors reported that the instability of the jets due to self-gravitating effects depends on the density ratio of the fluids. Segal and Polikhov (2008) and Muthukumaran and Vaidyanathan (2016*a*) also reported the effects of increased density ratio at high-pressure environments and also observed that the instability in liquid jets grow faster and resulted in increased atomization. Numerous experimental and numerical studies Eggers and Villermaux (2008); Elazab et al. (2012*a*,*b*); Eldabe et al. (2016); Faeth et al. (1995); Gorokhovski and Herrmann (2008); Hasan (2016*a*); Lasheras and Hopfinger (2000*b*); Lefebvre and McDonell (2017); Lin (2003); Lin and Lian (1989); Lin and Reitz (1998); Marmottant and Villermaux (2004); Reitz and Bracco (1982); Sirignano and Tryggvason (2000) in the past have been performed to understand the different aspects of instabilities and atomization.

1.4 Thermodynamic super-critical state

The fluid exists in solid, liquid, and vapour states at temperatures below the thermodynamic critical point. At subcritical temperatures, the fluid generally exists either in the solid-vapour or liquid-vapour state. At subcritical conditions, the liquid and vapour coexist with a distinct interface that is characterized by surface tension. With the increase in the temperature of the system, the vapour pressure of the system also increases, and the density of the liquid phase tend to decrease. When the temperature is near its critical point, the vapour pressure of the system approaches critical pressure and vapour density becomes almost equal to the density of the liquid phase and in addition to it, there is a drastic reduction in the surface tension (Anderson and Yang (1995)). At the critical point, the surface tension becomes zero and the distinct interface between the liquid and vapour phase no longer exists. For a pure substance, the whole system exists in a homogeneous state with physical properties like viscosity and density that lie in between the distinct values of liquid and vapour state. This homogeneous phase is often referred to as a supercritical state. In the supercritical state, the fluid possesses density that is nearly equal to half of the density of the liquid with many properties similar to that of the vapour (Zappoli (2003)). Also, in addition to it, the fluid exhibits various

anomalies such as infinite heat capacity, drastic reduction in thermal conductivity and latent heat of evaporation (Sengers (1985)). These various anomalies in the transport properties of the fluid near the critical and supercritical conditions make the modeling of jet dynamics at these conditions very challenging.

1.5 Liquid jets at supercritical conditions

In most of the propulsion applications, there is a general trend towards increasingly higher chamber pressures. A simple thermodynamic analysis of a liquid rocket engine indicates that higher the chamber pressures result in higher specific impulse and thereby increase the efficiency of the engine. Similarly, higher chamber pressures increase the power output and efficiency of diesel engines and gas turbines. In rocket applications, the chamber conditions are often supercritical to the fuels under consideration. The fluids injected into the supercritical ambient pressure often possess a subcritical initial temperature. The injected jet is then heated up beyond its critical temperature before it gets atomized, and mixes and undergo combustion in the combustion chamber. This process is often referred to as a 'transcritical' injection. To formulate an accurate physical model for improved design methodology, a better understanding of atomization, mixing, flow dynamics, and flame stabilization in high pressure subcritical and supercritical conditions is essential.

Most of the early works were focused on static droplets at elevated pressure and temperature conditions. The studies revealed that the droplet lifetime decreases with an increase in pressure at supercritical pressure conditions. The study of a fluid jet at transcritical and supercritical conditions is more complex when compared with the study of the droplets. The study on droplets is one of the several aspects of the behaviour of fluids at such conditions. The other characteristics of the jets such as shear layer geometry, spreading angle, and thermodynamic transition to the supercritical medium significantly influence the mixing characteristics of the jet.

Newman and Brzustowski (1971) initiated the study of jet injection into supercritical conditions. They performed experiments on the injection of liquid CO_2 into its supercritical environment, and also into an ambient medium consisting of N_2 and CO_2 mixture at various compositions. Finer sprays with smaller droplets were observed when the temperature reached the critical point. Behaviour of a single and coaxial jet from subcritical to supercritical conditions was investigated by Mayer et al. (H. Mayer et al. (1998); Mayer et al. (2000); Mayer and Tamura (1996)) and it was observed that beyond critical pressure the jet exhibited streaky like appearance. They also observed a change in the atomization process. Chehroudi, Talley and Coy (2002) revealed that the supercritical jet exhibits characteristic features similar

to those in variable density gaseous jet. The authors performed studies on the injection of liquid N_2 into gaseous N_2 at subcritical and supercritical conditions. The reviews by Bellan (2000), Oschwald*, Smith, Branam, Hussong, Sschik, Chehroudi and Talley (2006) and Chehroudi (2012) brought out major experimental efforts in recent decades in characterizing supercritical jets. Segal and Polikhov (2008) performed studies on subcritical fluoroketone jet injected into chamber conditions that varied from subcritical to supercritical, and reported that the jet exhibited supercritical behavior with the absence of droplet formation beyond critical pressure and temperature. At supercritical chamber conditions, as the chamber to injectant density ratio increases, the core length decreases (Roy and Segal (2010)). The recent work carried out by Muthukumaran and Vaidyanathan (2016*a*) on circular jet investigates the thermodynamic transition involved in the low-velocity jet at the supercritical condition. Their study probes the disturbance wave structure on a steady-state jet. It was found that the laminar subcritical jet injected into its supercritical chamber conditions remained intact for a certain downstream distance until the surface disturbances amplified, promoting mixing and thereby causing the jet transition to the supercritical state. The authors evaluated the decrease in the surface tension of the jet interface from the disturbance wavelength by assuming the disturbances to be capillary in nature. However, the nature of disturbance formed on the liquid jet surface is not completely understood.

The breakup and mixing process of the jet is predominantly determined by the thermodynamic properties of the injectant (Baab et al. (2018)). Wu et al. (1996, 1999) studied the expansion and mixing process of supercritical ethylene jets into subcritical and supercritical nitrogen environments. Experimental results showed that, when the injectant jet was at room temperature, the injected ethylene jet appeared to have an opaque region, which was caused by fuel condensation, and it gradually disappeared as the temperature of the jet was increased further. The authors also reported that the difference in the temperature of the jet influenced the heat transfer rate between the jet and the environment, which in turn affected the mixing process. Liu et al. (2018) studied the spray characteristics of diesel fuels injected at subcritical to supercritical conditions into atmospheric conditions. Their results showed that the spray characteristics were significantly affected when the injected fuel was at near-critical and supercritical temperatures as compared to those at subcritical temperatures. Studies by Doungthip et al. (2002) reported that the penetration depth of a supercritical jet is much lesser as compared to a subcritical jet at supercritical chamber conditions. The authors injected n-decane at sub-critical to super-critical conditions into a supercritical nitrogen environment. Similar observations were also reported by Liu et al. (2017); Muthukumaran and Vaidyanathan (2016*b*); Roy and Segal (2010). Though there are numerous studies (Chen (1994); Lin et al. (2006); Lin and Tavlarides (2013)) conducted in the past to understand the

behaviour of a supercritical jet in a sub-critical and super-critical environment, the literature is limited in providing the comprehensive understanding of interfacial instability of the jet associated with changes in the thermodynamic properties of the injectant.

It is widely assumed that the surface tension forces will cease to exist when the pressure and temperature of the liquid phase exceed its critical value. In a single component system, this theory of diminishing surface tension at high-pressure conditions was observed in many studies over the last few decades. However, for a multicomponent system, this is not the case in general. In a multi-component system, the surface tension forces need not diminish with the chamber pressure exceeding the critical value. Many studies in the past Dahms (2016); Dahms and Oefelein (2013, 2015); Muthukumaran and Vaidyanathan (2014, 2015); Newman and Brzustowski (1971); Woodward and Talley (1996) revealed that the liquid jet indicated the presence of surface tension at chamber pressure above critical value with distinct interface between liquid and vapour phase. Muthukumaran and Vaidyanathan (2014, 2015) studied the behaviour of an elliptical fluoroketone liquid jet at its supercritical conditions with ambient nitrogen environment. The study revealed that the elliptical liquid jet exhibited axis-switching phenomena, thereby indicating the presence of surface tension forces without undergoing a thermodynamic transition to the supercritical state. Experiments by Dahms and Oefelein (2015) reported the presence of surface tension at temperatures above the critical temperature. Recently Dahms (2016) proposed a linear gradient theory model in combination with a 32-term Benedict- Webb-Rubin equation of state to study the molecular two-phase interfacial structure of n-dodecane-nitrogen mixture at critical conditions. Their results showed that the interface might transition to the regime of continuum length scale at critical conditions due to the combined effects of reduced surface tension forces and molecular paths and the broadened interfaces. Manin et al. (2014) and Falgout et al. (2016) using high-speed imaging techniques provided experimental validation for the same.

1.5.1 Studies on co-axial injections

In applications like rocket engines, the liquid fuel jet is allowed to interact with a fast-moving gaseous fluid that enhances atomization. Atomizers/injectors based on this principle are generally known as air-blast injectors or co-axial injectors. A shear-coaxial jet consists of two potential cores, the one corresponding to the inner jet and the other related to the outer annular jet. There exist two shear layers associated with these cores: an outer shear layer between the ambient fluid and the outer annular jet, and another inner shear layer between the outer annular fluid and the circular inner jet. The development of perturbations on these shear layers and their interaction has a great influence on the eventual instability and atomization characteristics of the jet.

Co-axial injectors can be of two types: single-phase and two-phase. Single-phase co-axial injectors can be either gas-gas injectors or liquid-liquid injectors. Over the past many years good amount of fundamental studies (Alexander Schumaker and Driscoll (2012); Favre-Marinet and Schettini (2001); Rehab et al. (1997); Tang and Ko (1994); Tani et al. (2015)) have been carried out for single-phase co-axial injectors. These types of injectors find applications in turbofan engines, air blowers, and gas burners. Two-phase co-axial injectors find applications in fields like cryogenic rocket engines. Many studies (Branam et al. (2002); Chigier and Farago (1992); Lasheras and Hopfinger (2000*a*); Lasheras et al. (1998)) were conducted in the past to explore the various aspects of two-phase co-axial injectors. Depending on the inner jet Reynolds number and gas Weber number, Chigier and Farago (1992) categorized the liquid jet breakup into five modes namely, axisymmetric Rayleigh mode, non-axisymmetric Rayleigh mode, membrane breakup mode, fiber-type breakup mode, and super pulsating mode. In a co-axial injector, determining the liquid jet breakup length is very important since it indicates the location at which the multiphase region becomes active. Aerodynamic instabilities between the liquid and gas jets were studied by Lasheras and Hopfinger (2000*a*). The authors provided a correlation between the liquid core length and the momentum flux ratio between liquid and gas. Many studies carried out by various researchers reported that breakup length is greatly influenced by the injecting Reynolds number and Weber Number which are directly coupled with nozzle geometry and the momentum ratio (Charalampous et al. (2009); Dumouchel (2008); Eroglu et al. (1991); Kumar and Sahu (2018*a*,*b*); Lasheras and Hopfinger (2000*a*); Leroux et al. (2007); Liu et al. (2006); Porcheron et al. (2002)), and also on the density ratio of the co-flowing fluids (Alexander Schumaker and Driscoll (2012); Chehroudi, Cohn and Talley (2002); Chehroudi, Talley and Coy (2002); Porcheron et al. (2002); Reitz and Bracco (1982)).

Studies on co-axial injectors at trans-critical and supercritical conditions were initiated in the later years of the 19th century. Injection of cryogenic Nitrogen jet with gaseous Nitrogen as co-flow at transcritical and supercritical conditions were studied by many researchers (Chehroudi (2012); Chehroudi, Talley and Coy (2002); Davis and Chehroudi (2006); Davis (2006); Leyva et al. (2007); Mayer et al. (2000); Schmitt et al. (2012); Tani et al. (2015)). Mayer et al. (2000) used gaseous Helium as co-flow instead of Nitrogen. Studies by Chehroudi, Talley and Coy (2002) revealed that the co-flowing outer jet has a great influence on the mixing of the inner jet into the chamber environment. The authors studied the acoustic effects on the length of the inner core jet and its spreading angle and proposed that those can be the ideal indicators to study the mixing behaviour. Studies at the German Aerospace Center (DLR) by Oschwald et al. (1999); Oschwald*, Smith, Branam, Hussong, Schik, Chehroudi and Talley (2006) reported that the temperature of the centerline

jet is greatly influenced by the thermodynamic transition at super-critical conditions. They studied the behaviour of cryogenic nitrogen-gaseous helium coaxial jets using Raman scattering measurements. There are several numerical studies carried out by various researchers (Balarac and Metais (2005); Balarac, Métais and Lesieur (2007); Balarac, Si-Ameur, Lesieur and Métais (2007); Hosangadi et al. (2008); Lacaze and Oefelein (2013); Matsuyama et al. (2010)) on the cryogenic coaxial jets at transcritical and supercritical conditions.

1.5.2 Fractal Analysis

Often the experimental characterization in the atomization regime is limited to the determination of parameters like spray angle and breakup length. The description of the liquid-gas interface during atomization is very much essential for the prediction of drop size distribution in any liquid spray applications (Dumouchel et al. (2005)). Liquid-gas interface geometry appears to be very complex in high-pressure environments and in such cases, the fractal dimension is very useful in characterizing the geometry of the interface. The fractal dimension gives a measure of the space-filling nature of the jet surface. Fractal dimensions were used by Sreenivasan and Meneveau (1986) to analyze the geometry of the turbulent jet interfaces. Chehroudi et al. (1999) used the Minkowski or the box-counting method to study the fractal nature of liquid nitrogen injected into supercritical nitrogen. Later Chehroudi and Talley (2004) used the fractal concept to characterize the boundary of a fluid spray under atmospheric conditions. The fractal dimension of the liquid-gas interface was measured by Shavit and Chigier (1995) from the experimentally obtained images. The authors reported that the fractal dimension increased from 1 to a peak value and then decreased at different axial locations from the jet orifice. Heidorn et al. (2008) through numerical simulations proposed a dynamic model and their analysis showed that the fractal dimension for a liquid jet boundary is near to 1.27. Similar results were obtained from the experimental study conducted by Taylor and Hoyt (1983). Muthukumaran and Vaidyanathan (2016*b*) employed fractal analysis for near-critical and supercritical fluoroketone jet into subcritical and supercritical chamber conditions. The authors used Helium and Nitrogen as chamber environments. The fractal dimension for all the cases were between 1.25 and 1.35. The authors concluded that in a binary component system, behaviour of the supercritical jet at low injecting Re is similar to variable-density or gaseous jets and is independent of chamber conditions i.e, whether subcritical or supercritical.

1.5.3 Modal decomposition of jets

With the advancement of non-intrusive techniques like planar laser-induced fluorescence (PLIF), particle-image velocimetry (PIV), and high-speed imaging in recent years, researchers use modal decomposition techniques to extract coherent features of the flow. These modal decomposition techniques reveal the most energetic coherent structures in the flow which cannot be observed directly from the acquired data (for example, shadowgraphy or PIV images). Previous studies Arienti and Soteriou (2009); Berkooz et al. (1993); Charalampous et al. (2019); Charalampous and Hardalupas (2014); Kumar and Sahu (2019) on injector flow included the Proper Orthogonal Decomposition (POD) approach to reveal the most energetic pairs of the coherent structures but POD is not as efficient when it comes to handling the temporal details of the flow. Dynamic Mode Decomposition (DMD) decomposes the experimental snapshots into temporally and spatially coherent structures which allows a more thorough analysis of complex fluid dynamic processes. DMD has the capability to provide an accurate decomposition of a non-linear system into simple coherent structures in space and time, without any need for fluid and flow properties. It is completely a data-driven method and can be used for future step prediction of the system. Schmid (2010, 2011) performed DMD analysis to extract dynamically relevant coherent structures on a slow jet injected into a quiescent medium which was similar to the Arnoldi algorithm. The DMD analysis was used by many researchers for the modal decomposition of the flow (Hemati et al. (2014); Hyhlík et al. (2017); Roy et al. (2015); Seena and Sung (2011); Tirunagari et al. (2012)). Hua et al. (2016) used DMD analysis to capture robust modes in a shear co-axial injector flows. Stability analysis of Cu-water nanofluids past a square cylinder was studied using DMD analysis by Sarkar et al. (2013). Alessandri et al. (2019) applied the DMD technique over the experimentally acquired PIV data to identify stable and unstable regimes in transitional flows.

1.6 Inference from literature

It is widely assumed that the surface tension forces will cease to exist when the pressure and temperature of the liquid phase exceed its critical value. In a single-component system, this theory of diminishing surface tension at high-pressure conditions was observed in many studies over the last few decades. However, for a multicomponent system, this is not the case in general. In a multi-component system, the surface tension forces need not diminish when the chamber pressure starts exceeding the critical value. Many studies in the past revealed that the liquid jet indicated the presence of surface tension at pressures above critical value with a distinct interface between liquid and vapour phases. Despite many

significant contributions by many researchers over the past few decades, the fundamental phenomena which cause the thermodynamic transition from the regime of classical spray atomization to diffusion-dominated mixing, especially in a multi-component system are still not fully understood and pose some challenging questions. Most of the previous studies that investigated the binary component system used two different mediums for the injecting jet and ambient medium respectively. However, there are only limited studies (Newman and Brzustowski (1971), Woodward and Talley (1996)) that investigated a binary component system by employing the jet fluid itself as one of the components in the ambient environment.

Even though the study of liquid jets at transcritical and supercritical conditions was initiated in the 1970s by Newman and Brzustowski (1971), most of the researchers in the past studied the mixing of the jet at conditions similar to that of rocket engines. The mixing studies were studied by injecting at Re$>$10000. Studies in the past are performed to investigate the supercritical jet behaviour, and very little information is available on the effect of various flow and fluid properties on the thermodynamic transition. Also, the nature of instabilities at the near-critical and supercritical conditions and the mixing process of the jet is greatly influenced by the thermodynamic properties of the injectant. However, a comprehensive understanding of these aspects is not explored in detail and hence it is not fully understood. Hence, a low-velocity jet could reveal further insights on the influence of various transport properties on the instability nature and mixing nature of the jet.

In most of the experimental studies in co-axial injectors, the densities, and temperature of both the inner fluid and outer fluid are comparable, and the atomization and mixing process is largely dependent on the shearing action of the outer fluid over the inner fluid. There is hardly any study in the literature that essentially indicates the effect of a lower-density (compared with inner jet) outer jet on the atomization and mixing behaviour of the coaxial jet in general.

A thorough understanding and accurate description of the flow physics's coherent features and disturbance behaviour could greatly benefit many industrial applications like those in the combustion chamber of diesel or rocket engines. With the advancement of non-intrusive techniques like planar laser-induced fluorescence (PLIF), particle-image velocimetry (PIV), and high-speed imaging in recent years, modal decomposition techniques like POD, DMD are instrumental to extracting coherent features of the flow. These modal decomposition techniques reveal the most energetic coherent structures in the flow, which cannot be observed directly from the acquired data (for example, shadowgraphy or PIV images). The linear stability analysis typically helps to bring out the dominant modes. In contrast, modal analysis on the high-speed shadowgraphy images will reveal the range of instability modes that cause

the jet to disintegrate, leading to additional insights on the nature of instabilities that generate and propagate in the jet at near-critical and supercritical conditions.

1.7 Scope and Objective

The jet dynamics at transcritical and super-critical conditions involve strong coupling between fluid dynamics and the thermodynamic processes. At elevated pressure and temperature environments, the injected jet undergoes changes in transport properties which in turn alter the fluid dynamic properties. In the past, most of the studies were carried out with high injecting velocities. To understand the nature of the instabilities and reveal fundamental characteristics of mixing and thermodynamic transition, it is very much essential to study the jet at low injection velocity.

The main objective of the present work is to understand the effects of various flow and fluid properties on the nature of instabilities formed on the jet surface and interface, and the mixing of circular liquid jets at sub-critical to supercritical chamber conditions. The objectives are listed as follows:

1. The first objective of the present work is to perform the experiments in a single-component system i.e, the injecting jet is injected into its own vapour. Experiments are performed to study the effects of the chamber and injecting properties on the behaviour of the jets. Linear instability analysis and Modal decomposition techniques are applied to study the instability nature and extract different modes of the flow.

2. The second objective of the work is to perform the experiments in the binary component system. The work is divided into two parts:

    - to investigate and determine (i) the sufficient and necessary conditions for a liquid jet to undergo the thermodynamic transition to supercritical state and also to understand (ii) the effect of different compositions of the fluids in the chamber environment (nitrogen-fluoroketone) on the behaviour of liquid jet. Fractal analysis of the jet boundary is employed to comprehend the mixing nature of the liquid jet.
    - to investigate the atomization and mixing behaviour of a coaxial jet when a low-temperature low-density gaseous fluid is introduced as a co-flow for a sub-critical fluoroketone liquid jet at super-critical chamber conditions. The effect of the velocity of the outer jet is studied experimentally and proper orthogonal decomposition is employed to obtain the different spatial modes and temporal modes of the jet behaviour.

1.8 Thesis Outline

A brief introduction to the application of jet disintegration and mixing at supercritical conditions is presented in chapter 1.

In chapter 1, a brief introduction and the detailed literature review pertaining to the study of liquid jet breakup and mixing of a liquid jet at sub-critical to supercritical conditions is discussed. Finally, the scope and the objectives of the current study is presented.

In chapter 2, the details of the experimental facility and methodologies to analyse the jet behaviour are presented. The detailed mathematical formulation of fractal analysis, linear instability analysis and dynamic mode decomposition methods are presented. Also, an overview of the experimental conditions is presented.

In chapter 3, the detailed investigation of a circular jet at sub-critical to supercritical chamber conditions in a single component system (i.e. the liquid jet injected into its own vapour medium is presented. Experiments were carried out to investigate the effect of injectant and chamber conditions on the instability and mixing nature of the jet. Axi-symmetric linear instability analysis and dynamic mode decomposition is employed to study the instability of the jet.

In chapter 4, the detailed investigation of the mixing nature and thermodynamic transition of a circular jet in a binary component system is investigated. Experiments were carried out to study the effect of the compositions of fluids on the behaviour of the liquid jet. Fractal analysis was employed to compare the mixing nature of the single and binary component systems. Also, the behaviour of liquid jet in the presence of co-flowing gas at supercritical conditions is presented in chapter 4.

In chapter 5, the major conclusions from the current study are presented.

Chapter 2

Experimental Methods

In this chapter, the details of the experimental setup for single component and binary component system are discussed. Various components such as high pressure facility, various measurement technique, and data acquisition procedures are described. Also, the methodology of analsyis tools like linear instability analysis, fractal analysis and Dynamic mode decomposition are also presented in detail.

2.1 Experimental facility

The experiments were to be performed to comprehend the jet behaviour at thermodynamic sub-critical to supercritical conditions. An experimental facility constituting a high-pressure chamber along with provision for heating the chamber to desired temperatures was built in Advanced Propulsion and Laser Diagnostics (APLD) lab, IIST to conduct the experiments. The facility also consists of liquid and gas heaters and supply lines. The liquid and gas supply system consists of nitrogen cylinders, ball valves, metering valves, flow meters, pressure transducer, and thermocouples. A schematic view of the experimental setup is shown in fig.2.1.

- **High-pressure chamber**

  The high-pressure chamber is designed to withstand a pressure of 70bar and temperature up to 700K and is provided with quartz optical windows on four sides for the visualization of the jet. Four through-holes are provided on the corners of the main chamber body to insert the cartridge heaters. A circular orifice of a diameter 1mm is provided on the central top of the chamber through which the liquid jet is injected. The chamber is heated using cartridge heaters which are inserted into the through-holes

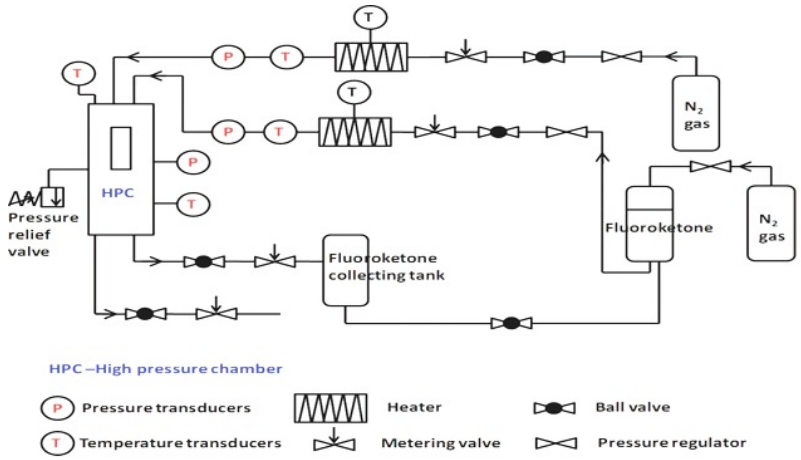

Figure 2.1: Experimental setup

provided in the four corners of the chamber. Two thermocouples, one near the orifice and the other at the bottom of the chamber are used to measure the temperature inside the chamber.

- **Pressure Measurements**
  The pressure readings are obtained using OMEGA dyne PX309-1KGV steady pressure transducers. It is highly accurate with errors less than 0.25% of the full scale reading with the pressure ranges upto 1000 psi gauge. The pressure transducer is excited with 5 VDC and the corresponding output of 0-10 mV is acquired. The output of the transducer is connected to the NI- PXIe-4331 card of National Instruments (NI) for acquiring the pressure data.

- **Temperature Measurements**

  The temperature of the chamber is maintained at the required level using PID controllers which have an error of less than 0.5%. The temperature measurements are taken using OMEGA K-type thermocouple having the temperature range from -100° to 1200° C with a maximum error of 1.1°. The thermocouples are connected to the PXIe-4353 card of NI system for acquiring the temperature readings. To ensure the uniformity in the temperature distribution, two theromocouples are provided in the chamber, one on the top and another at the bottom of the chamber.

- **Flow measurements**

  1. **Liquid mass flow rate:** The EMERSON Coriolis mass flow meter is used for flow rate measurements which uses coriolis principle for measuring the flow rates.

Table 2.1: Uncertainity in measurements

Measurement	Maximum Uncertainity
Pressure	0.9%
Temperature	1.1°C
Mass flow rate	1.1%
Length measurement	15%

The flow meter is excited with 18-24 VDC and provides an output of 4-20 mA. The output of the flow meter is connected to the NI PXIe-6239 card of the NI system for acquiring the flowmeter readings.

2. **Gas mass flow rate:** For the co-axial studies, the flow rates in gas lines are obtained using the SWAGELOCK S-series metering valves. The flow rate is obtained by the equation:

$$q = N_2 C_v P_1 (1 - \frac{2\Delta P}{3P_1}) \sqrt{\frac{2\Delta P}{P_1 G_g T_1}} \tag{2.1}$$

where P_1 and P_2 are the inlet and outlet pressures across the metering valve, C_v is the coefficent of velocity which depends upon the number of turns of on the valve, G_g is the specific gravity of the gas, q is the flow rate, $\Delta P = P_1 - P_2$, T_1 is the absolute upstream temperature in K, and N_2 is a constant.

- **Flow visualization**

  The jet behaviour studies rely primarily on the flow visualization technique because of its non-intrusive nature. In the presnt study, high speed shadowgraphy technique is used to capture the jet images. For acquiring high speed images, PHANTOM high speed camera is used with Nikkor 105mm macro lens. Backlighting is provided using Green hardsoft Illuminator light source. Triggering of the camera is done by Labview programme yhrough BNC-2120 card of NI system.

- **Data Acquisition**

  All the temperature, presure and the mass flow readings are fed to the National Instruments (NI) data acquisition system (Instruction Manual, National Instruments).The hardware/software interface is made using the LABVIEW software. The LABVIEW is a viual programming language from National Instruments (NI) generally used for instrumentation control and data acquisition. For the present study, the real time

Table 2.2: Fluoroketone properties

Chemical formula	$CF_3CF_2C(O)CF(CF_3)_2$
Boiling point	322 K
Molecular Weight (M)	316 g/mol
Critical Temperature (T_c)	441.8 K
Critical pressure (P_c)	18.6 bar
liquid density (ρ_l)	1600 kg/m^3
Absolute Viscosity (μ)	0.64 cP
Surface tension (σ)	10.8 m/Nm

readings of the pressure, temperature and mass flow rate readings are acquired, and the output is stored in a MICROSOFT excel file.

- **Fluids**

Injecting liquid, Fluoroketone

An engineering fluid Dodecafluoro-2-methylpentan-3-one ($CF_3CF_2C(O)CF(CF_3)_2$) commonly referred as fluoroketone (Fk) or Novec-649 is used for the study of liquid jets at critical conditions primarily because of its low critical pressure P_c=18.6 bar and critical temperature T_c=441.8K (Owens (2002)). Many researchers DeSouza and Segal (2017); Muthukumaran and Vaidyanathan (2016*a*, 2014, 2015, 2016*b*); Roy and Segal (2010); Segal and Polikhov (2008) in the recent years used the same for the study at critical condtions. It is a fire suppressant and it is thermally stable upto a temperature of 773K. The properties of fluoroketone at various conditions are obtained from NIST Reference Fluid Thermodynamics and Transport Properties-REFPROP Database 23 (Version 9.1). The properties of the fluoroketone are detailed in table2.2.

Other fluids

Nitrogen(N_2) and Helium(He) are used as the gaseous fluids in the present study. The critical pressures of N_2 and He are 33 bar, 2.27 bar respectively and their molecular weights are 14 and 4 respectively.

2.2 Fractal Analysis: Box counting Method

Mandelbrot (1982) proposed that the concept of fractals can be applied to the study of turbulence since turbulence possess the nature of self-similarity. Fractal analysis is a branch

of mathematics which allows the description of complex boundaries and it becomes very useful in the studies of a liquid-gas interface at critical conditions. Fractal dimension gives a measure of the tortuosity, fragmentation or roughness of a line or surface that is self-similar over a range of scales when observed at different magnifications. In a plane, the fractal dimension for a straight line is 1 and if the line is tortuous and if it covers the whole plane then the fractal dimension will be 2. The larger fractal dimension indicates the presence of corrugated interface that exists between the injected jet and the chamber environment or in other words the fractal dimension gives a measure of the space filling nature of the jet in the medium. The application of fractal concept has its own limitations as the existence of self-similarity occurs only over a certain range of scales when observed at different magnifications. In the current study, the box-counting algorithm is used for obtaining the fractal dimension of the injected fluid. Fractal analysis is carried out for subcritical fluoroketone injected to a) its own environment and b) mixture of nitrogen-fluoroketone environment. Fractal dimensions were evaluated for lengths up to 25 jet diameters downstream of the injected jet from the orifice. The iso-density contour of the injected jet boundary is obtained by imposing a specific threshold intensity value of the visualized jet image. The fractal dimension is obtained for the resulting jet boundary. To calculate the the fractal dimension, the fractal objects are overlapped with the evenly spaced grid and the boxes that cover the set are counted. The fractal dimension depends on the number of boxes that cover the fractal set and it changes as the grid becomes finer. the fractal dimension is defined as

$$Df = \frac{Log(N(\in))}{Log(1/N(\in))} \tag{2.2}$$

where $N(\in)$ is the number of boxes of side $\in$ that was required to cover the fractal set.

2.3 Instability Analysis

To explore further insight into the liquid jet characteristics, linear instability analysis was performed. The surrounding medium of the jet was considered inviscid and quiescent. From the studies of Ibrahim and Marshall (2000), a jet with a uniform velocity profile is more unstable as compared to the one with a parabolic profile. In the present study, the profile of the jet is assumed to be uniform. The studies of Muthukumaran and Vaidyanathan (2016*a*) and Segal and Polikhov (2008) also reported that the assumption is valid. The linearized equations for mass and momentum conservation equations (in r and z-direction) are:

$$\frac{1}{r}\frac{\partial(ru_i)}{\partial r} + \frac{\partial u_i}{\partial z} = 0 \tag{2.3}$$

$$\frac{\partial u_i}{\partial t} + \delta_{1i} u_l \frac{\partial u_i}{\partial z} = -\frac{1}{\rho}\frac{\partial p_i}{\partial r} + \delta_{1i}\nu[\bigtriangledown^2 u_i - \frac{u_i}{r^2}] \tag{2.4}$$

$$\frac{\partial w_i}{\partial t} + \delta_{1i} u_l \frac{\partial w_i}{\partial z} = -\frac{1}{\rho}\frac{\partial p}{\partial z} + \delta_{li}\nu \bigtriangledown^2 w_i \tag{2.5}$$

where u and w are the velocity components in radial and axial directions, p is the pressure, ν is the viscosity, and index 'i' represents the liquid(i=1) and vapour phase(i=2) respectively. δ=1 when i=1 and δ=0 when i=2 i.e, for gas phase the viscosity is assumed to be zero.

The perturbations are considered to be Fourier mode of the form:

$$F(x,t) = f(x,t)exp[i(kx + m\theta + \omega t)] \tag{2.6}$$

where k(=πd/λ) represents the non-dimensional wave number and ω represents the non-dimensional temporal oscillation; here v is the velocity of the injecting jet and 'd' is the diameter of the jet. The parameter m corresponds to the azimuthal mode of disturbance. In the present study, the disturbances are considered to be axis-symmetric in nature; therefore the parameter is taken as m=0. For other cases, the parameter m=1 represents the sinuous mode and m=2 corresponds to the screw-like mode. The perturbations in pressure and velocity components are:

$$p_i = P_i(r)exp(j(kz + \omega t)) \tag{2.7}$$

$$u_i = U_i(r)exp(j(kz + \omega t)) \tag{2.8}$$

$$w_i = W_i(r)exp(j(kz + \omega t)) \tag{2.9}$$

In the present work, the dispersion relation for instability analysis of viscous jet into a gaseous medium as presented by Segal and Polikhov (2008) is employed. This dispersion relation is similar to the one obtained by Sterling and Sleicher (1975).

$$\begin{aligned}(\omega+k)^2\frac{I_0(k)}{I_1(k)} - \frac{2ik^2}{Re_l}(\omega+k)[\frac{I_0(k)}{I_1(k)} + \frac{I_0'(k)}{I_1'(k)}] + \omega^2 Q\frac{K_0(k)}{K_0'(k)} \\ -\frac{4k^3}{{Re_l}^2}[k\frac{I_1'(k)}{I_1(k)} - l\frac{I_1'(l)}{I_1(l)}] + \frac{k}{We_l}(1-k^2) = 0\end{aligned} \tag{2.10}$$

where $k = k_r + k_i$ and $\omega = \omega_r + \omega_i$, with -$k_i$ and $-\omega_i$ representing the spatial growth rate and temporal growth rate and k_r and ω_r being spatial oscillation and temporal oscillation respectively. I and K of equation 2.10 are the modified Bessel function of the first and second kind and their subscripts 0 and 1 correspond to the zeroth-order and first order of the functions respectively. Re, We and Q in equations 2.11,2.12 and2.13 represent the injecting Reynolds Number, Weber number and density ratio (gas(ρ_g)/liquid(ρ_l)) respectively with V

representing the velocity of the jet, d diameter of the jet, μ dynamic viscosity and σ surface tension.

$$Re = \frac{\rho_l V d}{\mu} \tag{2.11}$$

$$We = \frac{\rho_l V^2 d}{\sigma} \tag{2.12}$$

$$Q = \frac{\rho_g}{\rho_l} \tag{2.13}$$

2.4 Dynamic Mode Decomposition

Dynamic Mode Decomposition is one of the decomposition techniques which is based on the time-resolved sequence of flow field measurements as similar to Proper Orthogonal Decomposition(POD). Unlike POD, the correlated spatial modes are associated with a given temporal frequency accompanying a growth or decay rate. The method relies on taking snapshots of data $\mathbf{X}_k$ from a dynamical system along the time scale t_k where k= 1,2,3,...,n. With DMD analysis, the nonlinear problem can be represented by linear dynamics $\mathbf{X}_{k+1}$=$\mathbf{A}\mathbf{X}_k$, where A is chosen such that it minimizes $||\mathbf{X}_{k+1}$-$\mathbf{A}\mathbf{X}_k||$ where k = 1,2,3,...,n-1 and n denotes the number of snapshots. The primary function of DMD is to resolve the low-rank structures in complex systems. Usage of DMD is also associated with predicting the future dynamic model using the previously derived dominant spatiotemporal structures.

Mathematical Background and Architecture

The dynamic system can be represented as :

$$\frac{dX}{dt} = \mathrm{f}(X, t; \eta) \tag{2.14}$$

where $\mathbf{X}(t) \in \mathbb{R}^n$ is the state of the system at time t,η represents the variables in the system and function f denotes the dynamic function. In this context $\mathbf{X}$ can be a multidimensional vector derived from the computation of a complex system or can be a measure of pixel values in a given frame or a snapshot of a video stream. The evolution of $\mathbf{X}$ during $\Delta\mathbf{t}$,denoted by $\mathbf{F}$ is given by:

$$X_{k+1} = F(X_k) \tag{2.15}$$

A solution to the non-linear system of eqn.2.14 is not possible. This is where an equation-free numerical solution comes to the aid, and the same can be used to predict the future states.

Only the data measurements are used to approximate the dynamics. Therefore with those measurements, DMD produces a liner dynamical system

$$\frac{dX}{dt} = \alpha X \tag{2.16}$$

The solution to (2.16) with initial condition X(0) is:

$$X(t) = \sum_{k=1}^{n} \phi_k \exp(\omega_k t) b_k = \phi \exp(\omega_t) b \tag{2.17}$$

where ϕ_k and ω_k are eigenvectors and eigenvalues of the matrix α, and the coefficients b_k are the coordinates of X(0) in the eigenvector basis.

The DMD Algorithm

1. The Singular Value Decomposition(SVD) of X is,

$$X \approx U\Sigma V^* \tag{2.18}$$

   where V^* denotes the complex conjugate of V and U $\in \mathbb{C}^{n*r}$, $\Sigma \in \mathbb{C}^{r*r}$, V $\in \mathbb{C}^{m*r}$ and r is the rank of the reduced SVD approximation to X; also $U*U = I$ and $V*V = I$.

2. From X, that we have obtained from SVD, the matrix A can be formed by:

$$A = X'V\Sigma^{-1}U^* \tag{2.19}$$

   The r*r projection of full matrix A onto DMD modes is given by:

$$\tilde{A} = U^*AU = U^*X'V\Sigma^{-1} \tag{2.20}$$

3. Next the eigen vectors and eigen values of $\tilde{A}$ are found by:

$$\tilde{A}W = W\Lambda \tag{2.21}$$

   where eigen vectors are represented by the columns of W and eigen values λ_k by the diagonal matrix Λ. The loarithmic mapping of the eigen values λ_k gives the amplitude $(Re(\lambda_k)/\Delta t)$ and frequency $(Im(\lambda_k)/\Delta t)$.

4. With the values of eigen vectors and eigen values from (2.21) the eigen value decomposition of the original matrix A can be found by:

$$\phi = X'V\Sigma^{-1}W \tag{2.22}$$

The modes obtained form (2.22) are called the DMD modes. With the eigen values and vectors obtained from low rank approximation we can reconstruct the future time step as given by:

$$x(t) \approx \sum_{k=1}^{r} \phi_k \exp(\omega_k) b_k = \phi \exp(\Omega t) b, \tag{2.23}$$

where $\omega_k = \ln(\lambda_k)/\Delta t$ and b_k is the initial amplitude of each mode. i.e for time $t_1 = 0$, equation (2.23) gives $x_1 = \phi$ b

2.5 Experimental conditions an-overview

Table2.3 shows an overview of the experimental conditions for the studies in single component system, binary component system and co-axial injection. In single component system, the fluoroketone jet is injected into its own vapour environment whereas in binary component system studies, the fluoroketone is injected to chamber with different composition of nitrogen and fluoroketone. In co-axial studies, the another co-flow gas is injected along with fluoroketone jet into the fluorketone vapour environment. For all the cases, the temperature of the chamber is always maintained at supercritical condition with respect to the fluoroketone jet. Studies are conduected for different chamber pressure and injecting conditions of the jet.

Table 2.3: Experimental Conditions

Study	Working Fluids	Chamber Temperature	Chamber Pressure	Chapter
Single component system	Fk	supercritical	subcritical to supercritical	Chapter 3
Binary component system	Fk, N_2, He	supercritical	subcritical to supercritical	Chapter 4

Chapter 3

Single component system

In this chapter, experiments were carried out for single component system i.e, the injecting jet is injected into its own vapour. The effect of the chamber pressure and thermodynamic properties of the injecting jet on the instability nature and mixing characteristics were studied. Axis-symmetric linear instability analysis is performed to derive further insight from jet characteristics caused by the flow and fluid properties. Dynamic Mode Decomposition is employed to extract different instability modes of the flow.

3.1 Effect of chamber pressure

Single component studies were conducted by injecting the liquid jet into its own medium as the chamber environment. The desired chamber pressure was obtained by introducing a sufficient amount of fluoroketone into the heated chamber. The required chamber condition was achieved prior to the injection of the fluoroketone jet. The term subcritical or supercritical conditions were referenced with respect to the critical conditions of injectant fluid, fluoroketone. The experimental conditions are detailed in the table.3.1.a.

Fig.3.1 shows the behaviour of a subcritical fluoroketone jet injected into its own environment at varying chamber pressure from subcritical to supercritical conditions. The liquid jet was observed to exhibit classical atomizing behaviour with the formation of instabilities on the jet surface which eventually leads to the droplet formation. The droplet size decreased as the chamber pressure was increased. The mixing of the jet into the chamber medium was observed to occur at chamber pressure P_r=0.95 as in fig.3.1.e. Also the jet was observed to appear like a turbulent gaseous jet at near-critical chamber conditions. There are hardly any observations in the literature that a liquid jet undergoes a thermodynamic transition at a pressure less than its critical pressure. In the studies conducted by Guang et al. (2011), the authors reported that when a liquid jet or drop at atmospheric temperature is

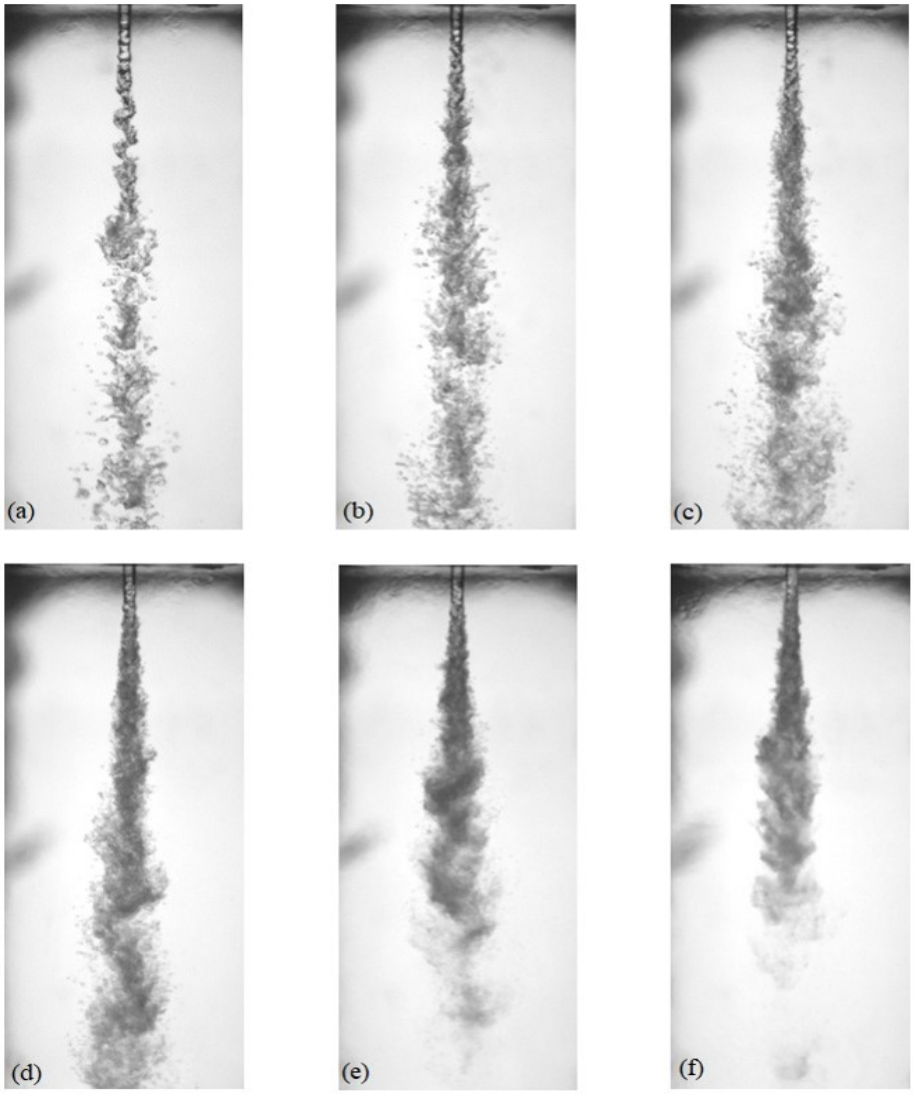

Figure 3.1: Subcritical fluoroketone jet injected into its own environment at different chamber pressures (subcritical to super-critical) and at fixed supercritical temperature of 475K (T_r=1.07).Reduced chamber pressure (P_r=$P_{chamber}$/$P_{critical}$)= 0.718(a), 0.761(b), 0.819(c), 0.862(d), 0.95(e), 1.01(f) and injection Re = 1333(a), 1293(b), 1452(c), 1492(d), 1492(e), 1512(f).

Table 3.1: Experimental Conditions

Sl No	Chamber Environment	Reduced Injection Temperature $T_i = \frac{T_{injection}}{T_{critical}}$	Reduced Chamber Temperature $T_r = \frac{T_{chamber}}{T_{critical}}$	Reduced Chamber Pressure $P_r = \frac{P_{chamber}}{P_{critical}}$	Injection Reynolds Number Re_i
(a)	Fluoroketone	0.68-0.93	1.07	0.5 - 1.09	497 - 14000

injected into a gaseous environment at high temperature, evaporation takes place at rapid jet velocities. Images were taken using a long-distance microscope to visualize the jet surface more closely and to identify the possibility of formation of finer drops near the jet surface at high subcritical conditions and Re. Fig.3.2 shows the zoomed-in images of the liquid jet at high subcritical chamber conditions. It is clear from fig.3.2 (a) that the liquid jet does exhibit the presence of surface tension with the formation of very small droplets near its surface. In fig.3.2 (b) drop formations with distinct interface is not observed. It was observed that before the drop forms and gets ejected from the jet surface, it starts vaporizing. At high Re, the breakup of the liquid jet due to the formation of turbulent eddies caused the liquid jet surface to bulge the jet. At high turbulent intensities, droplets are formed from these bulges. Tseng et al. (1992) proposed the relation for the characteristic time for the separation of these bulges that form in the jet and eventually lead to the formation of drops. The author proposed that the characteristic timescale is inversely proportional to the square root of surface tension. Hence, as the pressure approaches critical condition, and with the surface tension decreasing, the characteristic time for the separation of the bulges increases. When the chamber pressure was increased beyond the critical pressure of the fluid, the jet was observed to have a thermodynamic transition at all injecting Re.

3.2 Effect of injection Reynolds Number

Fig.3.3 shows the injection of fluoroketone into its own environment at chamber pressure around 17 bar (P_r = 0.92) at varying Re. At Re=875, the liquid jet is laminar up to a few diameters downstream as seen in fig.3.3(a) and there could be a significant increase in temperature of the jet, thereby resulting in a decrease in surface tension. This decrease in surface tension and aerodynamic drag due to heavy dense ambient fluid resulted in shorter wavelength disturbances on the laminar jet which resulted in the breakup of the liquid jet with very fine droplets. As the Re of the injected jet was increased as in fig3.3, it was observed

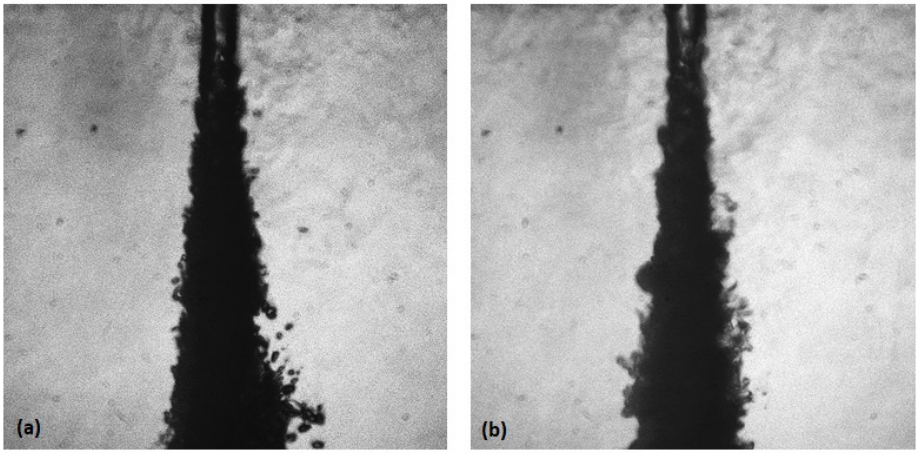

Figure 3.2: Zoomed in images of fluoroketone injected into its own environment with chamber at high subcritical pressure and fixed supercritical chamber temperature of 475K (T_r=1.07). P_r=$P_{chamber}$/$P_{critical}$= 0.925(a), 0.97(b) and injection Re = 1742(a), 1552(b). The field of view is 10mmx12mm.

that the coarse features at the surface of the jet (fig.3.3.a) transitioned to finer ones (fig.3.3.b). At Re= 1044, the jet undergoes vaporization and gets mixed with the environment at around 30 jet diameters downstream (fig.3.3(b)). When the Re was further increased to 1989 as in fig.3.3(d), the jet appeared like a turbulent gaseous jet. The jet was not observed to get mixed with the ambient environment as in the case of lower Re.

When the chamber pressure was increased to a very high subcritical condition as shown in fig.3.4, the jet was observed to behave like a turbulent gaseous jet. Due to the higher aerodynamic drag, the jet gets disintegrated rapidly. At Re above 1000, the jet was not observed to have any drop formation.

When the chamber pressure was increased beyond the critical pressure of the fluid, the jet was observed to have a thermodynamic transition at all injecting Re as observed in fig.3.5. In many previous studies, the liquid jet injected into the supercritical medium was observed to behave like a supercritical jet instantly. This is primarily due to high injecting Re. At high injecting Re (fig 3.5 d), the injectant jet is turbulent and is more prone to interfacial disturbances which grow rapidly and expedite the thermodynamic transition to the ambient medium. At low injecting Re, the jet didn't break up instantly as it enters the chamber (fig 3.5.a and b) because of the comparatively less aerodynamic drag. Similar observations were reported in the experiments by Muthukumaran and Vaidyanathan (2016*a*). In their study, the subcritical circular liquid jet exhibited a distinct interface for a few jet diameters downstream at its supercritical environment. Dahms and Oefelein (2013) also reported that the interface may exhibit the presence of finite surface tension and it never attains critical

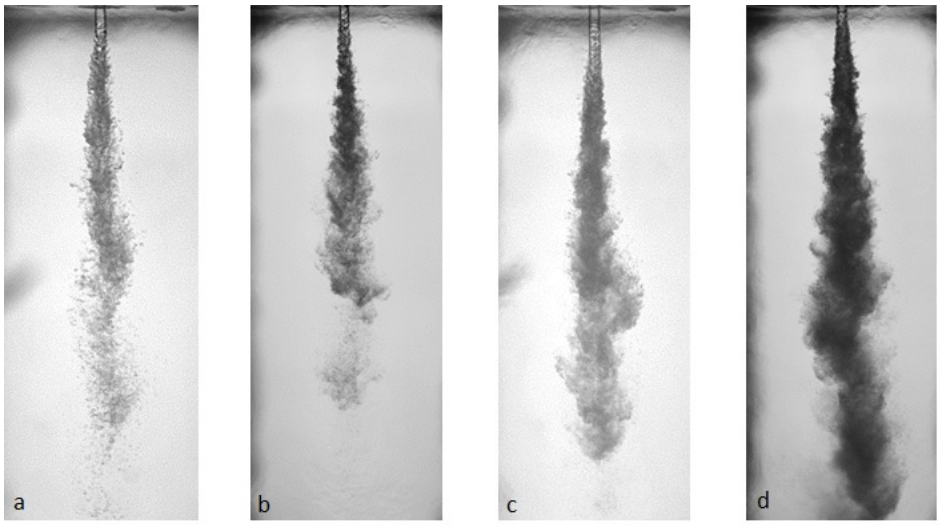

Figure 3.3: Fluoroketone injected into its own environemnt with chamber at subcritical pressure and fixed supercritical chamber temperature of 475K (T_r=1.07). from left to right chamber pressure P_r=$P_{chamber}$/$P_{critical}$= 0.92(a), 0.93(b), 0.92(c), 0.92(d) and injection Re_i = 875(a), 1044(b), 1452(c), 1989(d).

condition instantly as the jet enters into a supercritical environment. The observations are in excellent agreement with the studies carried out by various researchers in the past few decades. The initial divergence angle (α_d) is directly related to the rate of mixing of the jet into the environment. The higher divergence angle indicates faster mixing. It can be noted from fig.3.5(d), at Re=3316, that the jet divergence angle is more as compared to those at other lower Re. This increasing trend in divergence angle indicates faster mixing of the jet into the chamber environment. This is due to the increased aerodynamic drag acting on the jet at higher Re. Chehroudi, Cohn and Talley (2002) was the first to quantitatively measure the jet spreading angle using the images obtained from a cryogenic N_2 jet injected into gaseous N_2 under both subcritical and supercritical pressures. The initial divergence angle of the jet was measured at the jet exit and these were compared with the divergence angle of other mixing layer flows. The results were in good agreement with the theory of incompressible but variable density gaseous mixing layers.

3.3 Effect of Injecting Temperature

Experiments associated with the single-component system were carried out by injecting a circular fluoroketone jet into its own environment. The temperature of the incoming jet is varied from 300K (0.68) to 410K (0.93) by preheating the liquid jet using a liquid heater. The properties of fluoroketone at various conditions are obtained from NIST data.

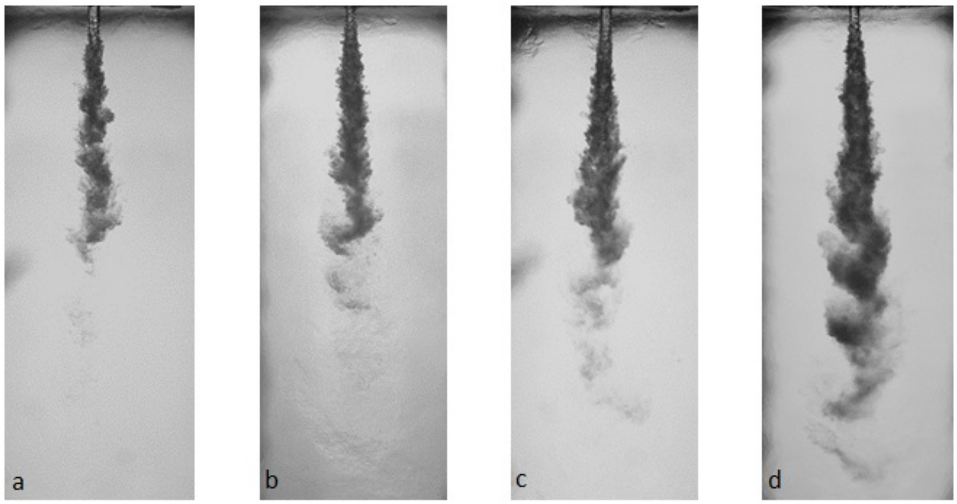

Figure 3.4: Fluoroketone injected into its own environemnt with chamber at high subcritical pressure and fixed supercritical chamber temperature of 475K (T_r=1.07). from left to right chamber pressure P_r=$P_{chamber}$/$P_{critical}$= 0.96(a), 0.97(b), 0.97(c), 0.96(d) and injection Re = 796(a), 1061(b), 1631(c), 1807(d).

Fig.3.6. shows the effect of preheating on the behaviour of a circular fluoroketone jet injected into its own environment with chamber pressure maintained around 12.2 bar (P_r=0.66) and chamber temperature at 470K (T_r=1.07). When the liquid jet at room temperature was injected into the chamber as shown in fig.3.6.a, the jet was observed to develop disturbances on its surface at a few jet diameters downstream. The non-dimensionalized undisturbed length 'l_b' (i.e,$l_b = l/d$ the distance from jet orifice till the onset of instability) was 4 and the non-dimensionalized disturbance wavelength (λ_d=λ/d) was 1, where λ is the disturbance wavelength measured from the figure and d is the jet diameter. As the temperature of the injecting liquid was increased to 338K by preheating the liquid as in fig.3.6.b, it was observed that both the undisturbed length and disturbance wavelength decrease to 2 and 0.6 respectively. When the temperature of the jet was further increased to its near-critical temperature (T_i=0.93), the jet was observed to exhibit faster mixing as evident from fig.3.6.d. It is evident from fig.3.6 that, the undisturbed length and disturbance wavelength decreases as the temperature of the injecting jet increases. Similar observations were earlier reported by Chen (1994) and Roy and Segal (2010). Their studies showed that the spray penetration length decreased as the temperature of the jet increased. This decrease in penetration was attributed to the decrease in density of the jet with an increase in temperature. In addition to the decrease in density of the injectant, there will be a significant reduction in surface tension and viscosity of the liquid as a result of heating. Fig.3.7,3.8 shows the variation in Re and We with respect to temperature for m=1.3g/s and P=13bar. This along with intense

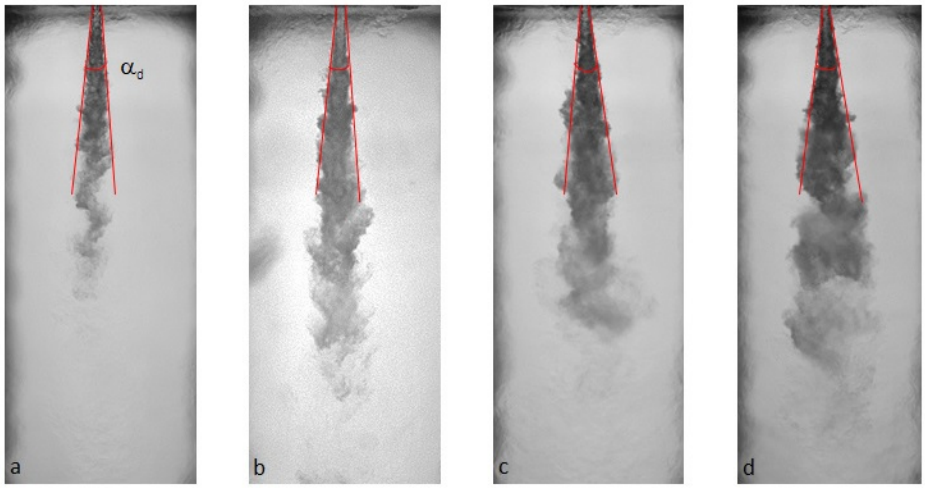

Figure 3.5: Fluoroketone injected into its won environment with chamber at supercritical pressure and fixed supercritical chamber temperature of 475K (T_r=1.07). from left to right chamber pressure P_r=$P_{chamber}$/$P_{critical}$= 1.04(a), 1.04(b), 1.03(c), 1.04(d) and injection Re = 1061(a), 1512(b), 2321(c), 3316(d)

interaction of the ambient medium makes the fluid more vulnerable to the disturbances and the jet atomizes more rapidly.

Fig.3.9,3.10 shows the injection of fluoroketone jet into its own environment at high sub-critical (near critical) chamber pressure around 18 bar (P_r=0.96) and super-critical condition with P_r=1.06 and at chamber temperature of 470K (T_r=1.07). In these cases also, the jet was observed to have a decrease in undisturbed length as the temperature of the injected jet was increased. Also, faster mixing was observed when the injectant temperature is near the critical temperature of the jet as evident from fig.3.9.d. It is to be noted from fig.3.6.d, 3.9.d and 3.10.d that the liquid jet mixed with the ambient medium when the injectant temperature condition is near to its individual critical condition. Similar results were also reported in the past Kurschat et al. (1992); Simões-Moreira et al. (2002). With near-critical values of injection temperature, the surface tension coefficient decreases rapidly to zero as the jet interface temperature approaches the critical temperature. This decrease in surface tension helps in faster disintegration of the jet and thereby leading to faster mixing of the jet into the chamber environment.

3.3.1 Axis-symmetric Instability Analysis

The dispersion relation was solved numerically for different injecting mass flow rates and chamber pressures. The temperature of the chamber was kept constant at 470K. Therefore each chamber pressure corresponds to a unique density ratio Q. The properties of the

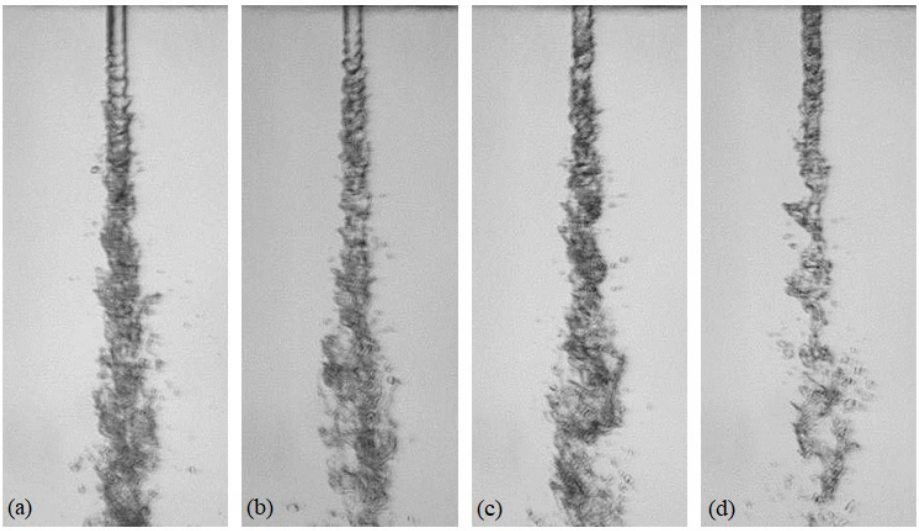

Figure 3.6: Fluoroketone injected into its own environemnt with chamber at subcritical pressure P_r=0.66 and fixed supercritical chamber temperature of 475K (T_r=1.07). from left to right injecting temperature of fluoroketone T_i= 0.68(a), 0.77(b), 0.825(c), 0.93(d); injection mass flow rate ($\dot{m}$)=1.5(a), 1.2(b), 1.38(c), 1.35(d); injection Re = 2780(a), 3747(b), 6212(c), 13033(d); and injection We = 703(a), 648(b), 1236(c), 3651(d)

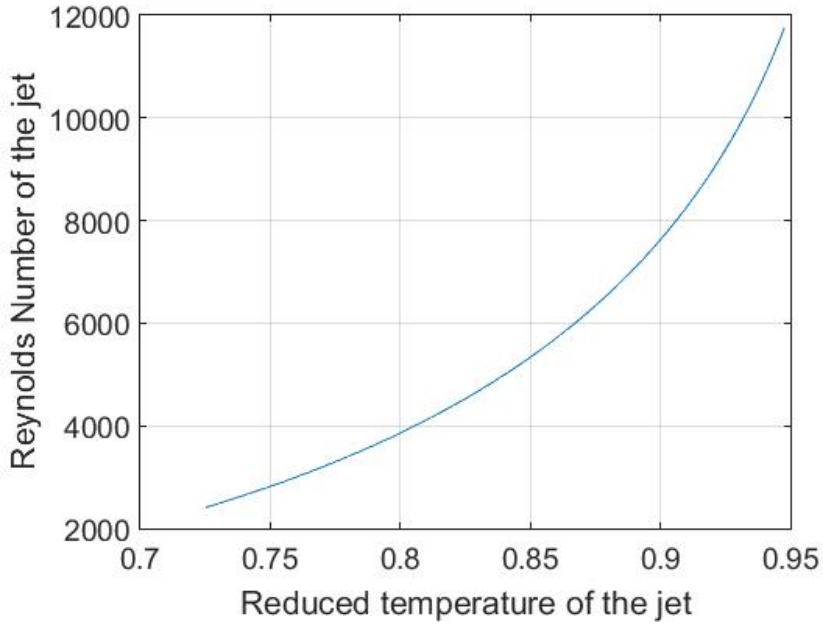

Figure 3.7: Variation of Reynolds Number of the jet at different injecting Temperature at pressure P=13bar

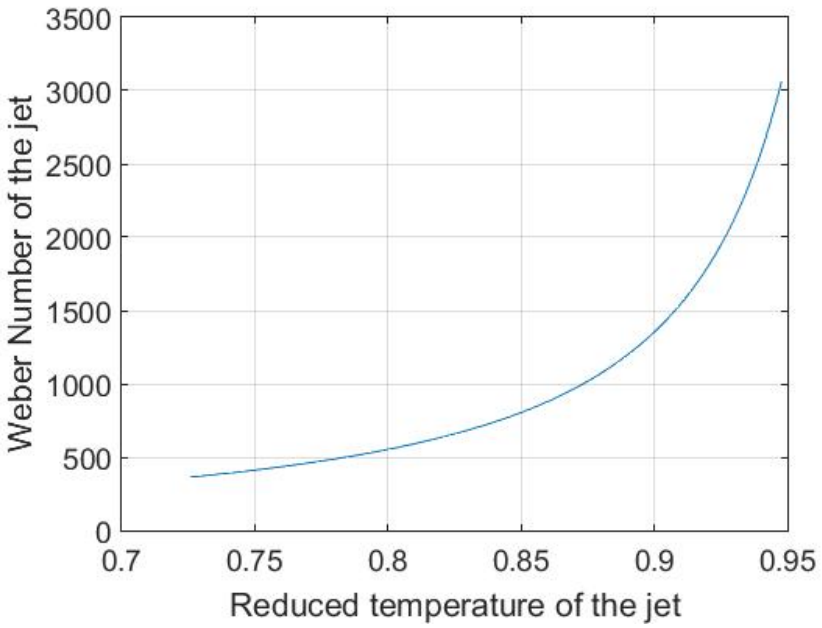

Figure 3.8: Variation of Weber Number of the jet at different injecting Temperature at pressure P=13bar

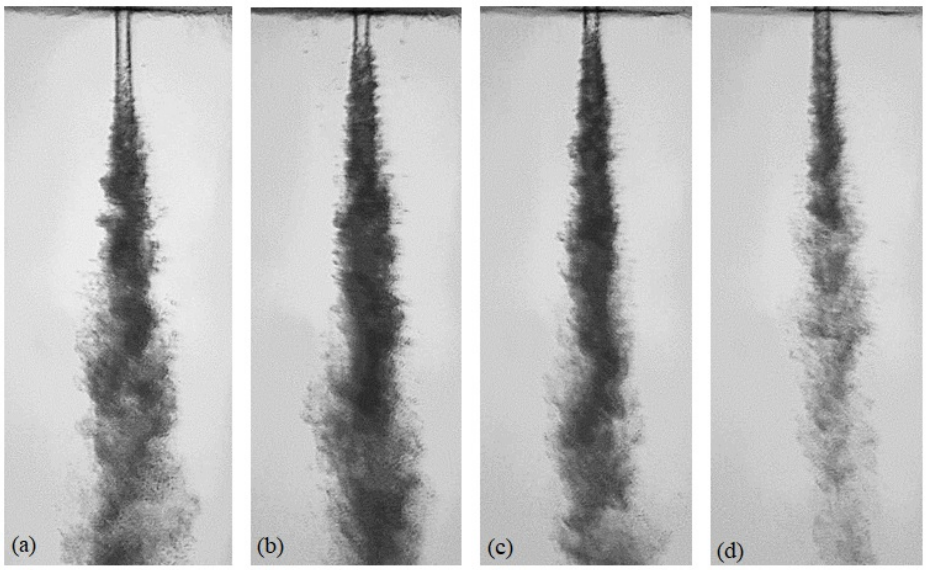

Figure 3.9: Fluoroketone injected into its own environemnt with chamber at high subcritical pressure P_r=0.96 and fixed supercritical chamber temperature of 475K (T_r=1.07). from left to right injecting temperature of fluoroketone T_i= 0.68(a), 0.77(b), 0.825(c), 0.93(d); injection mass flow rate ($\dot{m}$)=1.35(a), 1.33(b), 1.27(c), 1.27(d); injection Re = 2389(a), 4314(b), 5667(c), 14683(d); and injection We = 538(a), 815(b), 1078(c), 5628(d)

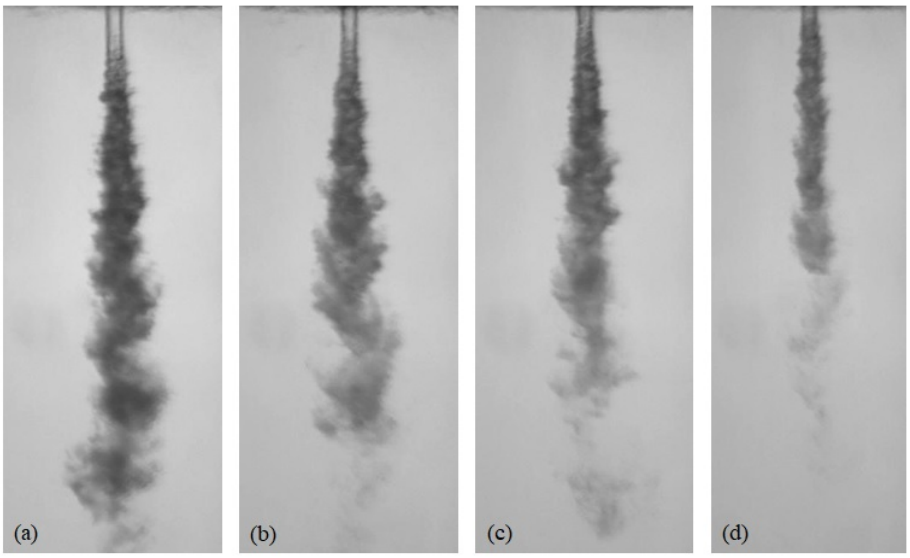

Figure 3.10: Fluoroketone injected into its own environemnt with chamber at supercritical pressure P_r=1.06 and fixed supercritical chamber temperature of 475K (T_r=1.07). from left to right injecting temperature of fluoroketone T_i= 0.68(a), 0.77(b), 0.825(c), 0.93(d); injection mass flow rate ($\dot{m}$)=0.74(a), 0.74(b), 0.83(c), 0.8(d); injection Re = 1301(a), 2357(b), 3684(c), 7089(d); and injection We = 162(a), 257(b), 460(c), 1294(d)

fluoroketone fluid at different conditions were obtained from the NIST database. The resulting disturbance wavelength with respect to the injecting mass flow rate was plotted for each chamber condition as shown in fig.3.11. The non-dimensional disturbance wavelength is obtained from the wave number k_i. It can be observed from fig.3.11 that, at low injecting mass flow rate $\dot{m}$=0.5 g/s, the disturbance wavelength is very much dependent on the density ratio of the fluid. At Q=0.0463, the disturbance wavelength is approximately $\sim$1.45, whereas, for Q=0.1613, the disturbance wavelength is near to 0.5. As the injecting mass flow rate increases, the effect of the density ratio on the disturbance wavelength decreases. At $\dot{m}$=1.5 g/s, the disturbance wavelength is almost 0.2-0.3 for all the density ratios in the range 0.0463$<$Q$<$0.1347. This is mainly due to the effect of an increase in the inertia of the liquid jet at a higher injecting mass flow rate. The shorter wavelength disturbance is more dominant at a higher injecting mass flow rate or higher density ratio.

The instability analysis was also performed to study the effect of preheating of the injected liquid jet. Fig.3.12 shows the variation in disturbance wavelength for various mass flow rates and at different injection temperatures of the jet. The results obtained were congruous with the experimental observations in the previous section. The disturbance wavelength reduced considerably when the temperature of the injecting jet was increased and could lead to better atomization and mixing of the liquid jets in the chamber environment.

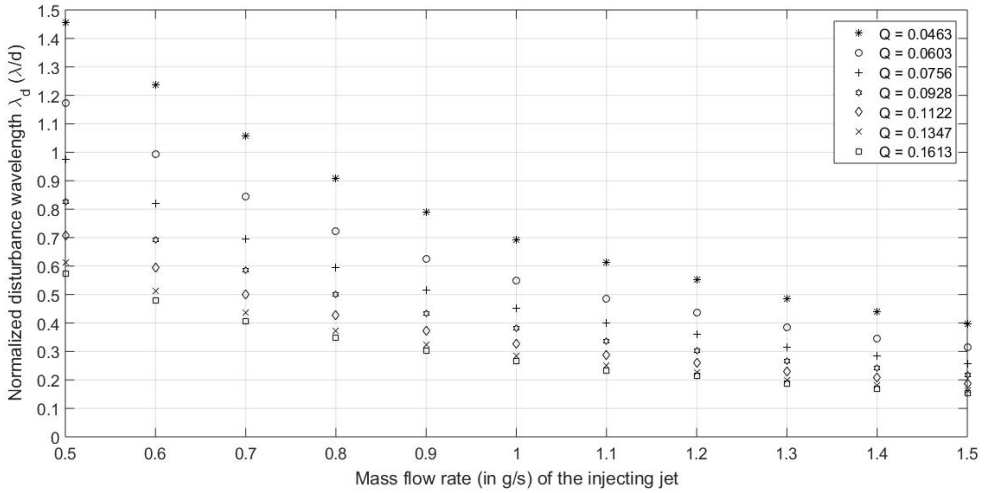

Figure 3.11: Variation of normalized disturbance wavelength with injection mass flow rate for different density ratios

3.4 Dynamic Mode Decomposition

Fig.3.13 represents the high-speed shadowgraphy images of a subcritical circular liquid jet at Re_i=1637 injected into a chamber at subcritical chamber pressure P_r=0.47 and supercritical temperature T_r=1.07. The jet was observed to develop disturbances on its surface after a few jet diameters from the jet orifice which is explicitly marked as ovals in fig.3.13 The effect of chamber density was not high enough to destabilize the inertia of the jet to completely atomize the jet. Hardly any droplet formation was observed in this condition. The instability waves developed on the jet surface in fig.3.13 grow in amplitude and propagate only in the downstream direction which indicates that the instabilities are convective in nature.

The shadowgraphy images provide only very limited information on the jet dynamics and they do not quantitatively provide detailed insight into the prevalent perturbation dynamics. Also, it is very difficult to extract the characteristics of the disturbances developed on the liquid jets as a result of interaction with the ambient medium. For this reason, dynamic mode decomposition was applied, which is very effective in detecting and extracting the relevant dynamic features of the flow. Dynamic mode decomposition (DMD) was applied to the image-based flow visualization of a circular liquid jet, that is injected into a quiescent medium and the corresponding DMD modes obtained are shown in fig.3.14 and 3.15; it also shows the amplitude(growth/decay rate) versus frequency for the same.

The major observable feature of the modes was a set of uniformly spaced black and white patterns as seen in fig.3.14 b-e. These patterns represent the travelling waves or the instabilities formed on the jet surface. Their wavelengths can be estimated by directly

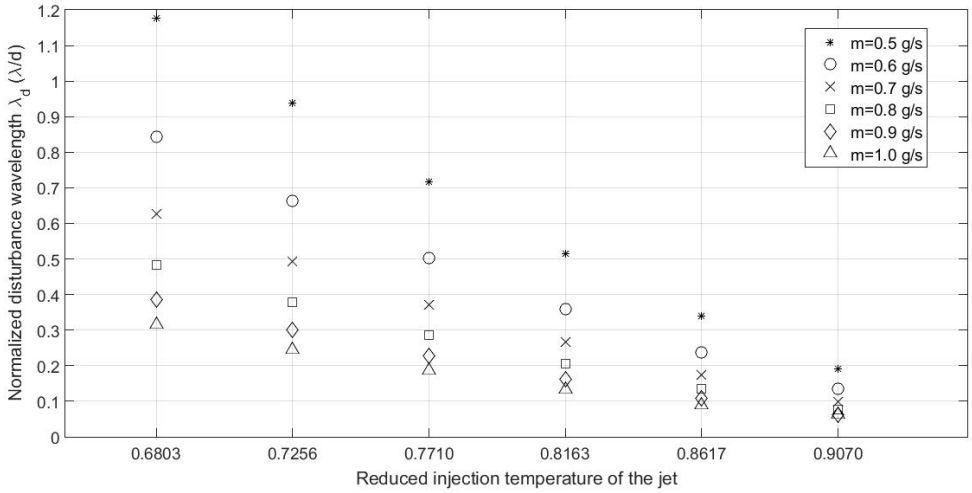

Figure 3.12: Variation of normalized disturbance wavelength for preheated jet for different mass flow rate when chamber is at subcritical condition P_r=0.54

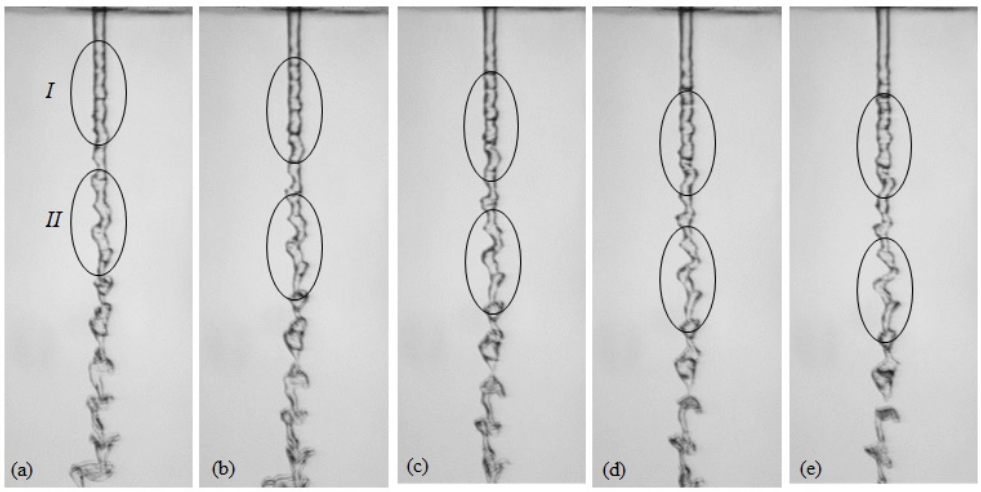

Figure 3.13: High speed shadowgraphy images of subcritical liquid jet at Re_i=1637 and We=236 injected to chamber at P_r=0.47, T_i=0.68, T_r=1.07 and Q=0.05. Time of acquisition of images (a)-(e)=0μs, 1321μs, 2624μs, 3963μs, 5284μs, 6605μs.

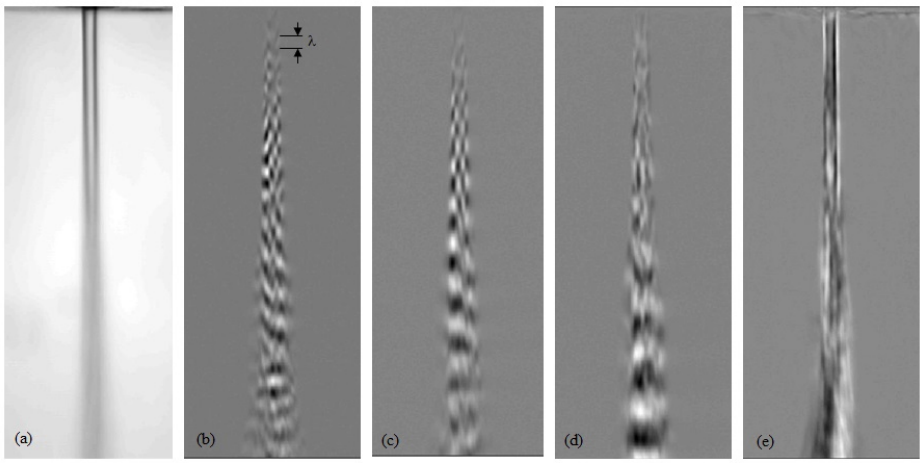

Figure 3.14: DMD modes of flow corresponding to fig.3.13

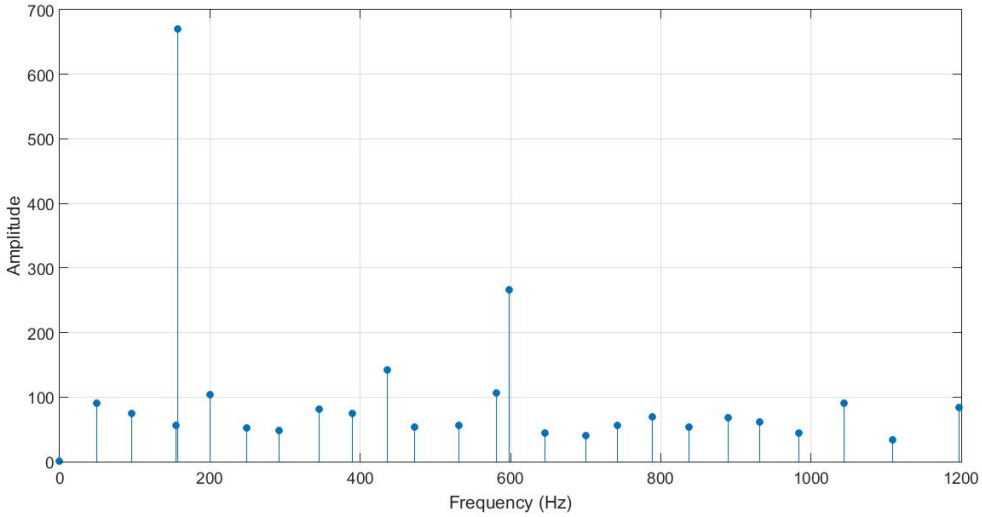

Figure 3.15: Amplitude vs ferquency plot for fig.3.13

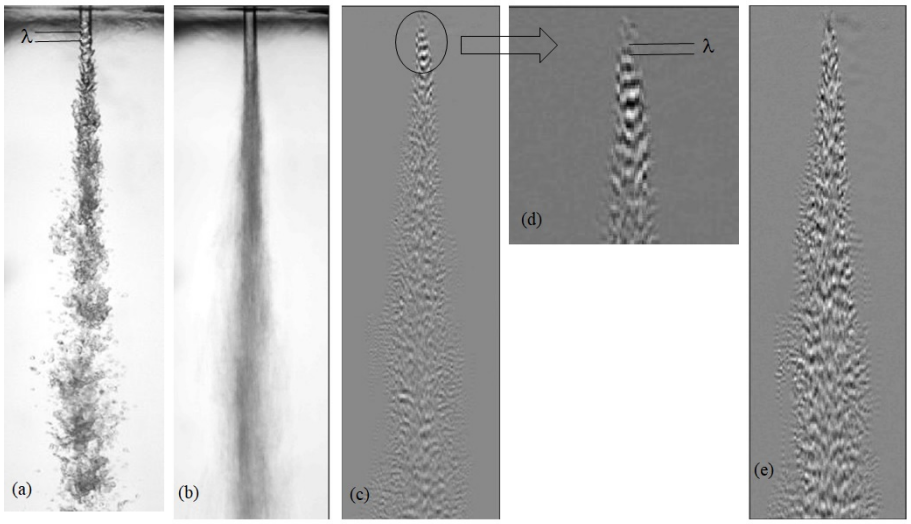

Figure 3.16: Shadowgraphy image (a) and DMD modes(b-e) for the condition P_r=0.77,T_r=1.07,T_i=0.68, Re=1169, We=125

counting the pixels between the consecutive peaks. The mode corresponding to the highest amplitude in fig.3.15 corresponds to the mode in fig.3.14.b. Fig.3.14.a is the mean mode and fig.3.14.c-e correspond to other modes. It can be also noted in fig.3.13 that the instability waves are marked as *I* in fig.3.13.a is moving downstream in time. The mean mode is the mode that also corresponds to the average image obtained from all the image sequences. Since the instability in fig.3.13 is convective in nature, the position of perturbations continues to move downstream in time and space. When the average image is obtained, the moving perturbations will not be captured. This is the reason why the undisturbed length in mean mode is observed to be longer. The mean mode does not capture the dynamic features of the jet. The wider black and white patterns in the modes in fig.3.14 d and e correspond to the sinuous waves II shown in fig.3.13.

Fig. 3.15 shows the amplitude versus the frequency of the first 51 modes obtained from DMD analysis. The remaining modes were found to be noisy as seen in fig.3.14 (e), which contain small-scale structures, which typically span the entire flow domain. The frequency of the dominating mode (shown in fig.3.15) is 156.6Hz and its amplitude is nearly 6-7 times larger than the rest of the modes. The dynamic mode decomposition provides a more visual insight into the exploration of the nature of instabilities in a quantitative manner. The axisymmetric disturbance wavelength predicted from solving the dispersion relation is compared with the wavelength obtained from the DMD modes. It is interesting to observe that the wavelength of the dominating DMD mode is closer to the one obtained from solving dispersion relation. The non-dimensionalized wavelength obtained from solving dispersion

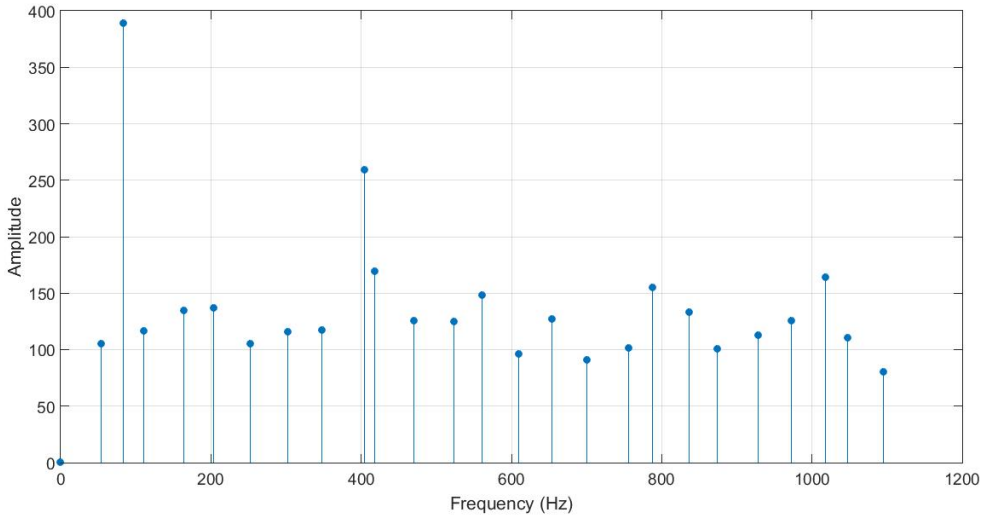

Figure 3.17: Amplitude vs ferquency plot for fig.3.16

relation was 0.47 whereas the wavelength obtained from the fringe pattern in the mode is 0.5±0.06.

Fig.3.16.a shows the shadowgraphy image and the dynamic modes (b-e) obtained for injection of a subcritical jet into a chamber which is maintained at pressure P_r=0.77 and T_r=1.07. With the increased chamber pressure, the drag acting on the jet is much higher as compared to that in the previous case (P_r=0.47). As a result of this, the jet was observed to have a shorter undisturbed length and the non-dimensionalized disturbance wavelength decreased from 0.5 to 0.4 as shown in fig.3.16. The energy (amplitude) versus the frequency of the first 51 modes is shown in fig.3.17. The frequency of the most dominant mode is 83Hz and the corresponding mode is shown in fig.3.16.c. The disturbance wavelength obtained by solving the dispersion relation at this condition was 0.38. The wavelength measured from the fringe patterns for mode 1 (zoomed-in view can be seen in fig.3.16.d) was 0.37±0.06 which was closer to that obtained from dispersion relation(=0.38).

The instability nature of circular jets at near-critical and supercritical chamber conditions were also analysed using DMD and the resulting dynamic modes are shown in fig.3.18,3.20 and 3.22 and the corresponding amplitude versus frequency plots are shown in fig.3.19,3.21, and 3.23. As seen in the previous cases, the overall structural appearance of the mean mode is almost similar to the actual jet. Since the mean mode is free from any disturbances, the unmixed or undisturbed length can be measured from the mean mode more accurately than from the shadowgraphy image. The black and white fringe patterns with short-wavelength disturbances observed in the DMD modes in fig.3.20(c) and 3.22 (c) near to the jet orifice

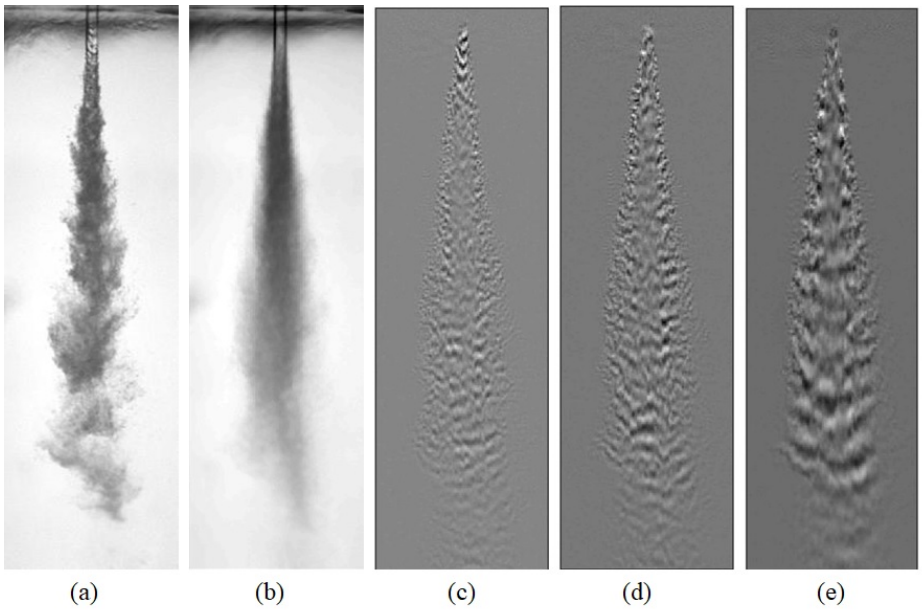

Figure 3.18: Shadowgraphy image (a) and DMD modes (b-e) for the condition P_r=0.924,T_r=1.07,T_i=0.68, Re=1313, We=157

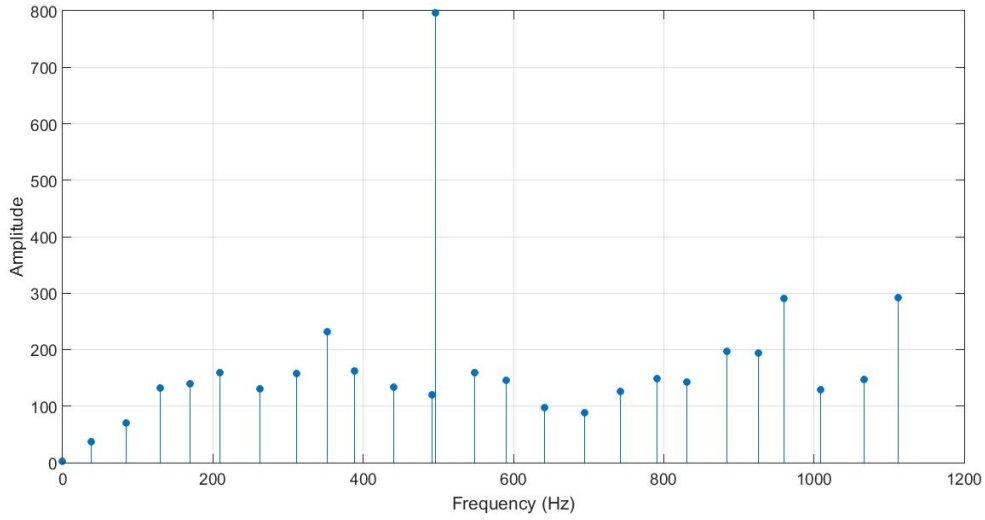

Figure 3.19: Amplitude vs ferquency plot for fig.3.18

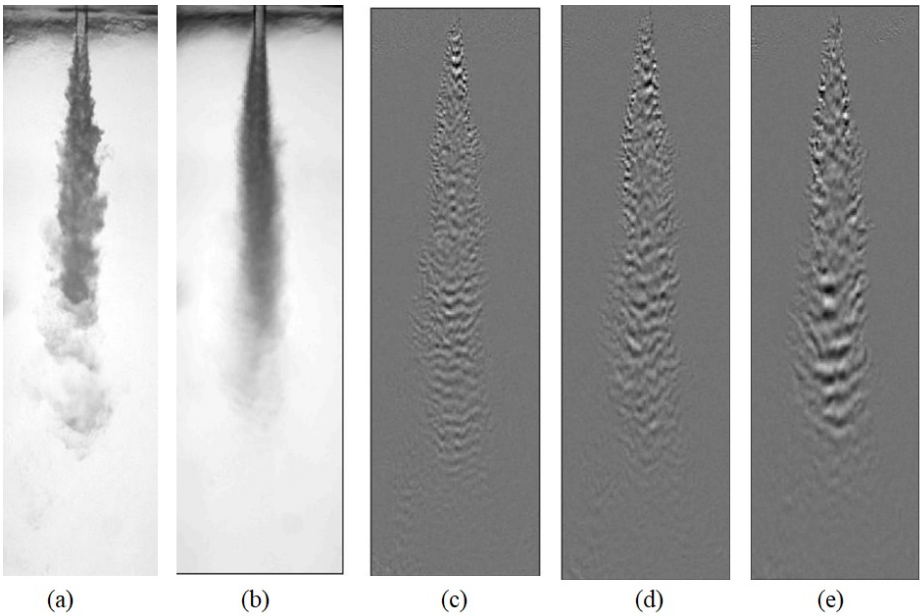

Figure 3.20: Shadowgraphy image (a) and DMD modes(b-e) for the condition P_r=1.01,T_r=1.07,T_i=0.68, Re=1313, We=157

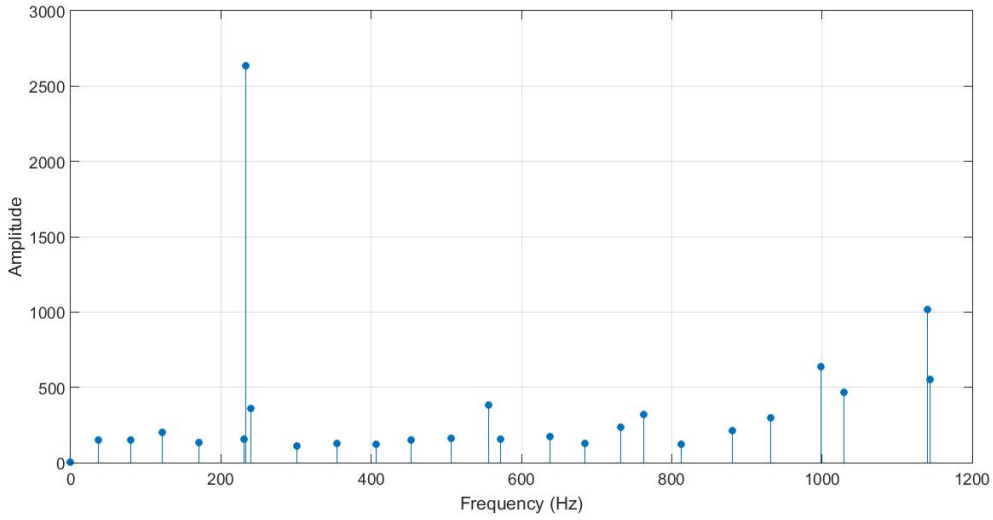

Figure 3.21: Amplitude vs ferquency plot for fig.3.20

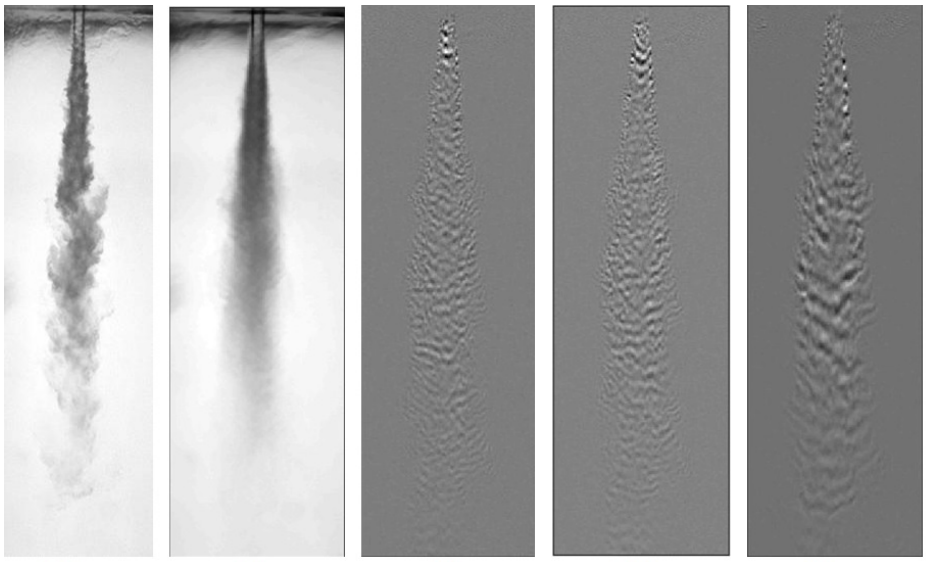

Figure 3.22: Shadowgraphy image (a) and DMD modes(b-e) for the condition P_r=1.05,T_r=1.07,T_i=0.68, Re 1300, We 150

indicate that the subcritical liquid jet when injected into a supercritical environment does not undergo transition immediately as it enters the chamber.

It can be observed that as the intensity of the atomization increases, the amplitude of the modes also increases. The amplitude of the modes for the condition P_r=0.77 is lower as compared to the case where P_r=0.47. This may be attributed to the fact that the instability of the flow for these two conditions is different in nature. The instability nature for P_r=0.47 is convective with hardly any jet breakup whereas for the other cases the instability nature is absolute and the jet completely atomizes after a few jet diameters downstream. The influence of the instability modes on the amplitudes and frequency of the modes have to be explored in detail to derive further insight.

Table 3.2 shows the comparison of the disturbance wavelength obtained by solving dispersion relation and also from DMD modes. For sub-critical chamber conditions, the wavelength obtained from solving the dispersion relation was in close agreement with the wavelengths obtained from DMD modes. But at near-critical and super-critical chamber conditions, the wavelengths obtained from the two different analyses are found to be different. At super-critical chamber conditions, the liquid jet gets heated rapidly and results in a significant reduction in surface tension. Therefore the actual Weber number of the jet will be larger than the respective value at the injection conditions. Hence, the wavelength obtained from instability analysis is higher as compared to the ones obtained from DMD analysis at

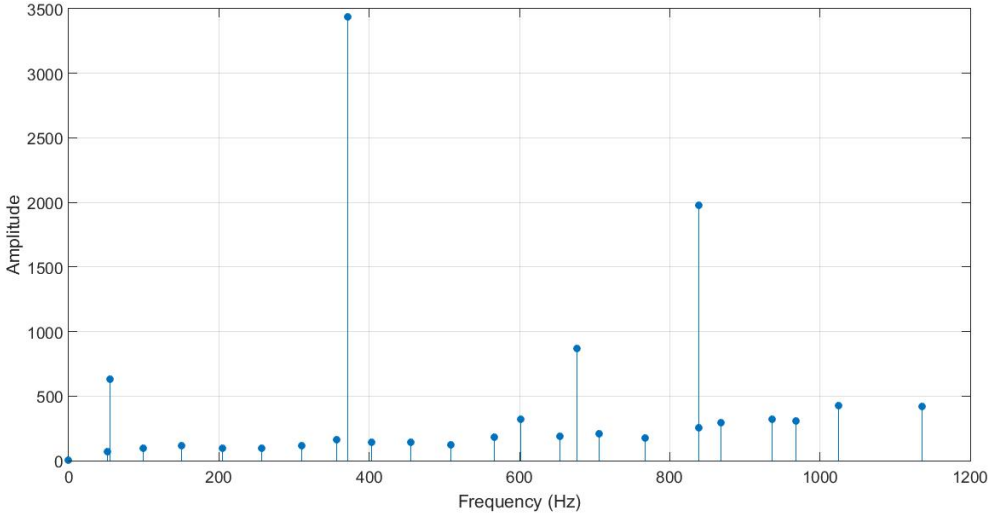

Figure 3.23: Amplitude vs ferquency plot for fig.3.22

Table 3.2: Comparision of wavelength from DMD and dispersion relation

Chamber Pressure P_r	λ_{disp}	λ_{dmd}	Main Observations
0.47	0.47	0.5±.0.06	• continous fringes shows the liquid jet do not atomize completely • wavelength of dominant mode close to the wavelength obtained from dispersion relation.
0.77	0.3845	0.37±0.06	• alternate fringes dissappear after few jet diameters downstream; indicates complete atmozization of liquid jet • wavelength of dominant mode close to the wavelength obtained from dispersion relation.
0.925	0.278	0.21±0.06	• growth rate (amplitude) increases with atomization
1.005	0.266	0.22±0.06	• no specific pattern observed, may be due to the faster thermodynamic transition into supercritical state • difference in wavelenth obtained from dispersion and DMD analysis; attributed to decrease in surface tension
1.05	0.2415	0.18±0.06	• No specific pattern observed, may be due to the faster thermodynamic transition into supercritical state • difference in wavelenth obtained from dispersion and DMD analysis; attributed to decrease in surface tension

near-critical and super-critical chamber conditions. Similar observations were also reported by Muthukumaran and Vaidyanathan (2016*a*). In cases and conditions where the fluid and flow properties are not distinctly accessible, DMD methodology is employable to find the dominant mode and the instability wavelength as obtained in this study at supercritical conditions.

3.4.1 Pre-heated liquid jets

Dynamic mode decomposition(DMD) analysis was also carried out for pre-heated liquid jets. Fig.3.24 & fig.3.26 modes shows the dominant modes for the preheated jet at sub-critical and super-critical chamber conditions respectively. Fig.3.25 & fig.3.27 represent the energy vs frequency plot for the modes for sub-critical and super-critical conditions. For the pre-heated jet experiments, 200 images at 5297fps were used for the DMD analysis. It is observed from fig.3.25 & fig.3.27 that the maximum frequency of the DMD modes for both subcritical and super-critical chamber conditions is constant for all injecting conditions. Also, it can be observed that the energy of the modes highly depended on the injecting condition than the chamber pressure. It can be inferred that at high subcritical to super-critical chamber conditions, the behaviour of the fluids is significantly influenced by the thermodynamic properties of the injecting fluids than on the chamber conditions.

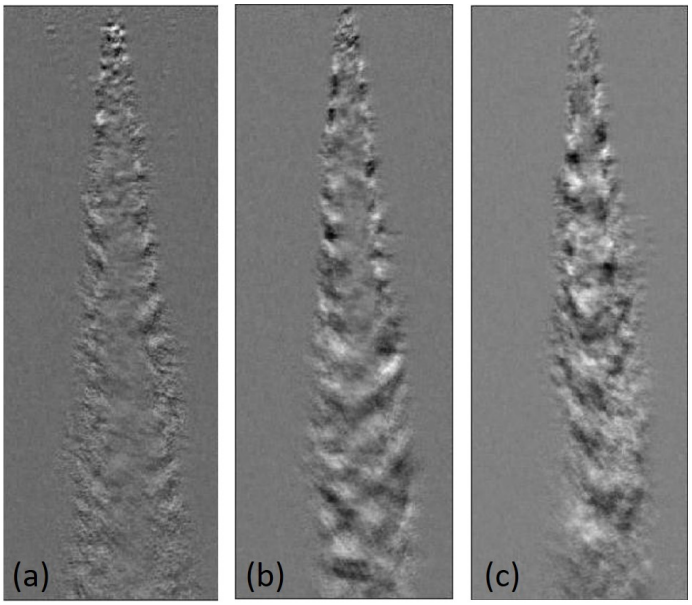

Figure 3.24: Dominant modes for Fluoroketone injected into its own environemnt with chamber at high subcritical pressure P_r=0.96 and fixed supercritical chamber temperature of 475K (T_r=1.07). from left to right injecting temperature of fluoroketone T_i= 0.77(a), 0.825(b), 0.93(c); injection mass flow rate ($\dot{m}$)= 1.33(a), 1.27(b), 1.27(c); injection Re = 4314(a), 5667(b), 14683(c); and injection We = 815(a), 1078(b), 5628(c).(Shadowgraphy images corresponding to fig.3.9)

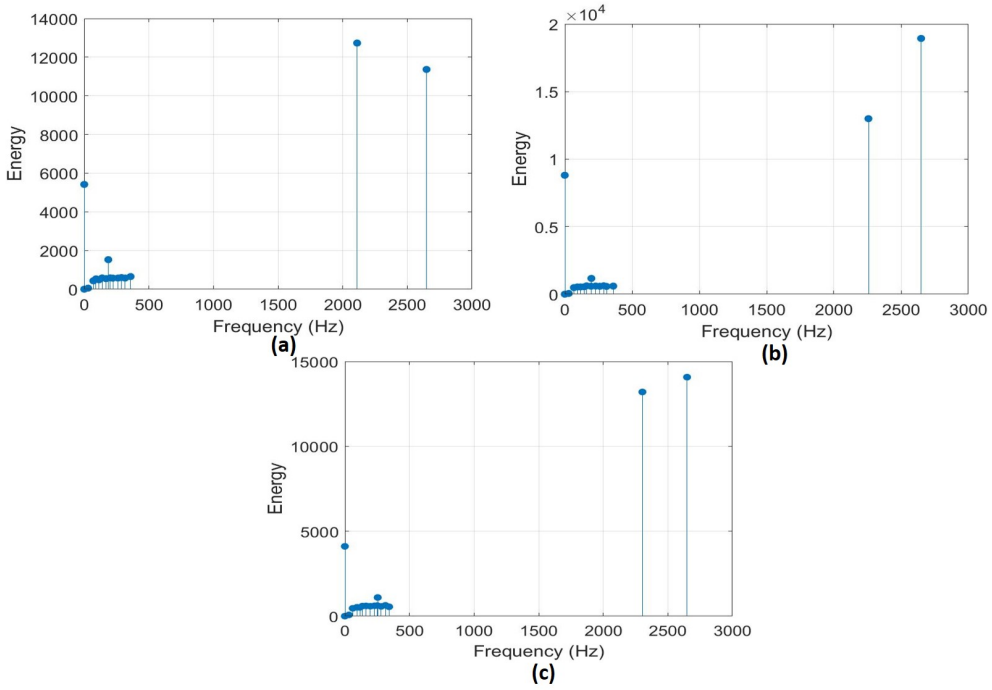

Figure 3.25: Energy vs frequency plots for the conditions shown in fig.3.24.a,b,c

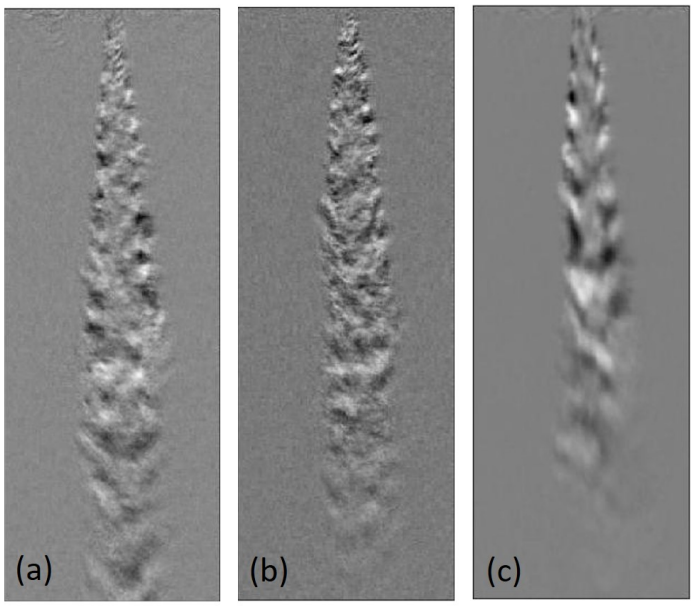

Figure 3.26: Dominant modes for Fluoroketone injected into its own environemnt with chamber at supercritical pressure P_r=1.06 and fixed supercritical chamber temperature of 475K (T_r=1.07). from left to right injecting temperature of fluoroketone T_i= 0.77(a), 0.825(b), 0.93(c); injection mass flow rate ($\dot{m}$)= 0.74(a), 0.83(b), 0.8(c); injection Re = 2357(a), 3684(b), 7089(c); and injection We = 257(a), 460(b), 1294(c).(Shadowgraphy images corresponding to fig.3.10)

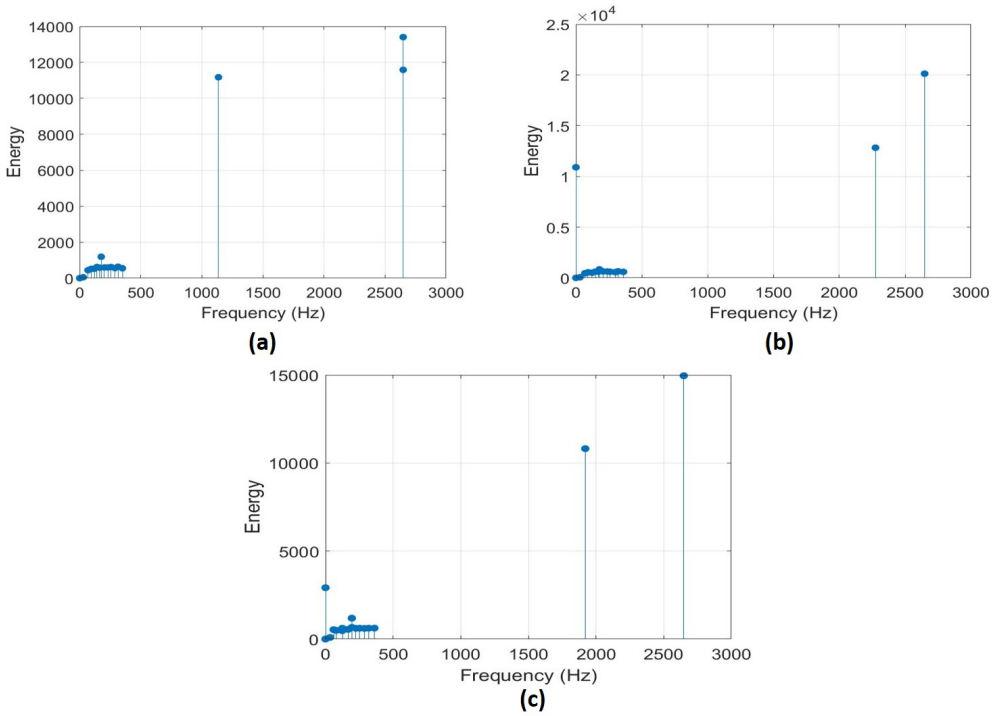

Figure 3.27: Energy vs frequency plots for the conditions shown in fig.3.26.a,b,c

Chapter 4

Binary Component system

In this chapter, experiments were carried out for binary component system; the objectives were to determine (i) the sufficient and necessary conditions for a liquid jet to undergo a thermodynamic transition to a super-critical state and also to understand (ii) the effect of different compositions of the fluids in the chamber environment (nitrogen-fluoroketone) on the behaviour of liquid jet, and (iii) the atomization and mixing behaviour of a co-axial jet when a relatively low-temperature, low-density gaseous fluid was introduced as a co-flow for a subcritical fluoroketone liquid jet at super-critical chamber conditions.

4.1 Effect of compositions of fluids in the chamber

The studies by Newman and Brzustowski (1971) revealed that the composition of gases in the environment significantly influences the behaviour of the liquid jet. It was evident from the previous studies that in a multi-component system, the ambient pressure conditions alone are not sufficient for the thermodynamic transition of the injected jet to take place. For example, the solubility of the gas phase in the liquid phase increases significantly at high pressure. This increase in solubility might lead to a newer critical pressure of the mixture, which may be either between the critical pressure of the pure phases of each component or it may be above the critical pressure of pure phases or, in other words, the critical point of a mixture of fluid depends on the composition of the fluids in which they are mixed. Hence, the main focus of the current section is to investigate the effect of the relative composition of fluids in the chamber environment on the behaviour of a circular liquid jet. Experiments were conducted by injecting subcritical fluoroketone jet into mixtures of Nitrogen and Fluoroketone that exist at a predetermined composition in the chamber. The experiments were conducted for varying injecting Reynolds numbers and at different compositions of fluoroketone and nitrogen in the chamber and are detailed in table 4.1.

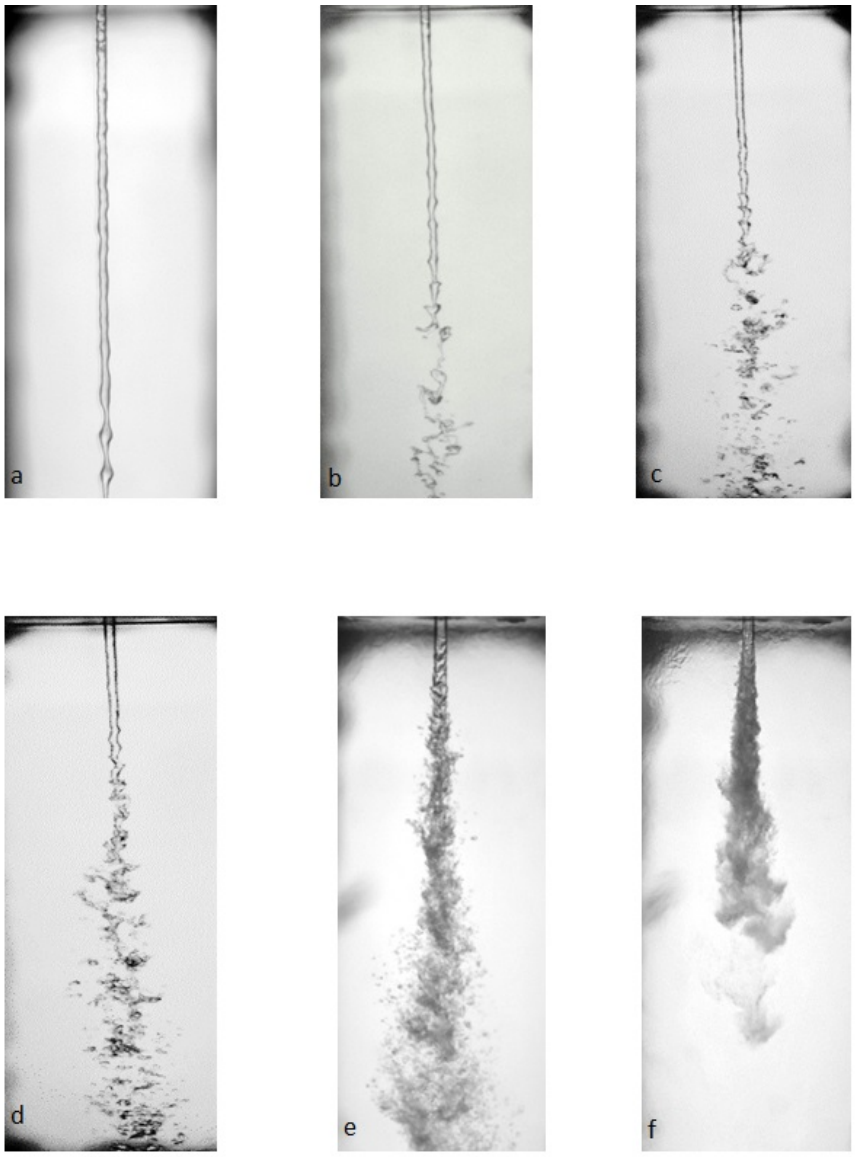

Figure 4.1: Subcritical fluoroketone jet injected into mixture of Nitrogen and Fluoroketone at different compositions with chamber at fixed supercritical chamber temperature of 475K (T_r=1.07). From (a)-(f): chamber composition (N_2:Fk) interms of mole fraction: 100% N_2(a), 3:2(b), 1:1(c), 2:3(d), 1:3(e), 100% Fk(f): Reduced chamber pressure (P_r=$P_{chamber}$/$P_{critical}$)= 1.085(a), 0.97(b), 1.01(c), 1.02(d), 1.01(e), 1.01(f) and injection Re = 1800(a), 1658(b), 1492(c), 1293(d), 1472(e), 1472(f).

Table 4.1: Experimental Conditions

Sl No	Chamber Environment	Reduced Injection Temperature $T_i = \frac{T_{injection}}{T_{critical}}$	Reduced Chamber Temperature $T_r = \frac{T_{chamber}}{T_{critical}}$	Reduced Chamber Pressure $P_r = \frac{P_{chamber}}{P_{critical}}$	Reduced Partial pressure of Fluoroketone $P_{Fk} = \frac{P_{Fluoroketone}}{P_{critical}}$	Injection Reynolds Number Re_i
(a)	N_2 - Fk ratio : 100% N_2, 3:2, 1:1, 2:3, 1:3	0.68	1.07	0.5 - 1.25	-	490 - 3700
(b)	N_2 - Fk mixture	0.68	1.07	0.5 - 1.25	0.282 - 1.03	490 - 3600

A mixture of nitrogen and fluoroketone was used as the ambient medium for conducting the experiments on the binary component system. Initially, a known quantity of nitrogen was injected into the chamber up to a known pressure. Then the fluoroketone was introduced to the chamber until the desired chamber pressure for the experimental condition was achieved. After the chamber environment was filled with the desired combination of nitrogen and fluoroketone, the fluoroketone jet was injected into the chamber, and the behaviour of the jet was closely monitored. The mole fraction of the individual species in the chamber environment was approximately estimated, $x_{Fk}=n_{Fk}/(n_{N_2}+n_{Fk})$, where x is the mole fraction, n is the number of moles which is calculated as the ratio of the mass of the respective fluid that was introduced into the chamber to the corresponding molecular mass of the fluid. Since the properties of the mixture at super-critical conditions are not fully understood, the aforementioned methodology based on mole fraction amounts to a first level estimate that represents the presence of the relative composition of each component in the mixture and also the relative distribution of each component in a combination of components known as the binary system. Since not many studies are available in the literature about the behaviour of the jet in a multi-fluid environment, it was decided to investigate the injected jet at different compositions (ratio of mole fraction of nitrogen to fluoroketone) of fluids in the chamber environment over a range of Re. The experimental conditions for the study of the binary component system are detailed in Table.4.1. It is to be noted that in the present chapter, the usage 'supercritical condition' means the chamber is at supercritical condition with respect to the injectant fluid.

When the chamber was filled with only nitrogen, the liquid fluoroketone jet was subjected to axisymmetric disturbances, which are longitudinal in nature. This is often referred to as the Rayleigh mode of instability, and the dominant disturbance is of longer wavelength as shown in fig.4.1.a. There was hardly any drop formation in a pure nitrogen environment. When fluoroketone was introduced into the nitrogen environment, the jet was observed to have changes in its behaviour. When the mole fraction ratio of nitrogen to fluoroketone

compositions in the environment approached 3:2 as in fig.4.1.b, the jet was observed to have Rayleigh mode of instability that had a relatively shorter wavelength for the dominant disturbance as compared to that of pure Nitrogen environment (fig.4.1.a). The undisturbed length (i.e. distance from the orifice up to which the jet maintained its shape without any disturbance) of the jet also decreased, and drops of the size of the order of jet diameter were observed about 40 jet diameters downstream. The decrease in undisturbed length is due to the increased ambient density and aerodynamic shear of the environment because of the presence of Fluoroketone in the chamber environment. As the mole fraction ratio of the composition approached 1:1 in the chamber (fig.4.1.c), the undisturbed length decreased further, and the instability mode was no longer in the Rayleigh regime; also the drops formed in this condition were smaller as compared to the case of nitrogen to fluoroketone 3:2 (fig.4.1.b) composition case. When the nitrogen to fluoroketone mole fraction ratio was changed to 2:3 (fig.4.1.d) in the chamber, the screw-like or helical mode appeared on the jet surface. Here, it was observed that the breakup length of the jet reduced even at a lower Re than in the case of fig.4.1.d which indicated that the changes in the jet behaviour are dominated by the change in the composition of the fluids in the environment than the changes in Re. Ohnesorge (1936) in his studies also reported screw-like disturbances. With further increase in Fluoroketone composition in the chamber with N_2:Fk as 1:3 (fig.4.1.e), the breakup mode shifted to the Taylor regime with the presence of very fine droplets. In the Taylor regime, atomization or breakup occurred immediately as the jet emanated from the orifice. It is to be noted that when the chamber pressure was critical with respect to the injecting fluoroketone, the presence of another gas delays not only the thermodynamic transition but also it influences and alters the atomization regimes. When nitrogen gas was introduced into a single component system, with the increase in the percentage of nitrogen in the environment: a) the undisturbed length increases, b) the disturbance wavelength increases, c) droplet size increases and d)atomization regime changes. Woodward and Talley (1996) also reported similar observations in their experiment when they injected liquid N_2 into gaseous N_2 environment. At super-critical chamber conditions, the liquid N_2 was observed to behave like a turbulent gaseous jet. When Helium was introduced into the super-critical nitrogen environment, liquid structures with distinct interfaces started to reappear, which indicated the presence of surface tension at super-critical conditions. The authors proposed that this re-appearance of liquid structure in nitrogen-helium medium was because of the solubility of Helium in LN_2. In fig.4.1.e, it was observed that when the mole fraction ratio of nitrogen to fluoroketone mixture is 1:3, the behaviour of the jet is comparable with that of the single-component system. Hence keeping this composition fixed, the behaviour of the jet is studied at various chamber pressure with varying injecting Re and is correspondingly compared with the single-component case.

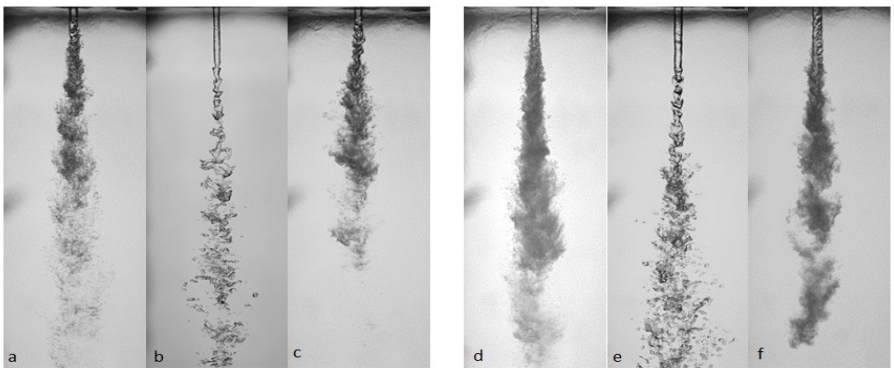

Figure 4.2: Comparision of single component system and binary component system at similar Re and chamber pressure.Fluoroketone jet injected into:(1) its own environment (a) and (d) ; (2) mixture of N_2-Fk environment at composition 1:3 (b),(c),(e) and (f). Reduced Chamber pressure P_r=$P_{chamber}$/$P_{critical}$= 0.92(a), 0.91(b), 1.09(c), 0.92(d), 0.92(e), 1.09(f) and injection Re = 890(a), 862(b), 980(c), 1452(d), 1492(e), 1492(f). Temperature of the chamber for all cases is 475K (T_r =1.07)

Effect of Partial Pressure

Fig.4.2 shows the comparison of the behaviour of subcritical fluoroketone jet in its own environment (fig.4.2.a and 4.2.d) and in Nitrogen-fluoroketone environment (fig.4.2.b, c, e and f). It is evident that at almost the same Re and chamber pressure, the behaviour of the injected jet is different in single and multi-component systems. From fig.4.2.c and 4.2.f, the behaviour of the jet was found to be similar to that of single-component system at similar Re (fig.4.2.a and 4.2.d) respectively. It was clear from the mole fraction composition studies that when the percentage of fluoroketone in the ambient increases, the liquid jet tends to behave as similar to that of a single component system. It is interesting to note that the partial pressure of fluoroketone in the chamber for a binary component system in fig.4.2.f is 0.937 and is nearly the same as the chamber pressure of fluoroketone in a single component system (fig.4.2.d). In other words, the individual partial pressure of the components in the chamber environment is adjudged to play a critical role in altering the behaviour of the jet in a multi-component system.

In this section, experiments that were carried out to study the effect of partial pressure of components in the environment on the behaviour of the injected liquid jet. The experiments were conducted for approximately the same injecting Reynolds number, and partial pressure of fluoroketone in the chamber environment was varied from its own subcritical to super-critical pressure by keeping the total pressure of the chamber nearly the same, which was always at a super-critical condition with respect to the injectant fluid. Initially, nitrogen was introduced into the chamber at a predetermined pressure; subsequently, fluoroketone was

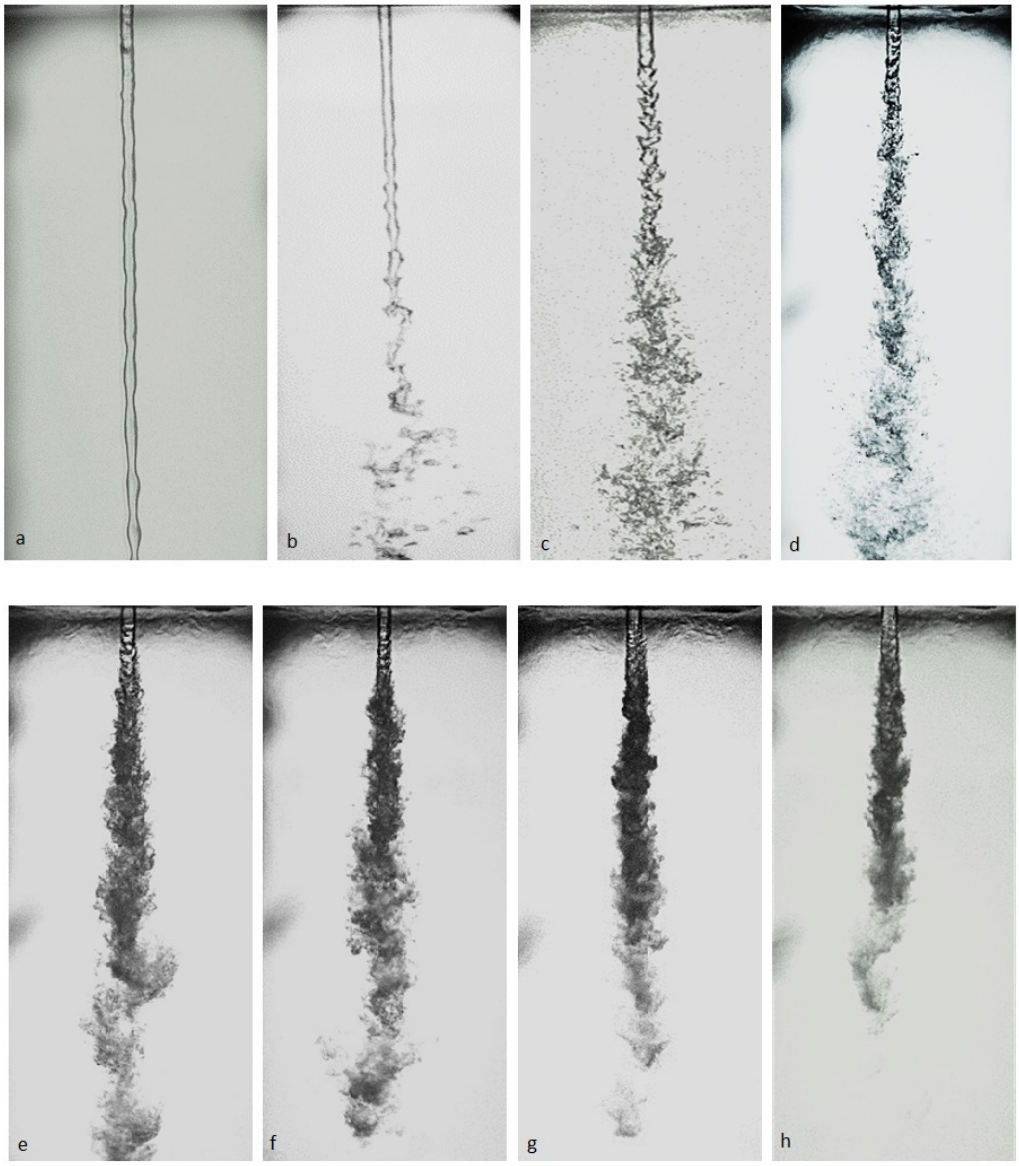

Figure 4.3: Fluoroketone jet injected into Nitrogen-fluoroketone mixture with chamber at supercritical pressure and fixed supercritical temperature of 475K (T_r=1.07) and varrying partial pressure of flouroketone in the chamber environment.From (a) - (h) Reduced Chamber pressure P_r=$P_{chamber}$/$P_{critical}$= 1.09(a), 1.05(b), 1.01(c), 1.01(d), 1.06(e), 1.07(f), 1.09(g), 1.17(h); Reduced partial pressure of fluoroketone in the chamber (P_{Fk}) = 0(a), 0.282(b), 0.558(c), 0.809(d), 0.90(e), 0.937(f), 1.01(g), 1.027(h) and injection Re = 1600(a), 1558(b), 1293(c), 1472(d), 1651(e), 1492(f), 1114(g), 1452(h)

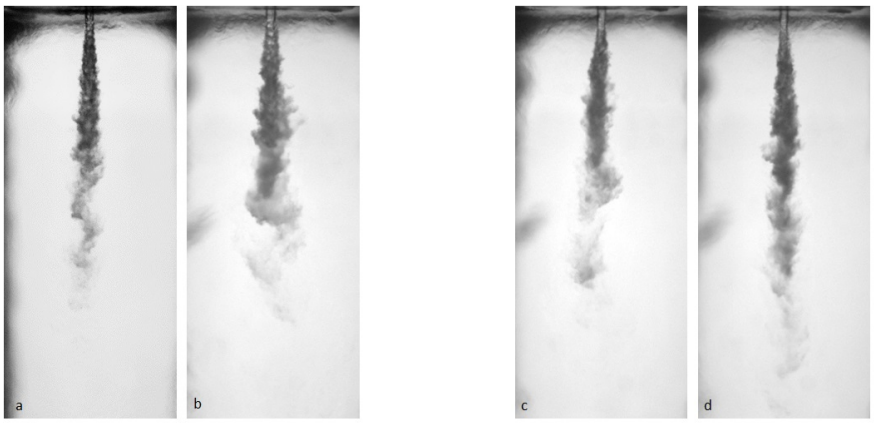

Figure 4.4: Fluoroketone injected to its own environment (a), (b) and Nitrogen-fluoroketone environment (c),(d), with the chamber at super-critical pressure and fixed super-critical temperature of 475K (T_r=1.07). Reduced chamber pressure P_r= 1.01(a), 1.02(b), 1.23(c), 1.18(d) ; Reduced partial pressure of fluoroketone in the chamber P_{Fk} = 1.02(c), 1.02(d) and injection Re = 1061(a), 1472(b), 1114(c), 1452(d)

Table 4.2: Fractal dimension results of single component and binary component system

Single Component System				Binary Component system				
P_r	Re	Fractal Dimension	Corresponding Image	P_r	P_{Fk}	Re	Fractal Dimension	Corresponding Image
1.01	1061	1.25	4.5.a	1.23	1.02	1114	1.25	4.5.c
1.02	1472	1.23	4.5.b	1.18	1.02	1452	1.28	4.5.d

added to the chamber environment. The mixture attains the required composition, and the components attain the required partial pressures for conducting the experiments.

When the subcritical liquid fluoroketone jet was injected into the pure Nitrogen medium at Re=1600 as in fig.4.3.a, the jet was observed to have Rayleigh mode of instability and was intact throughout the entire downstream distance without any drop formation. Here, the environment pressure and aerodynamic drag were insufficient to overcome the surface tension forces of the liquid jet. A similar observation was reported by Muthukumaran and Vaidyanathan (2016*a*). When fluoroketone was added to the chamber environment by keeping the total chamber pressure the same, the jet was observed to exhibit some changes in its behaviour as compared to the pure nitrogen environment. When the partial pressure of fluoroketone in the environment was around 5.3 bar (P_{Fk}=0.282) the jet was observed to exhibit Rayleigh instability (fig.4.3.b) with drop formation at around 20 jet diameters downstream distance and droplet size nearly of the order of jet diameter. When the partial

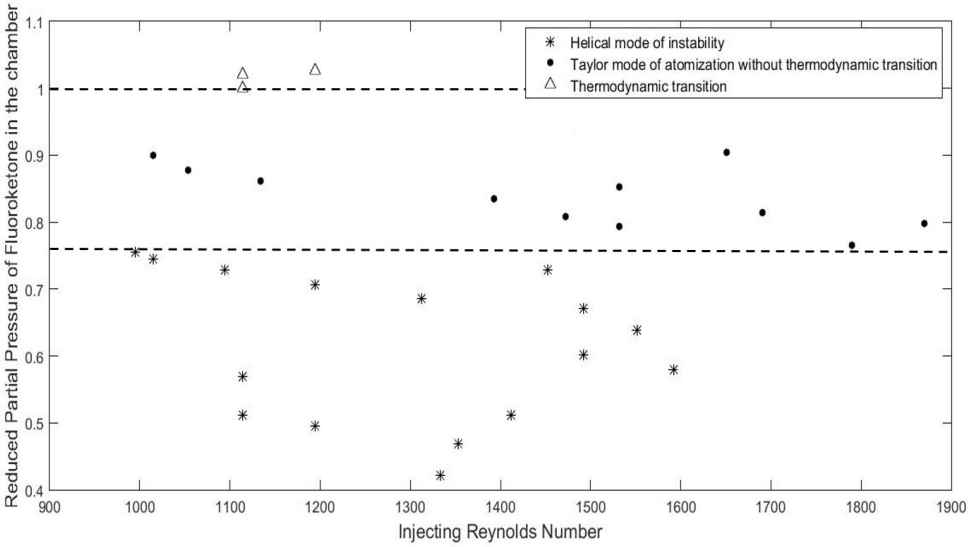

Figure 4.5: Various regimes of behavior of subcritical fluoroketone jet in a mixture of nitrogen-fluoroketone environemnt at fixed composition of 1:3.

pressure of fluoroketone was increased further to 10.5 bar (P_{Fk}=0.558) (fig.4.3.c), the jet is observed to have a wavy or screw-like mode of the asymmetric type of instability with very fine drops. The undisturbed length of fluoroketone liquid jet further decreased when the corresponding partial pressure was increased to P_{Fk}=0.809 as in fig.4.3.d. As the partial pressure of fluoroketone in the chamber environment is set at P_{Fk}=0.937 (fig.4.3.(f)), the jet was observed to have a phase change at far downstream distances. It was observed that when the partial pressure of the fluoroketone in the chamber environment is near to the critical pressure of fluoroketone, the injected jet exhibits features that are similar to those in the single-component system. The fluoroketone jet was observed to have a thermodynamic transition as in fig.4.3.g. The fluid jet behaved like a turbulent gaseous jet when the partial pressure of the fluoroketone in the environment exceeded its own individual critical pressure (fig.4.3.h). There was hardly any distinct visible interface downstream, thereby indicating the absence of surface tension forces. It is to be noted that in a single component system, the thermodynamic transition in super-critical chamber conditions occurs at a lower Re (fig.4.12.a) as compared to those in a binary component system (fig.4.3.g and 4.3.h).). The behaviour of the subcritical fluoroketone jet in a pure fluoroketone environment was compared with those in the nitrogen-fluoroketone environment as shown in fig.4.4. When the partial pressure of fluoroketone in the Nitrogen-fluoroketone environment reached its own critical pressure (fig.4.4.c and fig.4.4.d), the liquid jet was observed to exhibit thermodynamic transition. In a single-component system, at these injecting Re, the thermodynamic transition

occurred when the chamber pressure approached critical condition (fig.4.4.a and fig.4.4.c). The jet was observed to behave like a turbulent gaseous jet without any distinct interface. The fractal dimension of the injectant jet was obtained, and the details are provided in table.4.2. It was found that the fractal dimension is nearly 1.25 for all the cases in fig.4.4. This indicates that the interface features and mixing nature of the jet of a binary component system are similar to a single component system. This makes a clear indication that the necessary condition for a liquid jet to have a thermodynamic transition in a binary component system where one of the components in the medium is the same as the injectant fluid is that the partial pressure of the injectant fluid in the ambient medium must approach its individual critical condition.

Fig.4.5 shows the various regimes of the behaviour of the subcritical fluoroketone jet in a mixture of nitrogen-fluoroketone environment that is maintained at a fixed composition of 1:3. It can be noted that the changes in the behaviour of the jet are significantly influenced by the chamber conditions than the injecting conditions. The fluoroketone jet is observed to have a helical mode of instability till the partial pressure of fluoroketone in the chamber is in the range $0.4<P_{Fk}<0.78$. The Taylor mode of atomization is observed when the PFk is in the range $0.8<P_{Fk}<0.95$. The thermodynamic transition occurs when the partial pressure of the fluoroketone in the chamber approaches its individual critical condition (P_{Fk}=1).

4.2 Effect of injecting Reynolds Number

By keeping the overall composition of nitrogen to fluoroketone fixed at 1:3, experiments were conducted for the injection of liquid fluoroketone at subcritical temperature into the environment of Nitrogen-fluoroketone mixture at varying chamber pressure and injection Re (fig.4.6). It was observed that when the chamber pressure was near critical with respect to the injecting fluoroketone, at low Re=1194, the jet maintained its inherent structure up to around ten jet diameters downstream (fig.4.7.a) before it broke up into ligaments and droplets. The drops formed were slightly less than the order of jet diameter. The onset of instability is due to capillary pinching, and at low Re, the jet was observed to have a decrease in diameter as it moves downstream, which is due to the influence of gravity. This decreasing trend in jet diameter was not observed at higher Re. When the Re was increased to 1790 as in fig.4.6(b), the undisturbed length decreased to a few diameters, the droplet sizes are found to decrease, and there wass an increase in the number of droplets. The atomization regime at this Re was similar to the screw-like mode. As the Re was further increased to 1989, the undisturbed length reduced further (fig.4.6.(c). At this condition, the disturbance wavelength was found to be much shorter. When the Re was increased to Re=2321, the jet resembled the Taylor

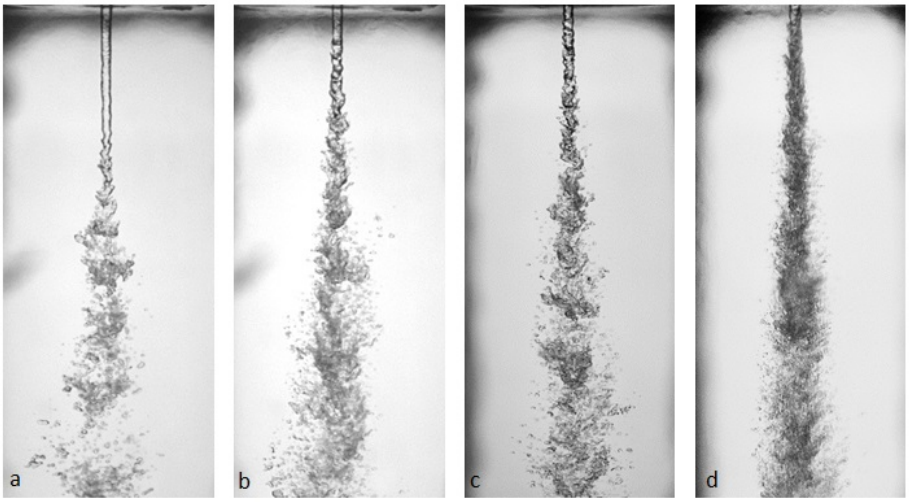

Figure 4.6: Fluoroketone jet injected into Nitrogen-fluoroketone mixture (mole fraction ratio 1:3) with chamber at high subcritical pressure and fixed supercritical temperature of 475K (T_r=1.07). Reduced Chamber pressure P_r=$P_{chamber}$/$P_{critical}$= 0.91(a), 0.95(b), 0.94(c), 0.97(d) and injection Re = 1194(a), 1790(b), 1989(c), 2321(d)

regime as in fig.4.6(d), with the jet breakup occurring just downstream of the orifice. At this regime, the droplets were very much finer, but there was no thermodynamic transition happening even for the finer droplets at the downstream locations.

Fig.4.7 shows the behaviour of the fluoroketone jet at chamber pressure that is around the critical pressure of the injectant fluoroketone. At Re=1532 (fig.4.7.a), the jet was observed to have an undisturbed length of a few diameters downstream before the formation of shorter wavelength disturbances which resulted in the breaking up of the jet. It was observed that as the Re was increased, the aerodynamic drag on the jet increased: (a) the undisturbed length decreased, (b) the number of drops formed increased, and (c) the divergence angle of the jet increased (fig.4.7.b, c, and d). The jet exhibited classical atomization and didn't exhibit any kind of vapourization or thermodynamic transition occurring even at high Re (fig.4.7.d), which indicated the presence of surface tension.

When the chamber pressure was further increased to high super-critical pressure (fig.4.8), the jets were observed to exhibit features similar to that of a single component system. At low injecting Re=829 (fig.4.8.a), the liquid jet was observed to develop instabilities leading to the formation of finer droplets. As the injecting Re was increased, there was no visible droplet formation, and the jet was observed to undergo mixing into the chamber environment. But it is very difficult to conclude whether the liquid jet undergoes thermodynamic transition at higher Re with these experiments. Studies by Segal and Polikhov (2008) observed the thermodynamic transition of fluoroketone jet into pure Nitrogen environment. The injecting

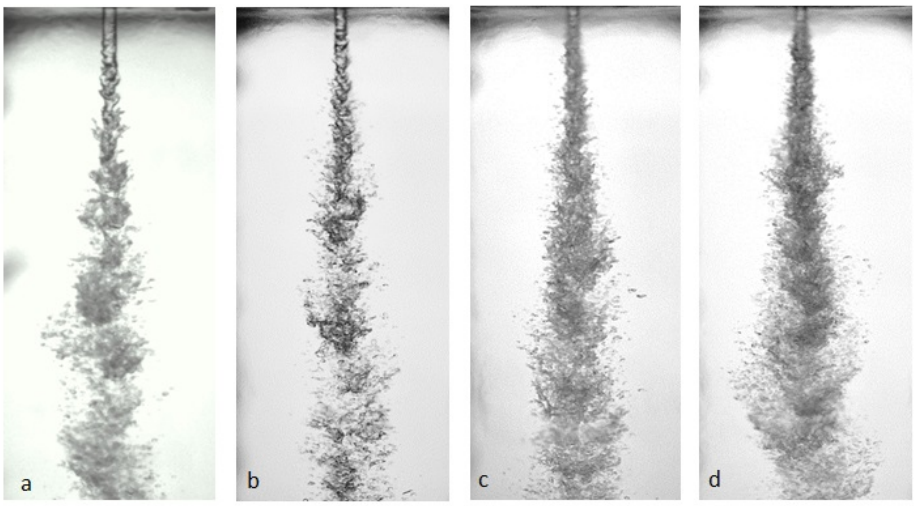

Figure 4.7: Fluoroketone jet injected into Nitrogen-fluoroketone mixture (mole fraction ratio 1:3) with chamber approximately at critical pressure and fixed supercritical temperature of 475K (T_r=1.07). Reduced Chamber pressure P_r=$P_{chamber}$/$P_{critical}$= 0.995(a), 0.995(b), 1.01(c), 1.02(d) and injection Re = 1532(a), 1823(b), 2155(c), 2818(d)

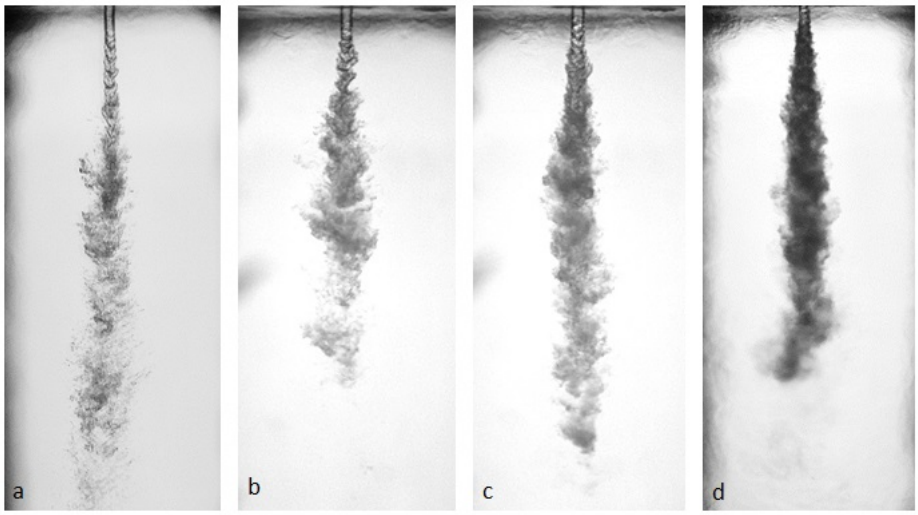

Figure 4.8: Fluoroketone jet injected into Nitrogen-fluoroketone mixture (mole fraction ratio 1:3) with chamber at supercritical pressure and fixed supercritical temperature of 475K (T_r=1.07). Reduced Chamber pressure P_r=$P_{chamber}$/$P_{critical}$= 1.09(a), 1.09(b), 1.09(c), 1.15(d) and injection Re = 829(a), 1015(b), 1492(c), 2487(d)

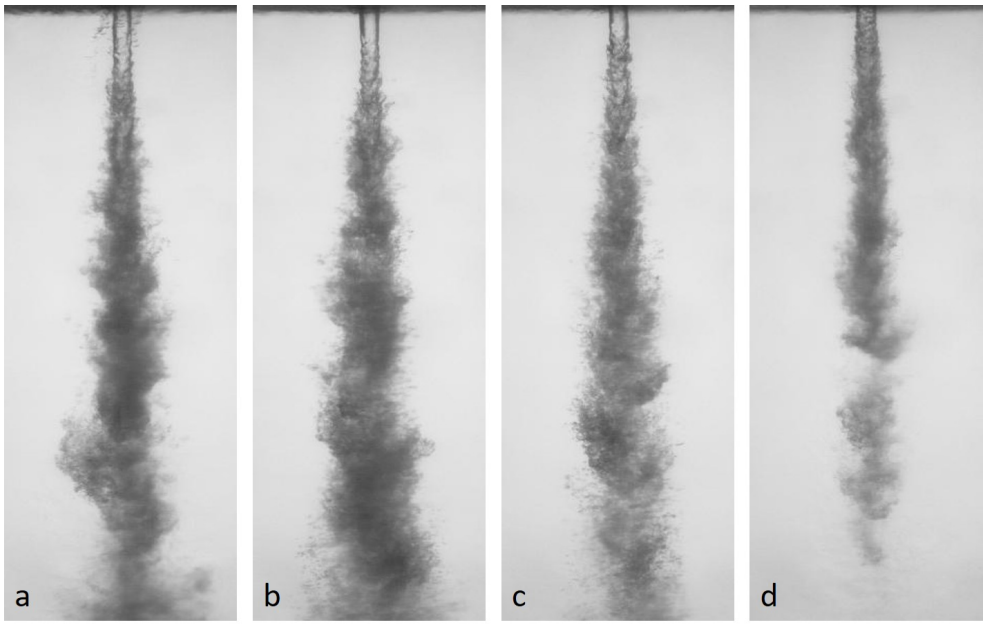

Figure 4.9: Fluoroketone jet injected into Nitrogen-fluoroketone mixture (mole fraction ratio 1:3) with chamber at supercritical pressure and fixed supercritical temperature of 475K (T_r=1.07). Reduced Chamber pressure P_r=$P_{chamber}$/$P_{critical}$= 1.05(a), 1.01(b), 1.01(c), 1.01(d) ; injection mass flow rate $\dot{m}$ *(g/s)* = 1.01 (a), 0.97(b), 0.97(c), 0.89(d) and Reduced injection temperature pressure T_i=$T_{injection}$/$T_{critical}$= 0.68(a), 0.734(b), 0.802(c), 0.85(d)

Reynolds number in their studies were very much higher compared to the experiments presented here.

4.3 Effect of injection temperature

To study the effect of injecting temperature on the jet behaviourt in a binary component system, experiments were conducted with preheated fluoroketone jet injected into the chamber mixed with nitrogen and fluoroketone. The results are shown in fig.4.9. With the increase in temperature of the injecting jet, the fluoroketone jet was observed to have a decreasing trend in the undisturbed length. The jet was observed to undergo faster mixing into the chamber medium when the injecting temperature of the fluoroketone was more than 350K (T_i >0.8), but it is very difficult to conclude on the thermodynamic transition of the jet.

4.4 Effect of Co-flow

For the co-axial experiments, an injector with an inner tube diameter of 1.5mm with a wall thickness of 0.5mm and length nearly 20mm is employed. Since the main objective of the study was to investigate the effect of the annular jet on the mixing behaviour, to reduce the shear force between the two fluids, no flare or step provision was included on the inner tube. The thickness of the annular region for Nitrogen gas is 0.5mm. A PHANTOM high-speed camera was used to acquire the jet images at 2500fps. Experiments were conducted to study the effect of a co-flowing fluid on the instability and the mixing nature of the fluoroketone jet into the chamber environment. The properties of fluoroketone and nitrogen at various conditions were obtained from NIST data. The details of the experimental conditions are detailed in table.4.3.

Table 4.3: Experimental Conditions for the co-axial experiments

Reduced Chamber pressure P_c	velocity of fluoroketone v_{fk} (m/s)	velocity of nitrogen v_{N_2} (m/s)	velocity ratio v_{N_2}/v_{fk}	mass flow rate of fluoroketone m_{fk} (g/s)	mass flow rate of nitrogen m_{N_2} (g/s)
1.06	0.4-0.90	0-60	0-100	1.1-2.5	0-3

4.4.1 Nitrogen co-flow

Figs.4.10 shows the effect of a co-flowing fluid on the behaviour of a subcritical fluoroketone jet injected into a chamber which was maintained at super-critical conditions. The velocity of the fluoroketone jet was maintained at around 0.4 m/s and the velocity of the co-flowing nitrogen jet was increased to observe its effect on the fluoroketone jet for different velocity ratios. When a sub-critical fluoroketone jet was injected into a chamber which was maintained at super-critical condition, in the absence of a co-flow, the liquid jet was observed to have a rapid thermodynamic transition to the super-critical chamber medium as observed in fig.4.10.a. The surface of the subcritical fluoroketone upon injection gets heated continuously

Table 4.4: Experimental Conditions for fig.4.10

Reduced Chamber pressure P_c	velocity of fluoroketone v_{fk} (m/s)	velocity of nitrogen v_{N_2} (m/s)	velocity ratio v_{N_2}/v_{fk}	mass flow rate of fluoroketone m_{fk} (g/s)	mass flow rate of nitrogen m_{N_2} (g/s)	coresponding figure
1.06	0.4±0.01	-	-	1.18	-	4.10.a
1.06	0.39±0.01	10.9±1	27	1.17	0.057	4.10.b
1.06	0.42±0.01	32±1	77	1.18	0.168	4.10.c
1.06	0.41±0.01	40.3±1	98	1.17	0.211	4.10.d

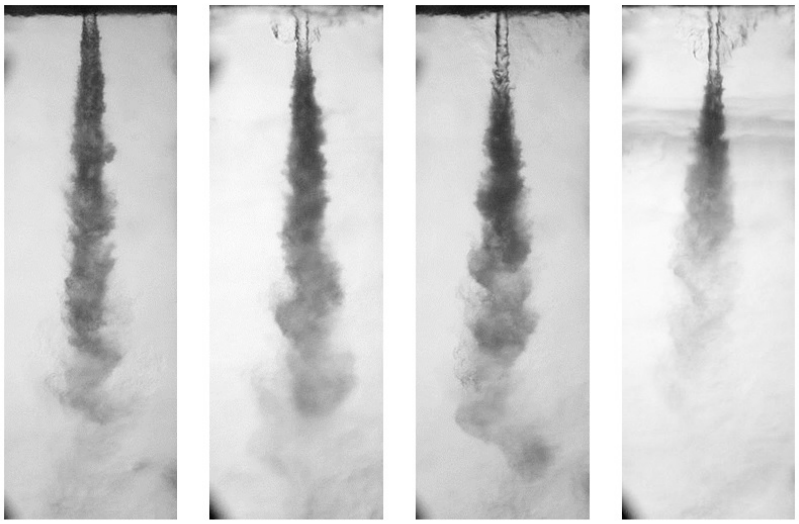

Figure 4.10: Effect of co-flowing nitrogen jet on sub-critical fluroketone jet at velocity v_fk=0.4m/s at super-critical chamber conditions. Experimental conditions of each image is detailed in table.4.4.

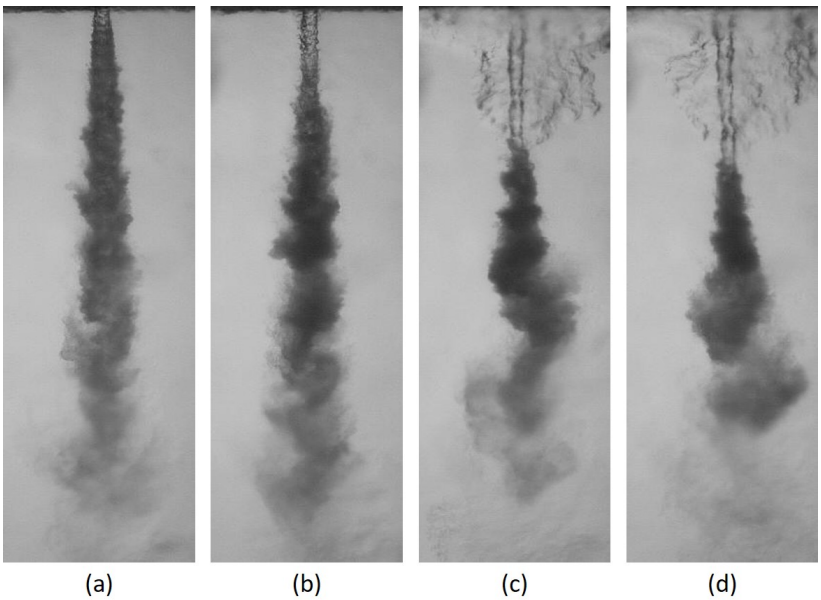

Figure 4.11: Effect of co-flowing nitrogen jet on sub-critical fluroketone jet at velocity v_fk=0.55m/s at super-critical chamber conditions. Experimental conditions of each image is detailed in table..4.5.

Table 4.5: Experimental Conditions for fig.4.11

Reduced Chamber pressure P_c	velocity of fluoroketone v_{fk} (m/s)	velocity of nitrogen v_{N_2} (m/s)	velocity ratio v_{N_2}/v_{fk}	mass flow rate of fluoroketone m_{fk} (g/s)	mass flow rate of nitrogen m_{N_2} (g/s)	coresponding figure
1.06	0.57±0.01	-	-	1.62	-	4.11.a
1.06	0.57±0.01	11.2±1	20	1.62	0.059	4.11.b
1.06	0.57±0.01	40.3±1	71.02	1.62	0.211	4.11.c
1.06	0.55±0.01	55.7±1	100	1.57	0.292	4.11.d

Table 4.6: Experimental Conditions for fig.4.12

Reduced Chamber pressure P_c	velocity of fluoroketone v_{fk} (m/s)	velocity of nitrogen v_{N_2} (m/s)	velocity ratio v_{N_2}/v_{fk}	mass flow rate of fluoroketone m_{fk} (g/s)	mass flow rate of nitrogen m_{N_2} (g/s)	coresponding figure
1.06	0.85±0.01	-	-	2.4	-	4.12.a
1.06	0.85±0.01	11.17±1	13	2.4	0.058	4.12.b
1.06	0.85±0.01	40.7±1	48	2.4	0.213	4.12.c
1.07	0.85±0.01	55.9±1	66	2.4	0.292	4.12.d

by the super-critical chamber medium and the interaction with the high dense chamber medium enhances atomization. When a subcritical nitrogen gaseous jet was introduced as a co-flow to the fluoroketone jet, the sudden thermodynamic transition of the fluoroketone jet was delayed as observable in fig.4.10.b,4.10.c and 4.10.d. The co-flowing subcritical nitrogen acts as a shield to the fluoroketone jet, thereby delaying the process of heating the jet due to the ambient high-temperature medium. The shielding distance depended on the inertia which is directly related to the velocity of the co-flowing nitrogen jet. As the velocity of the nitrogen jet was increased, the shielding was also increased, despite the effect of increased shearing on the inner jet. It can also be noted that even though the rapid thermodynamic transition into the super-critical medium was slightly delayed by the nitrogen jet, the overall mixing time or the length of the fluroketone jet into the super-critical medium was increased with respect to the increase in nitrogen velocity, which is evident in fig.4.10.c and fig.4.10.d.

Fig.4.11and 4.12 shows the effect of co-flow at higher velocities of the injecting fluoroketone jet with velocities around 0.55m/s in fig.4.11 and 0.85m/s in the fig.4.12; the corresponding experimental conditions are detailed in table 4.5 and 4.6 respectively. The co-flowing nitrogen jet was observed to shield the fluoroketone up to a certain distance which depended on the velocity of the nitrogen jet. The observations were similar to the cases in fig.4.10.

Because of the nebulous behaviour of the co-flowing nitrogen fluid, it is difficult to obtain the distance up to which the fluoroketone jet is shielded from the shadowgraphy images. To obtain the normalized shielding length, the Dynamic Mode decomposition (DMD)

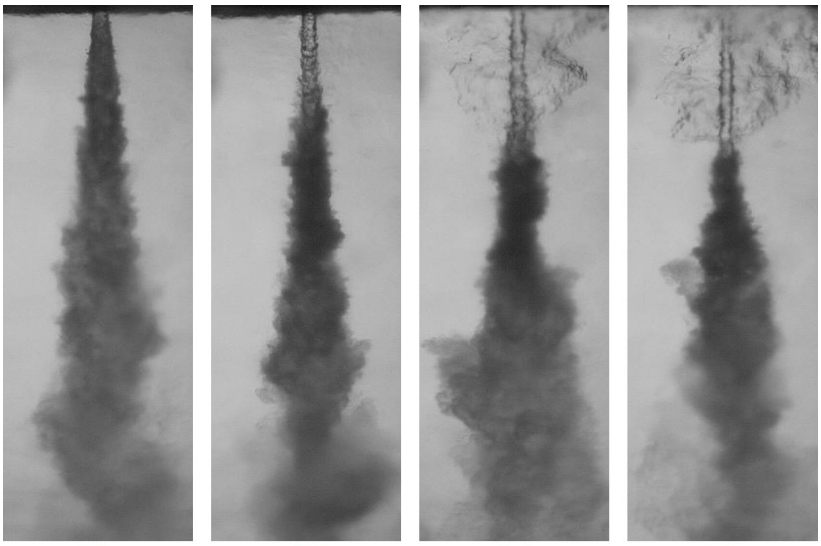

Figure 4.12: Effect of co-flowing nitrogen jet on sub-critical fluroketone jet at velocity v_fk=0.85m/s at super-critical chamber conditions. Experimental conditions of each image is detailed in table.4.6.

Table 4.7: Normalized shielding length obtained from mean DMD modes shown in fig.4.13

POD mode figure	velocity of fluoroketone v_{fk} (m/s)	velocity of nitrogen v_{N_2} (m/s)	Normalized shield length (with respect to inner jet diameter)	corresponding shadowgraphy image
4.13.a	0.39±0.01	10.9±1	6±0.06	4.10.b
4.13.b	0.42±0.01	32±1	9±0.06	4.10.c
4.13.c	0.41±0.01	40.3±1	13.7±0.06	4.10.d
4.13.d	0.57±0.01	11.2±1	6±0.06	4.11.b
4.13.e	0.57±0.01	40.3±1	12.91±0.06	4.11.c
4.13.f	0.57±0.01	55.7±1	13.5±0.06	4.11.d
4.13.g	0.85±0.01	11.17±1	5±0.06	4.12.b
4.13.h	0.85±0.01	40.7±1	13.3±0.06	4.12.c
4.13.i	0.8±0.15	55.9±1	13.6±0.06	4.12.d

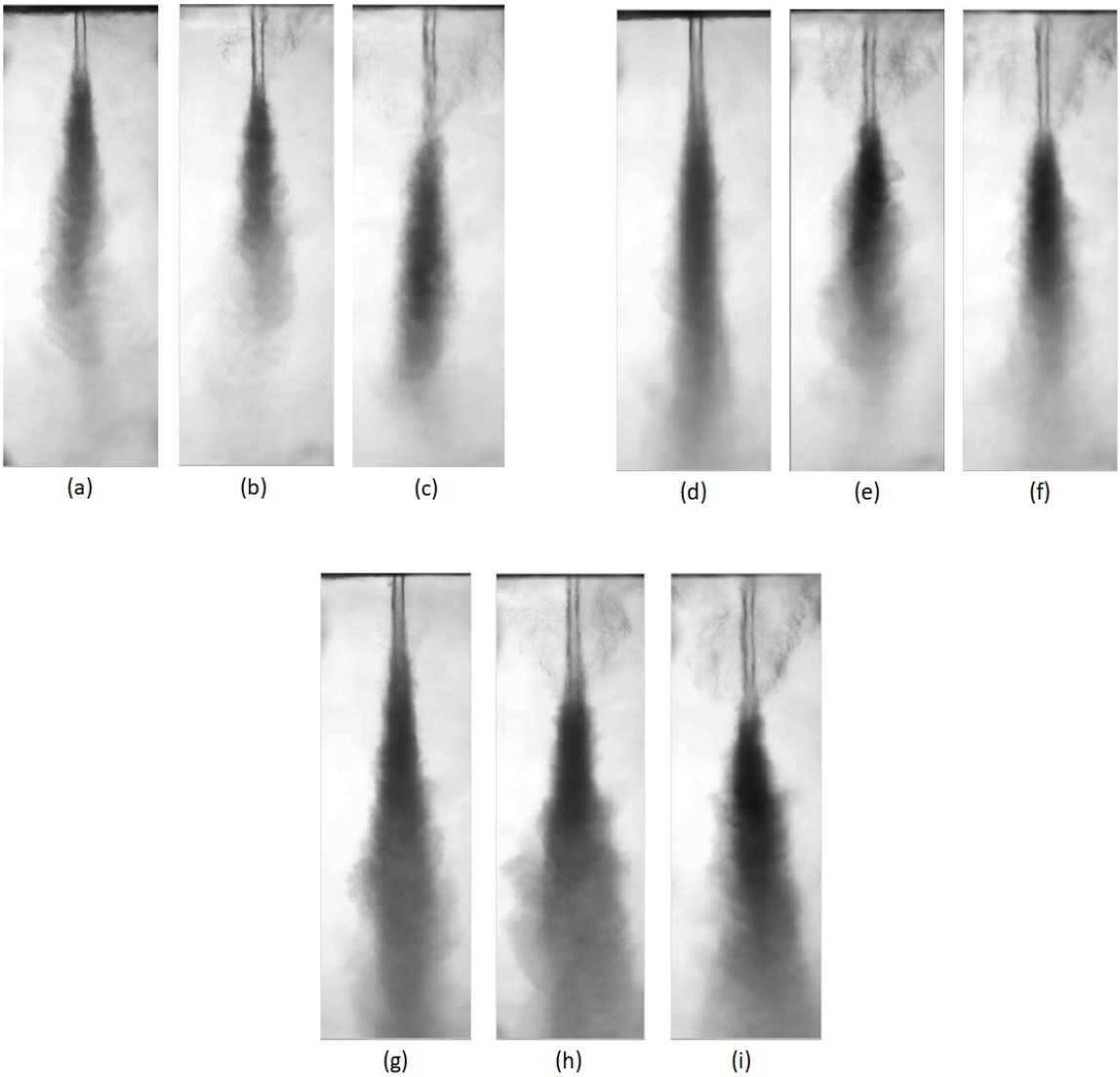

Figure 4.13: Mean modes obtained from DMD analysis. 'a','b','c','d','e','f,'g','h','i' corresponds to the experiemntal conditions shown in fig.4.10.'b','4.10.c','4.10.d', '4.11.b','4.11.c', '4.11.d', '4.12.b', '4.12.c', '4.12.d'

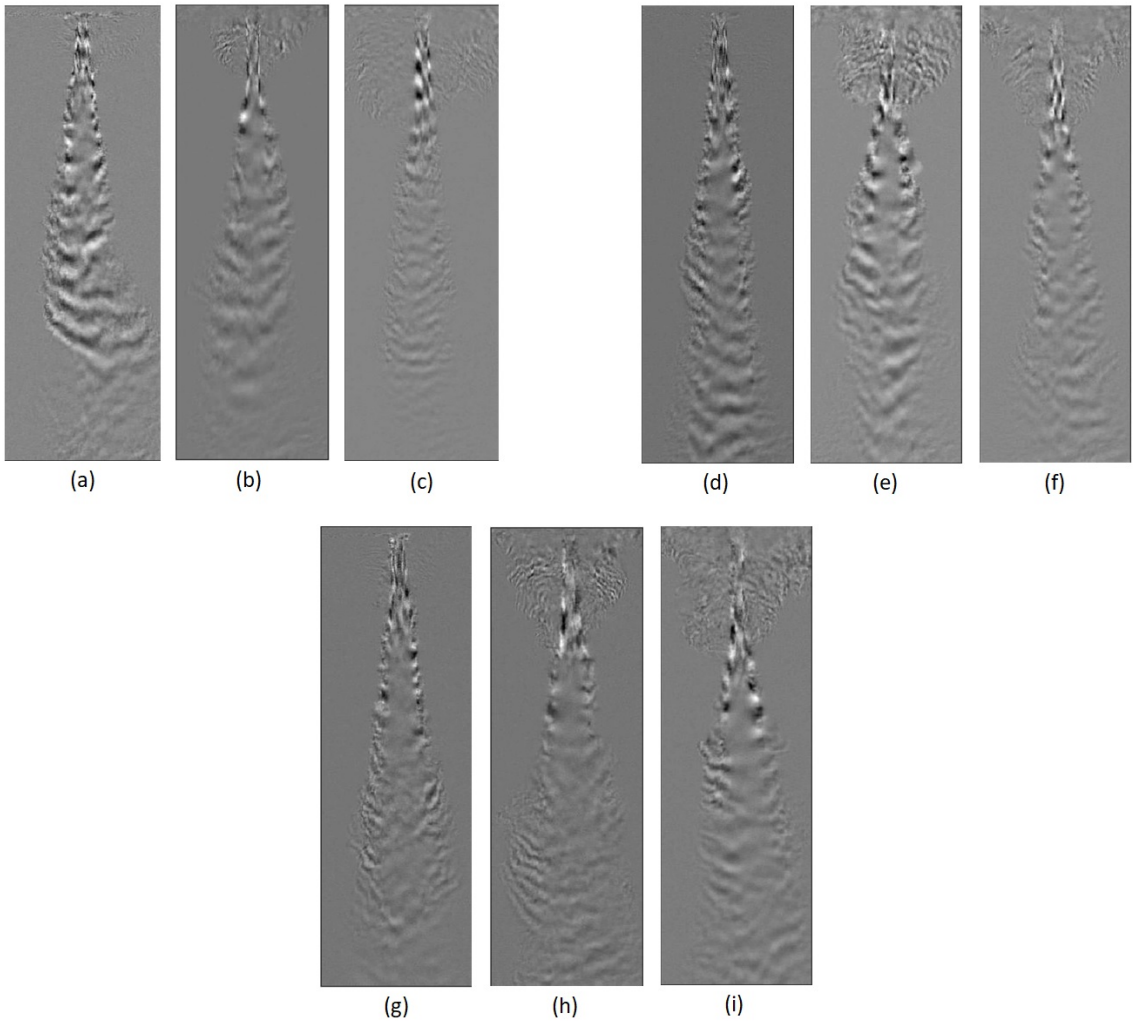

Figure 4.14: Most energetic DMD modes of the conditions shown in table.4.7. 'a','b','c','d','e','f,'g','h','i' corresponds to the experiemntal conditions shown in fig.4.10.'b','4.10.c','4.10.d', '4.11.b','4.11.c', '4.11.d', '4.12.b', '4.12.c', '4.12.d'

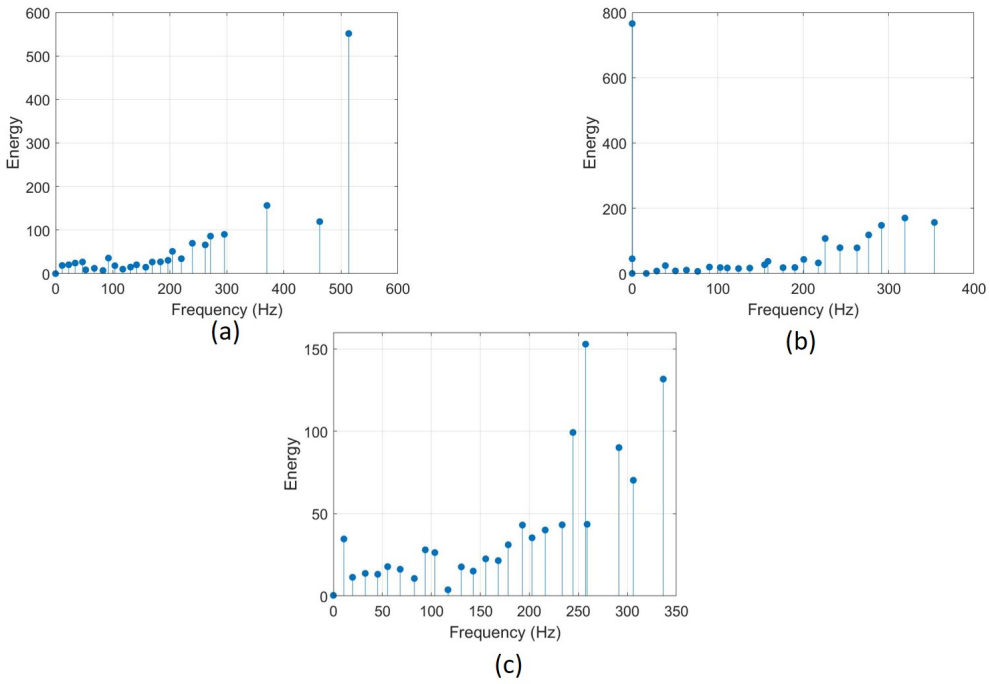

Figure 4.15: Amplitude versus frequency plot for Nitrogen co-flow shown in fig.4.11

method was employed. The mean modes obtained from the DMD analysis for different flow conditions from fig.4.10,4.11 and 4.12 are shown in fig.4.13 and the corresponding normalized shielding lengths (with respect to the inner jet diameter) are compiled in table 4.7. The most dominant modes for each flow condition are shown in fig.4.14. The alternate black and white fringe patterns in the modes represent the instabilities formed on the liquid jet surface. It is evident from all the cases in fig.4.14 that the subcritical fluoroketone jet does not undergo a rapid thermodynamic transition in the presence of a nitrogen co-flow. Also, it is very evident from table 4.7 that the shielding length is largely dependent on the velocity of the nitrogen jet than on the velocity ratio. In other words, the higher the inertia of the nitrogen jet to penetrate through the fluoroketone environment, the larger will be the shielding length. This shielding continued till the nitrogen gas got heated up and mixed with the ambient fluoroketone vapour. For the same velocity of the co-flowing nitrogen gas, the shielding length was nearly the same irrespective of the velocity ratio. It indicates that the shielding length directly depended on the velocity of the co-flowing fluid than on the velocity ratio. However, this aspect needs to be widely explored for a range of conditions employing co-axial jets at super-critical conditions. Fig.4.15 shows the amplitude versus frequency plot for different modes obtained for the cases shown in fig.4.11. It can be observed that the maximum frequency has a decreasing trend with increase in the velocity of the Nitrogen co-flow. This decrease in energy was due to the presence of a larger undisturbed length of

the liquid jet. In single-component system studies, it was shown that the energy of the modes of the liquid increased as the undisturbed length of jet decreased when the changer pressure was increased from sub-critical to super-critical chamber conditions.

4.4.2 Helium co-flow

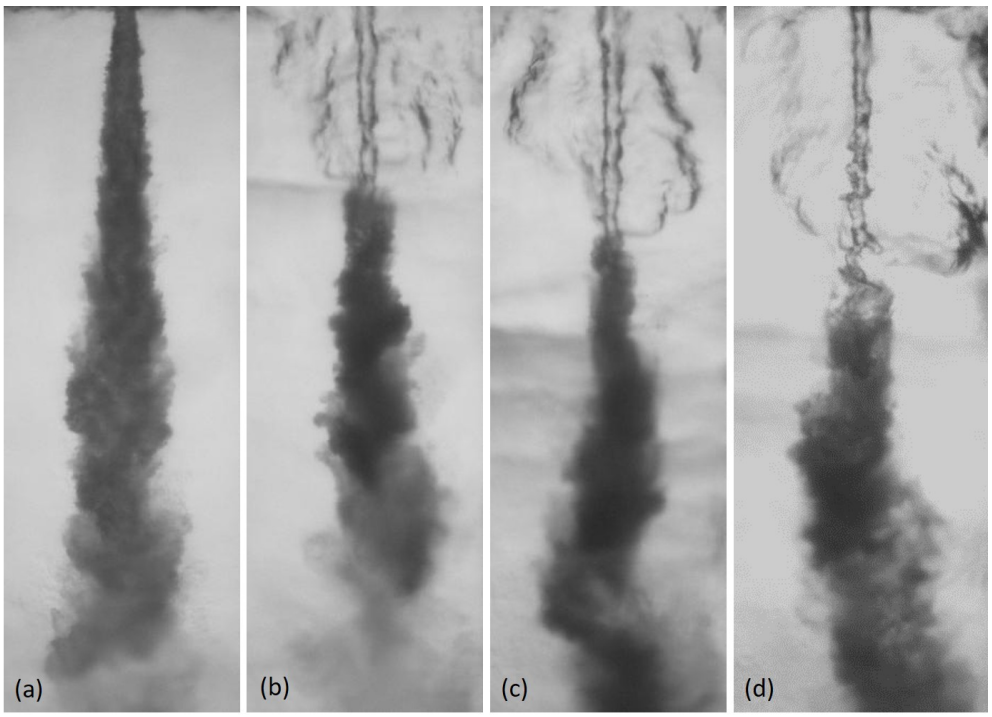

Figure 4.16: Effect of co-flowing Helium jet on sub-critical fluroketone jet at velocity v_fk=0.50m/s at super-critical chamber conditions. Experimental conditions of each image is detailed in table..4.8.

Table 4.8: Experimental Conditions for Helium co-flow shown in fig.4.16

Reduced Chamber pressure P_c	velocity of fluoroketone v_{fk} (m/s)	velocity of helium v_{He} (m/s)	velocity ratio v_{he}/v_{fk}	mass flow rate of fluoroketone m_{fk} (g/s)	mass flow rate of Helium m_{He} (g/s)	coresponding figure
1.06	0.5±0.01	-	-	1.25	-	4.16.a
1.06	0.48±0.01	30±1	62.5	1.28	0.161	4.16.b
1.06	0.51±0.01	71±1	139.21	1.5	0.355	4.16.c
1.06	0.5±0.01	93±1	186	1.35	0.2491	4.16.d

Co-axial experiments were also carried out with Helium as the co-flow as presented in fig.4.16 respectively. The observations were similar to that of the co-flow with nitrogen. The co-flowing gas was observed to act as a shield in both cases and the shielding length depended

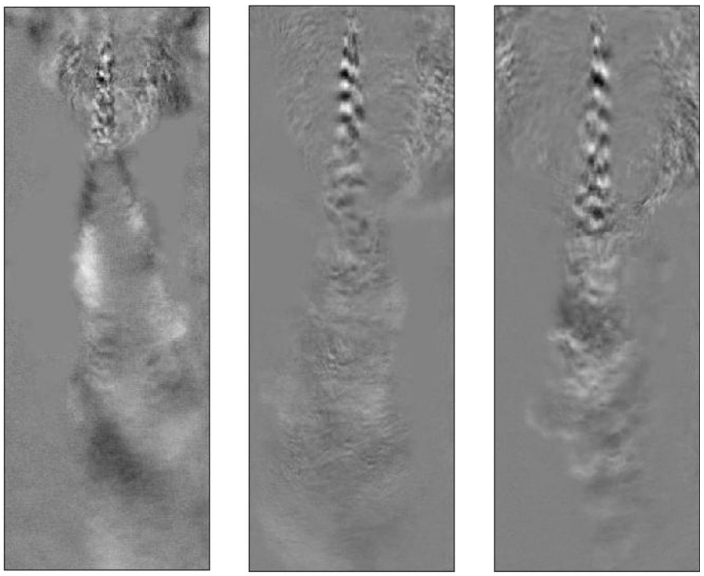

Figure 4.17: Dominant modes for Helium co-flow obtained from DMD analysis. 'a', 'b' and 'c' corresponds to the experimental condition shown in fig.4.16.'b',4.16.'c', 4.16.'d'

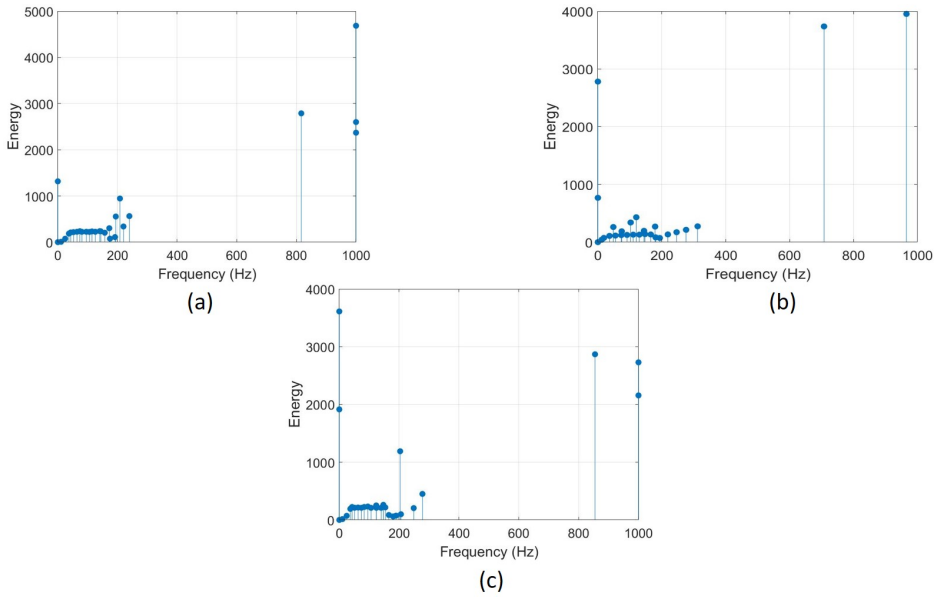

Figure 4.18: Amplitude vs frequency plot for Helium co-flow shown in fig.4.17

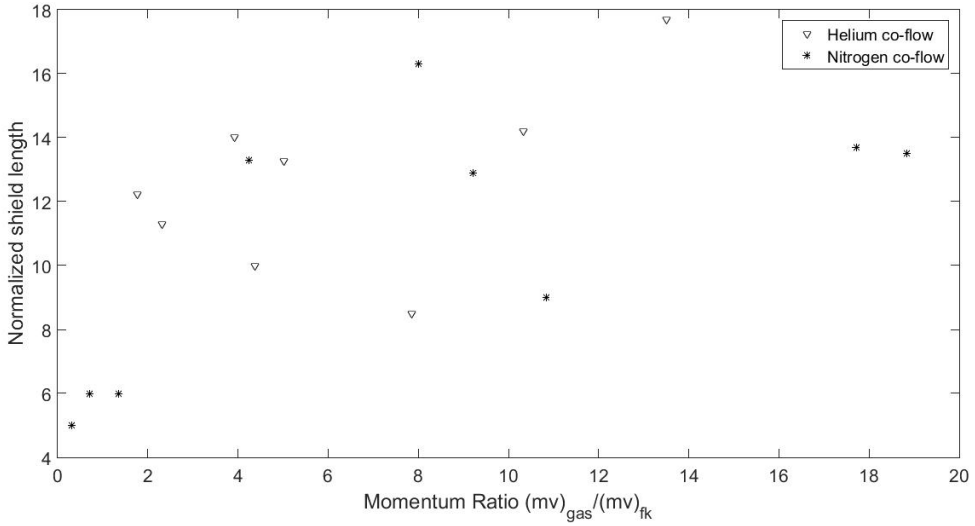

Figure 4.19: Normalized shield length vs Momentum ratios

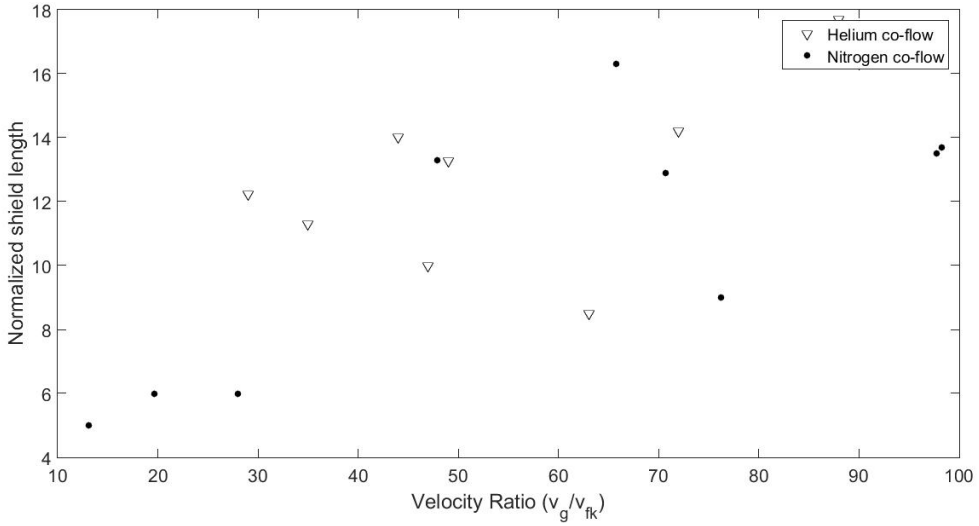

Figure 4.20: Normalized shield length vs Velocity ratios

on the velocity of the co-flowing gas. Dynamic mode decomposition was performed, and the resulting dominant modes for the cases in fig.4.16 is shown in fig.4.17, and the corresponding amplitude versus frequency for each modes plots are presented in fig.4.18. The presence of alternate black and white fringe patterns in the dominant mode indicated the presence of instability waves, as explained in chapter-3 for a single-component system. It can be observed that the energy of the most dominant mode decreases with respect to an increase in the Helium velocity, whereas the maximum frequency for all cases was close to 1000 Hz. In the case of nitrogen co-flow, the energy of the most dominant mode is 4-5 times larger than its second-highest mode and there was visibly one peak in the amplitude versus frequency plot as observed in fig.4.15. However, in the case of Helium co-flow, there are hardly any differences in the energy levels of the dominant modes. This may be due to the fact the in the case of nitrogen co-flow, the heat transfer rate of the inner fluoroketone jet is relatively reduced as compared to the case of Helium co-flow. This was observable in the shadowgraphy images that the inner jet is observed to be more unstable in Helium co-flow compared to that of the Nitrogen co-flow.

Fig.4.19 and fig.4.20 shows the variations in normalized shield length with respect to the momentum ratio (co-flow gas with respect to fluoroketone jet) and velocity ratios for Nitrogen and Helium co-flow cases at super-critical chamber conditions. From the set of experiments conducted, no specific trend could be observed on the dependency of shield length on the momentum and velocity ratios. Detailed experiments at different flowrates need to be conducted in this regard. But it is evident that, at a constant fluoroketone jet velocity, the shield length increases with an increase in the co-flow velocity of the gas.

Chapter 5

Conclusions

In the present experimental study, the behaviour of a subcritical laminar fluoroketone liquid jet injected into its own environment and in a mixture of N_2-fluoroketone environment at varying Reynolds number and chamber pressure (subcritical to supercritical) conditions are investigated. High-speed imaging techniques are employed to understand the jet behaviour, and fractal analysis of the jet boundary and dynamic mode decomposition is used to comprehend the mixing nature of the liquid jet. The instability nature and the thermodynamic transition of a jet at critical conditions is significantly influenced by the local conditions, mainly temperature at the interface between jet surface and the ambient fluid, and composition of the fluids in the chamber environment.

For a single component system, the thermodynamic transition of the liquid jet depends upon the injecting Reynolds number and chamber pressure, whereas in a binary component system, the transition depends heavily on the partial pressure of the injecting fluid in the chamber environment. Experiments carried out by preheating the injectant (from room temperature to near-critical temperature) showed that the nature of instabilities formed on the jet surface at the near-critical and supercritical conditions and the mixing process of the jet are greatly influenced by the thermodynamic properties of the injectant. With the introduction of a sub-critical gaseous jet as a co-flow, at super-critical chamber conditions, the sudden thermodynamic transition of the fluoroketone jet was not observed and the co-flow jet insulated the fluoroketone jet from the surrounding environment. This shielding distance is directly dependent on the velocity of the co-flow jet. The following conclusions are obtained from the study:

- For a single component system, at low subcritical pressure and low jet Re$<$1000, the jet exhibited classical characteristics. However, as the chamber pressure was increased shorter wave disturbances were observed after a few diameters from the injection

orifice. This is attributed to the high aerodynamic drag because of the dense chamber environment. As the chamber pressure became supercritical, the distinct interface was observed to diminish which indicated the absence of surface tension and the injected jet behaved like a turbulent gaseous jet.

- It was observed that at P_r=0.97, the jet started behaving like a turbulent gaseous jet without any drop formation at Re>1500 for a single component system. At low Re$\sim$1000, the jet was observed to have drop formation but at higher Re, the drop formation was not observed. This is attributed to high aerodynamic drag acting on the jet because of the increased Re. The bulges formed on the jet surface which were supposed to become droplets are vapourized before they separate from the jet surface.

- Experiments in the binary component system showed that the jet still possesses a distinct interface even above critical pressure and this clearly indicated the presence of surface tension. It was observed that the composition of the fluids in the chamber environment have a great influence on the behaviour of the liquid jet.

- When the chamber environment was pure Nitrogen, the jet underwent Rayleigh breakup without any drop formation. As the amount of fluoroketone was increased in the ambient environment the atomization regime was changed from the Rayleigh regime to the Taylor regime. When the N_2 to fluoroketone composition in the chamber was 1:3, the jet exhibited Taylor regime of atomization with features that are comparable to the features of a single component system with very fine drops at subcritical chamber pressure, and the thermodynamic transition was observed at higher chamber pressure above P_r=1.15.

- The subcritical jet was observed to undergo a thermodynamic transition when the partial pressure of fluoroketone in the Nitrogen-fluoroketone environment approaches its individual critical pressure.

- Fractal analysis using the box-counting method was employed to study the fractal nature of the subcritical jet. The fractal dimension of the liquid jet in a single component system and binary component system matches when the partial pressure of the fluoroketone in the chamber environment approaches its own individual critical pressure.

- The temperature of the incoming jet has a greater effect on the nature of instabilities and mixing of the fluid into the medium. The mixing of the jet into the chamber medium becomes more rapid as the temperature of the incoming jet increases. This

is mainly attributed due to the decrease in surface tension and viscosity with increase in temperature. Linear stability analysis on the liquid jet showed that, the disturbance wavelength decreases with increase in injection temperature.

- Different coherent structures of the jets were obtained and the wavelength of these fringe patterns of the most dominant mode obtained from growth rate (amplitude) versus frequency plot modes was in close agreement with the disturbance wavelength obtained from the stability analysis at sub-critical chamber conditions. It was also observed that the magnitude of the growth rate of the modes increases as the chamber pressure increases. The dominant modes obtained at supercritical conditions differed from those obtained using linear stability analysis and is attributed to the drasctic reduction in surfce tension of the jet at those conditions.

- With the introduction of a sub-critical gaseous jet as a co-flow, at super-critical chamber conditions, the sudden thermodynamic transition of the fluoroketone jet was not observed and the co-flow jet insulated the fluoroketone jet from the surrounding environment. This shielding distance is directly dependent on the velocity of the co-flow jet. The shielding length increases with an increase in co-flow velocity or rather on the inertia of the co-flow jet, (iii) The temporal characteristics of the jet behaviour were studied using DMD analysis. As a result of the shielding, the DMD analysis shows a decresing trend in the energy of the dominat modes with increase in co-flow jet velocity.

5.1 Future Work

- It was observed that in binary component system, at near critical chamber conditions, the liquid jet was observed to disintegrate faster with increase in Reynold number. More detailed experiments can be carried out to understand the influence of injecting velocity on the mixing nature of the jet in multicoponent system at near critical chamber conditions.

- In co-axial injection, the low temperature gas delayed the thermodynamic transition of the fluoroketone jet at supercritical chamber conditions. Experiments need to be carried out to understand the behaviour of the jet when the co-flow gas is introduced at a higher temperature.

- The L/D ratio is an important aspect of the injector that will influence the jet characteristics. However in this study the effect of L/D variation was not attempted and this can be taken up as part of future studies.

Bibliography

Alessandri, A., Bagnerini, P., Gaggero, M., Lengani, D. and Simoni, D. (2019), 'Dynamic mode decomposition for the inspection of three-regime separated transitional boundary layers using a least squares method', *Physics of Fluids* **31**(4), 044103.

Alexander Schumaker, S. and Driscoll, J. F. (2012), 'Mixing properties of coaxial jets with large velocity ratios and large inverse density ratios', *Physics of Fluids* **24**(5), 055101.

Alhushaybari, A. and Uddin, J. (2019), 'Convective and absolute instability of viscoelastic liquid jets in the presence of gravity', *Physics of Fluids* **31**(4), 044106.
URL: *https://doi.org/10.1063/1.5089242*

Anderson, W. E. and Yang, V. (1995), *Liquid rocket engine combustion instability*, American Institute of Aeronautics and Astronautics.

Arienti, M. and Soteriou, M. C. (2009), 'Time-resolved proper orthogonal decomposition of liquid jet dynamics', *Physics of Fluids* **21**(11), 112104.

Baab, S., Lamanna, G. and Weigand, B. (2018), 'Two-phase disintegration of high-pressure retrograde fluid jets at near-critical injection temperature discharged into a subcritical pressure atmosphere', *International Journal of Multiphase Flow* **107**, 116–130.

Balarac, G. and Metais, O. (2005), 'The near field of coaxial jets: A numerical study', *Physics of Fluids* **17**(6), 065102.

Balarac, G., Métais, O. and Lesieur, M. (2007), 'Mixing enhancement in coaxial jets through inflow forcing: A numerical study', *Physics of fluids* **19**(7), 075102.

Balarac, G., Si-Ameur, M., Lesieur, M. and Métais, O. (2007), 'Direct numerical simulations of high velocity ratio coaxial jets: mixing properties and influence of upstream conditions', *Journal of Turbulence* (8), N22.

Bellan, J. (2000), 'Supercritical (and subcritical) fluid behavior and modeling: drops, streams, shear and mixing layers, jets and sprays', *Progress in energy and combustion science* **26**(4-6), 329–366.

Berkooz, G., Holmes, P. and Lumley, J. L. (1993), 'The proper orthogonal decomposition in the analysis of turbulent flows', *Annual review of fluid mechanics* **25**(1), 539–575.

Branam, R., Mayer, W., Telaar, J. and Schneider, G. (2002), Injection characteristics on the surface of a coaxial jet, *in* '38th AIAA/ASME/SAE/ASEE Joint Propulsion Conference & Exhibit', p. 3695.

Chandrasekhar, S. (2013), *Hydrodynamic and hydromagnetic stability*, Courier Corporation.

Charalampous, G., Hadjiyiannis, C. and Hardalupas, Y. (2019), 'Proper orthogonal decomposition of primary breakup and spray in co-axial airblast atomizers', *Physics of Fluids* **31**(4), 043304.

Charalampous, G. and Hardalupas, Y. (2014), 'Application of proper orthogonal decomposition to the morphological analysis of confined co-axial jets of immiscible liquids with comparable densities', *Physics of Fluids* **26**(11), 113301.

Charalampous, G., Hardalupas, Y. and Taylor, A. (2009), 'Novel technique for measurements of continuous liquid jet core in an atomizer', *AIAA journal* **47**(11), 2605–2615.

Chehroudi, B. (2012), 'Recent experimental efforts on high-pressure supercritical injection for liquid rockets and their implications', *International Journal of Aerospace Engineering* **2012**.

Chehroudi, B., Cohn, R. and Talley, D. (2002), 'Cryogenic shear layers: experiments and phenomenological modeling of the initial growth rate under subcritical and supercritical conditions', *International Journal of Heat and Fluid Flow* **23**(5), 554–563.

Chehroudi, B. and Talley, D. (2004), 'The fractal geometry of round turbulent cryogenic nitrogen jets at subcritical and supercritical pressures', *Atomization and Sprays* **14**(1).

Chehroudi, B., Talley, D. and Coy, E. (1999), Fractal geometry and growth rate changes of cryogenic jets near the critical point, *in* '35th Joint Propulsion Conference and Exhibit', p. 2489.

Chehroudi, B., Talley, D. and Coy, E. (2002), 'Visual characteristics and initial growth rates of round cryogenic jets at subcritical and supercritical pressures', *Physics of Fluids* **14**(2), 850–861.

Chen, L. D. (1994), Heat transfer, fouling, and combustion of supercritical fuels, Technical report, IOWA University, Dept of Mechanical Engineering.

Chigier, N. and Farago, Z. (1992), 'Morphological classification of disintegration of round liquid jets in a coaxial air stream', *Atomization and Sprays* **2**(2).

Chigier, N. and Reitz, R. D. (1996), 'Regimes of jet breakup and breakup mechanisms-physical aspects', *Recent advances in spray combustion: Spray atomization and drop burning phenomena.* **1**, 109–135.

Dahms, R. N. (2016), 'Understanding the breakdown of classic two-phase theory and spray atomization at engine-relevant conditions', *Physics of Fluids* **28**(4), 042108.

Dahms, R. N. and Oefelein, J. C. (2013), 'On the transition between two-phase and single-phase interface dynamics in multicomponent fluids at supercritical pressures', *Physics of Fluids* **25**(9), 092103.

Dahms, R. N. and Oefelein, J. C. (2015), 'Atomization and dense-fluid breakup regimes in liquid rocket engines', *Journal of Propulsion and Power* **31**(5), 1221–1231.

Davis, D. and Chehroudi, B. (2006), Shear-coaxial jets from a rocket-like injector in a transverse acoustic field at high pressures, *in* '44th AIAA Aerospace Sciences Meeting and Exhibit', p. 758.

Davis, D. W. (2006), On the behavior of a shear-coaxial jet, spanning sub-to supercritical pressures, with and without an externally imposed transverse acoustic field, Technical report, PENNSYLVANIA STATE UNIV UNIVERSITY PARK DEPT OF MECHANICAL AND NUCLEAR ....

DeSouza, S. and Segal, C. (2017), 'Sub-and supercritical jet disintegration', *Physics of Fluids* **29**(4), 047107.

Doungthip, T., Ervin, J. S., Williams, T. F. and Bento, J. (2002), 'Studies of injection of jet fuel at supercritical conditions', *Industrial & Engineering Chemistry Research* **41**(23), 5856–5866.

Dumouchel, C. (2008), 'On the experimental investigation on primary atomization of liquid streams', *Experiments in fluids* **45**(3), 371–422.

Dumouchel, C., Cousin, J. and Triballier, K. (2005), 'Experimental analysis of liquid–gas interface at low weber number: interface length and fractal dimension', *Experiments in fluids* **39**(4), 651–666.

Edwards, A. P. R., Osborne, B. P., Stoltzfus, J. M., Howes, T. and Steinberg, T. A. (2002), 'Instabilities and drop formation in cylindrical liquid jets in reduced gravity', *Physics of Fluids* **14**(10), 3432–3438.
URL: *https://doi.org/10.1063/1.1501825*

Eggers, J. and Villermaux, E. (2008), 'Physics of liquid jets', *Reports on progress in physics* **71**(3), 036601.

Elazab, S. S., Rahman, S. A., Hasan, A. A. and Zidan, N. A. (2012*a*), 'Axisymmetric hydromagnetic stability of a streaming resistive hollow jet under oblique varying magnetic field', *Journal of Mathematical and Computational Science* **2**(3), 473–500.

Elazab, S. S., Rahman, S. A., Hasan, A. A. and Zidan, N. A. (2012*b*), 'Stability of compressible hollow jet pervaded by a transverse varying magnetic field', *ISRN Mathematical Physics* **2012**.

Eldabe, N., Elogail, M., Elshaboury, S. and Hasan, A. A. (2016), 'Hall effects on the peristaltic transport of williamson fluid through a porous medium with heat and mass transfer', *Applied Mathematical Modelling* **40**(1), 315–328.

Eroglu, H., Chigier, N. and Farago, Z. (1991), 'Coaxial atomizer liquid intact lengths', *Physics of Fluids A: Fluid Dynamics* **3**(2), 303–308.

Faeth, G., Hsiang, L.-P. and Wu, P.-K. (1995), 'Structure and breakup properties of sprays', *International Journal of Multiphase Flow* **21**, 99 – 127. Annual Reviews in Multiphase Flow 1995.
URL: *http://www.sciencedirect.com/science/article/pii/0301932295000597*

Falgout, Z., Rahm, M., Sedarsky, D. and Linne, M. (2016), 'Gas/fuel jet interfaces under high pressures and temperatures', *Fuel* **168**, 14–21.

Favre-Marinet, M. and Schettini, E. C. (2001), 'The density field of coaxial jets with large velocity ratio and large density differences', *International journal of heat and mass transfer* **44**(10), 1913–1924.

Gorokhovski, M. and Herrmann, M. (2008), 'Modeling primary atomization', *Annu. Rev. Fluid Mech.* **40**, 343–366.

Guang, J., Rui, T., Xiao-Chuan, L. and Wen-fei, W. (2011), Experimental studies of droplet evaporation in high-temperature air and co2, *in* 'Measuring Technology and Mechatronics Automation (ICMTMA), 2011 Third International Conference on', Vol. 2, IEEE, pp. 124–126.

H. Mayer, W. O., A. Schik, A. H., Vielle, B., Chauveau, C., G-ograve, I., kalp, Talley, D. G. and Woodward, R. D. (1998), 'Atomization and breakup of cryogenic propellants under high-pressure subcritical and supercritical conditions', *Journal of Propulsion and Power* **14**(5), 835–842.

Hasan, A. A. (2016*a*), 'Electrogravitational stability of streaming compound jets', *International Journal of Biomathematics* **9**(02), 1650032.

Hasan, A. A. (2016*b*), 'Self-gravitating stability of a rotating fluid layer', *Journal of Applied Mechanics and Technical Physics* **57**(6), 1016–1021.
URL: *https://doi.org/10.1134/S0021894416060080*

Heidorn, D., Steiner, H. and Brenn, G. (2008), Modelling of the fractal dimension in the primary atomization of high-speed liquid jets, *in* '22th European Conference on Liquid Atomization and Spray Systems, ILASS 2008'.

Hemati, M. S., Williams, M. O. and Rowley, C. W. (2014), 'Dynamic mode decomposition for large and streaming datasets', *Physics of Fluids* **26**(11), 111701.

Hosangadi, A., Lee, C., Kannepalli, C. and Arunajatesan, S. (2008), Three-dimensional hybrid rans/les simulations of a supercritical liquid nitrogen jet, *in* '44th AIAA/ASME/SAE/ASEE Joint Propulsion Conference & Exhibit', p. 5227.

Hua, J.-C., Gunaratne, G. H., Talley, D. G., Gord, J. R. and Roy, S. (2016), 'Dynamic-mode decomposition based analysis of shear coaxial jets with and without transverse acoustic driving', *Journal of Fluid Mechanics* **790**, 5–32.

Hyhlík, T., Netřebská, H., Devera, J. and Kalinay, R. (2017), Analysis of turbulent synthetic jet by dynamic mode decomposition, *in* 'EPJ Web of Conferences', Vol. 143, EDP Sciences, p. 02040.

Ibrahim, E. and Marshall, S. (2000), 'Instability of a liquid jet of parabolic velocity profile', *Chemical Engineering Journal* **76**(1), 17–21.

Kumar, A. and Sahu, S. (2018*a*), 'Liquid jet breakup unsteadiness in a coaxial air-blast atomizer', *International journal of spray and combustion dynamics* **10**(3), 211–230.

Kumar, A. and Sahu, S. (2018*b*), 'Optical visualization and measurement of liquid jet core in a coaxial atomizer with annular swirling air', *Journal of Flow Visualization and Image Processing* **25**(3-4).

Kumar, A. and Sahu, S. (2019), 'Large scale instabilities in coaxial air-water jets with annular air swirl', *Physics of Fluids* **31**(12), 124103.

Kurschat, T., Chaves, H. and Meier, G. (1992), 'Complete adiabatic evaporation of highly superheated liquid jets', *Journal of Fluid Mechanics* **236**, 43–59.

Lacaze, G. and Oefelein, J. C. (2013), Modeling high-density-gradient flows at supercritical pressures, *in* '49th AIAA/ASME/SAE/ASEE Joint PropulsionConference', p. 3717.

Lasheras, J. C. and Hopfinger, E. (2000*a*), 'Liquid jet instability and atomization in a coaxial gas stream', *Annual review of fluid mechanics* **32**(1), 275–308.

Lasheras, J. C. and Hopfinger, E. J. (2000*b*), 'Liquid jet instability and atomization in a coaxial gas stream', *Annual Review of Fluid Mechanics* **32**(1), 275–308.
URL: *https://doi.org/10.1146/annurev.fluid.32.1.275*

Lasheras, J., Villermaux, E. and Hopfinger, E. (1998), 'Break-up and atomization of a round water jet by a high-speed annular air jet', *Journal of Fluid Mechanics* **357**, 351–379.

Lefebvre, A. H. and McDonell, V. G. (2017), *Atomization and sprays*, CRC press.

Leib, S. and Goldstein, M. (1986*a*), 'Convective and absolute instability of a viscous liquid jet', *The Physics of fluids* **29**(4), 952–954.

Leib, S. J. and Goldstein, M. E. (1986*b*), 'The generation of capillary instabilities on a liquid jet', *Journal of Fluid Mechanics* **168**, 479–500.

Leroux, B., Delabroy, O. and Lacas, F. (2007), 'Experimental study of coaxial atomizers scaling. part i: dense core zone', *Atomization and Sprays* **17**(5).

Leyva, I., Chehroudi, B. and Talley, D. (2007), Dark core analysis of coaxial injectors at sub-, near-, and supercritical conditions in a transverse acoustic field, *in* '43rd AIAA/ASME/SAE/ASEE Joint Propulsion Conference & Exhibit', p. 5456.

Lin, K.-C., Cox-Stouffer, S. K. and Jackson, T. A. (2006), 'Structures and phase transition processes of supercritical methane/ethylene mixtures injected into a subcritical environment', *Combustion Science and Technology* **178**(1-3), 129–160.

Lin, R. and Tavlarides, L. L. (2013), 'Thermal stability and decomposition of diesel fuel under subcritical and supercritical conditions', *The Journal of Supercritical Fluids* **75**, 101–111.

Lin, S., Hudman, M. and Chen, J. (1999), 'Absolute and convective instability of a liquid jet'.

Lin, S. and Jiang, W. (2003), 'Absolute and convective instability of a radially expanding liquid sheet', *Physics of Fluids* **15**(6), 1745–1754.

Lin, S.-P. (2003), *Breakup of liquid sheets and jets*, Cambridge university press.

Lin, S. P. and Lian, Z. W. (1989), 'Absolute instability of a liquid jet in a gas', *Physics of Fluids A: Fluid Dynamics* **1**(3), 490–493.
URL: *https://doi.org/10.1063/1.857419*

Lin, S. and Reitz, R. (1998), 'Drop and spray formation from a liquid jet', *Annual review of fluid mechanics* **30**(1), 85–105.

Liu, F., Gao, Y., Zhang, Z., He, X., Wu, H., Zhang, C., Zeng, F. and Hou, X. (2018), 'Study of the spray characteristics of a diesel surrogate for diesel engines under sub/supercritical states injected into atmospheric environment', *Fuel* **230**, 308 – 318.

Liu, H.-F., Li, W.-F., Gong, X., Cao, X.-K., Xu, J.-L., Chen, X.-L., Wang, Y.-F., Yu, G.-S., Wang, F.-C. and Yu, Z.-H. (2006), 'Effect of liquid jet diameter on performance of coaxial two-fluid airblast atomizers', *Chemical Engineering and Processing: Process Intensification* **45**(4), 240–245.

Liu, Y., Pei, Y., Peng, Z., Qin, J., Zhang, Y., Ren, Y. and Zhang, M. (2017), 'Spray development and droplet characteristics of high temperature single-hole gasoline spray', *Fuel* **191**, 97 – 105.

Mandelbrot, B. B. (1982), *The fractal geometry of nature*, Vol. 982, Freeman, San Francisco.

Manin, J., Bardi, M., Pickett, L., Dahms, R. and Oefelein, J. (2014), 'Microscopic investigation of the atomization and mixing processes of diesel sprays injected into high pressure and temperature environments', *Fuel* **134**, 531–543.

Marmottant, P. and Villermaux, E. (2004), 'On spray formation', *Journal of fluid mechanics* **498**, 73–111.

Matsuyama, S., Shinjo, J., Ogawa, S. and Mizobuchi, Y. (2010), Large eddy simulation of lox/gh2 shear-coaxial jet flame at supercritical pressure, *in* '48th AIAA Aerospace Sciences Meeting Including the New Horizons Forum and Aerospace Exposition', p. 208.

Mayer, W., Schik, A., Sch-aring, M., ffler and Tamura, H. (2000), 'Injection and mixing processes in high-pressure liquid oxygen/gaseous hydrogen rocket combustors', *Journal of Propulsion and Power* **16**(5), 823–828.

Mayer, W. and Tamura, H. (1996), 'Propellant injection in a liquid oxygen/gaseous hydrogen rocket engine', *Journal of Propulsion and Power* **12**(6), 1137–1147.

McKinley, G. H. and Renardy, M. (2011), 'Wolfgang von ohnesorge', *Physics of Fluids* **23**(12), 127101.

Mehring, C. and Sirignano, W. (2000), 'Axisymmetric capillary waves on thin annular liquid sheets. ii. spatial development', *Physics of Fluids* **12**(6), 1440–1460.

Muthukumaran, C. K. and Vaidyanathan, A. (2016*a*), 'Initial instability of round liquid jet at subcritical and supercritical environments', *Physics of Fluids* **28**(7), 074104.
URL: *https://aip.scitation.org/doi/abs/10.1063/1.4954312*

Muthukumaran, C. and Vaidyanathan, A. (2014), 'Experimental study of elliptical jet from sub to supercritical conditions', *Physics of Fluids* **26**(4), 044104.

Muthukumaran, C. and Vaidyanathan, A. (2015), 'Experimental study of elliptical jet from supercritical to subcritical conditions using planar laser induced fluorescence', *Physics of Fluids* **27**(3), 034109.

Muthukumaran, C. and Vaidyanathan, A. (2016*b*), 'Mixing nature of supercritical jet in subcritical and supercritical conditions', *Journal of Propulsion and Power* pp. 1–16.

Newman, J. A. and Brzustowski, T. (1971), 'Behavior of a liquid jet near the thermodynamic critical region', *AIAA journal* **9**(8), 1595–1602.

O'Donnell, B., Chen, J. N. and Lin, S. P. (2001), 'Transition from convective to absolute instability in a liquid jet', *Physics of Fluids* **13**(9), 2732–2734.
URL: *https://doi.org/10.1063/1.1387469*

Ohnesorge, W. V. (1936), 'Die bildung von tropfen an düsen und die auflösung flüssiger strahlen', *ZAMM-Journal of Applied Mathematics and Mechanics/Zeitschrift für Angewandte Mathematik und Mechanik* **16**(6), 355–358.

Oschwald, M., Schik, A., Klar, M. and Mayer, W. (1999), Investigation of coaxial ln2/gh2-injection at supercritical pressure by spontaneous raman scattering, *in* '35th Joint propulsion conference and exhibit', p. 2887.

Oschwald*, M., Smith, J., Branam, R., Hussong, J., Schik, A., Chehroudi, B. and Talley, D. (2006), 'Injection of fluids into supercritical environments', *Combustion science and technology* **178**(1-3), 49–100.

Oschwald*, M., Smith, J. J., Branam, R., Hussong, J., Sschik, A., Chehroudi, B. and Talley, D. (2006), 'Injection of fluids into supercritical environments', *Combustion Science and Technology* **178**(1-3), 49–100.
URL: *https://doi.org/10.1080/00102200500292464*

Owens, J. G. (2002), 'Physical and environmental properties of a next generation extinguishing agent', *NIST Special Publication* pp. 984–1.

Porcheron, E., Carreau, J.-L., Le Visage, D. and Roger, F. (2002), 'Effect of injection gas density on coaxial liquid jet atomization', *Atomization and Sprays* **12**(1-3).

Rehab, H., Villermaux, E. and Hopfinger, E. (1997), 'Flow regimes of large-velocity-ratio coaxial jets', *Journal of Fluid Mechanics* **345**, 357–381.

Reitz, R. and Bracco, F. (1982), 'Mechanism of atomization of a liquid jet', *The physics of Fluids* **25**(10), 1730–1742.

Roy, A. and Segal, C. (2010), 'Experimental study of fluid jet mixing at supercritical conditions', *Journal of Propulsion and Power* **26**(6), 1205–1211.

Roy, S., Hua, J.-C., Barnhill, W., Gunaratne, G. H. and Gord, J. R. (2015), 'Deconvolution of reacting-flow dynamics using proper orthogonal and dynamic mode decompositions', *Physical review E* **91**(1), 013001.

Sarkar, S., Ganguly, S., Dalal, A., Saha, P. and Chakraborty, S. (2013), 'Mixed convective flow stability of nanofluids past a square cylinder by dynamic mode decomposition', *International Journal of Heat and Fluid Flow* **44**, 624–634.

Schmid, P. J. (2010), 'Dynamic mode decomposition of numerical and experimental data', *Journal of fluid mechanics* **656**, 5–28.

Schmid, P. J. (2011), 'Application of the dynamic mode decomposition to experimental data', *Experiments in fluids* **50**(4), 1123–1130.

Schmitt, T., Rodriguez, J., Leyva, I. and Candel, S. (2012), 'Experiments and numerical simulation of mixing under supercritical conditions', *Physics of Fluids* **24**(5), 055104.

Seena, A. and Sung, H. J. (2011), 'Dynamic mode decomposition of turbulent cavity flows for self-sustained oscillations', *International Journal of Heat and Fluid Flow* **32**(6), 1098–1110.

Segal, C. and Polikhov, S. (2008), 'Subcritical to supercritical mixing', *Physics of Fluids* **20**(5), 052101.

Sengers, J. V. (1985), 'Transport properties of fluids near critical points', *International Journal of Thermophysics* **6**(3), 203–232.
URL: *https://doi.org/10.1007/BF00522145*

Shavit, U. and Chigier, N. (1995), 'The role of dynamic surface tension in air assist atomization', *Physics of Fluids* **7**(1), 24–33.
URL: *https://doi.org/10.1063/1.868725*

Simões-Moreira, J. R., Vieira, M. M., Angelo, E. et al. (2002), 'Highly expanded flashing liquid jets', *Journal of Thermophysics and heat transfer* **16**(3), 415–424.

Sirignano, W. A. and Tryggvason, G. (2000), 'Fluid dynamics and transport of droplets and sprays'.

Sreenivasan, K. and Meneveau, C. (1986), 'The fractal facets of turbulence', *Journal of Fluid Mechanics* **173**, 357–386.

Sterling, A. M. and Sleicher, C. (1975), 'The instability of capillary jets', *Journal of Fluid Mechanics* **68**(3), 477–495.

Tang, S. K. and Ko, N. (1994), 'Experimental investigation of the structure interaction in an excited coaxial jet', *experimental thermal and fluid science* **8**(3), 214–229.

Tani, H., Teramoto, S. and Okamoto, K. (2015), 'High-speed observations of cryogenic single and coaxial jets under subcritical and transcritical conditions', *Experiments in Fluids* **56**(4), 1–13.

Taylor, J. and Hoyt, J. (1983), 'Water jet photography—techniques and methods', *Experiments in Fluids* **1**(3), 113–120.

Tirunagari, S., Vuorinen, V., Kaario, O. and Larmi, M. (2012), 'Analysis of proper orthogonal decomposition and dynamic mode decomposition on les of subsonic jets', *CSI Journal of Computing* **1**(3), 20–26.

Tomotika, S. (1935), 'On the instability of a cylindrical thread of a viscous liquid surrounded by another viscous fluid', *Proceedings of the Royal Society of London. Series A-Mathematical and Physical Sciences* **150**(870), 322–337.

Tseng, L.-K., Ruff, G. and Faeth, G. (1992), 'Effects of gas density on the structure of liquid jets in still gases', *AIAA journal* **30**(6), 1537–1544.

Weber, C. (1931), 'Zum zerfall eines flüssigkeitsstrahles', *ZAMM-Journal of Applied Mathematics and Mechanics/Zeitschrift für Angewandte Mathematik und Mechanik* **11**(2), 136–154.

Woodward, R. and Talley, D. (1996), Raman imaging of transcritical cryogenic propellants, *in* '34th Aerospace Sciences Meeting and Exhibit', p. 468.

Wu, P.-K., Chen, T. H., Nejad, A. S. and Carter, C. D. (1996), 'Injection of supercritical ethylene in nitrogen', *Journal of Propulsion and Power* **12**(4), 770–777.

Wu, P.-K., Shahnam, M., Kirkendall, K. A., Carter, C. D. and Nejad, A. S. (1999), 'Expansion and mixing processes of underexpanded supercritical fuel jets injected into superheated conditions', *Journal of Propulsion and Power* **15**(5), 642–649.

Zappoli, B. (2003), 'Near-critical fluid hydrodynamics', *Comptes Rendus Mecanique* **331**(10), 713–726.

LIST OF PUBLICATIONS

International Journals

- **Ayyappan, D.**, Vaidyanathan, A., Muthukuamaran, C.K., and Nandakumar, K., “Transition of subcritical liquid jets in single and multicomponent systems”, Physics of Fluids , 30(10), 104106, 2018
- **Ayyappan, D.**,Kumar Ajith, Vaidyanathan, A., and Nandakumar, "Study on instability of circular liquid jets at subcritical to supercritical conditions using dynamic mode decomposition", Physics of Fluids, 32, 014107,2020
- **Ayyappan, D.**, Vaidyanathan, A., and Nandakumar, "Mixing nature of a circular jet with co-flow at supercritical chamber conditions", Propulsion and Power Research (*submitted*)

Book Chapter

- **Ayyappan, D.**, Muthukumaran, C.K., Vaidyanathan, A., and Nandakumar, K.,"Study of Instability Nature of Circular Liquid Jet at Critical Chamber Conditions", Advanced Engine Diagnostics, Springer, pp 205-217,2019.

Conference Proceedings

- **Ayyappan, D.**, Muthukumaran, C.K., Vaidyanathan, A., and Nandakumar, K., "Dynamics of Circular Liquid Jet at Supercritical Chamber Conditions", IHMTC2017-13-276, 24th National and 2nd International ISHMT-ASFTE Heat and Mass Transfer Conference (IHMTC 2017), BITS Pilani, Hyderabad, 27-30 Dec, 2017.
- **Ayyappan, D.**, Muthukumaran, C.K., Vaidyanathan, A., and Nandakumar, K., "Temperature Effects on the Instablity Nature of Liquid Jets at Subcritical and Supercritical Chamber Conditions", Proceedings of the 7th International and 45th National Conference on Fluid Mechanics and Fluid Power (FMFP), IIT Bombay, Mumbai, India, December 10-12, 2018